UNIVERSITÀ DEGLI STUDI
DI GENOVA

PhD Program in Biotechnology in Translational Medicine
PhD program in Translational Medicine
XXX Cycle

The Human Amniotic Fluid Stem Cell Secretome as a powerful tool to unlock endogenous mechanisms of Cardiac Repair and Regeneration.

Candidate: Carolina Balbi
Supervisor: Prof. Sveva Bollini,

Alla mia Mamma,
perché manchi come l'aria.
Ti amo.

UNIVERSITÀ DEGLI STUDI
DI GENOVA

PhD Program in Biotechnology in Translational Medicine
PhD program in Translational Medicine

XXX Cycle

The Human Amniotic Fluid Stem Cell Secretome as a powerful tool to unlock endogenous mechanism of cardiac repair and regeneration.

Candidate: Carolina Balbi
Supervisor: Prof. Sveva Bollini,
Regenerative Medicine Lab,
Department of Experimental Medicine (DIMES),
University of Genoa

SUMMARY

Human amniotic fluid stem cells (hAFS) are immature fetal mesenchymal progenitors with promising paracrine potential, as previously shown by a study in a preclinical rat model of ischemia/reperfusion injury. Nevertheless, little is known about the comprehensive analysis of their *secretome*, which is represented by the whole of soluble secreted factors and extracellular vesicles (EV) released in the cell conditioned medium (hAFS-CM).

The aim of this PhD project is to characterise in details the hAFS secretome paracrine modulatory capacity, including the role of their extracellular vesicles, for future cardiac regenerative medicine.

The cardioprotecive potential of the hAFS-conditioned media (hAFS-CM) has been first assessed in a model of doxorubicin-induced cardiotoxicity *in vitro*. Indeed, the anthracycline doxorubicin is widely used in oncology, but it may cause cardiomyopathy with dismal prognosis that cannot be effectively prevented. Following hypoxic preconditioning, hAFS-CM demonstrated to actively antagonizes senescence and apoptosis of cardiomyocytes and cardiac progenitor cells, two major features of doxorubicin cardiotoxicity.

In order to fully understand the pro-active role of hAFS-EV in mediating paracrine regenerative effects, the second part of my PhD project has been dedicated to analyse the hAFS-derived EV (hAFS-EV) potential in providing proliferative, pro-survival, immunomodulatory and angiogenic effects. In particular, the role of hypoxic preconditioning on hAFS cells in priming their EV has been here evaluated as well. *In vitro* analyses on target cells defined their role as biologically mediators of paracrine effects by direct transfer of regenerative microRNAs, while the *in vivo* analysis in a preclinical mouse model of skeletal muscle atrophy study confirmed their modulatory role in decreasing pathological inflammation.

Finally, I confirmed the cardioactive profile of the hAFS secretome in a preclinical mouse model of myocardial infarction (MI), by specifically focusing on the enhancement of cardiac repair and the reactivation of the endogenous mechanism of regeneration via stimulation of cardiac progenitor cell in situ and of resident cardiomyocyte proliferation. Intra-myocardial injection of hAFS-CM soon after MI provided substantial cardioprotection, curbed down inflammation in the short term, while also sustaining angiogenesis and boosting cardiomyocyte proliferation. Notably, the hAFS secretome also induced the increase of endogenous epicardial progenitor cells within a week from MI, with a possible more specific role of hAFS-EV in unlocking their activation as well as rescuing cardiac function.

These encouraging findings suggest the hAFS secretome as an appealing source of therapeutic paracrine factors for the development of a *future medicinal advanced* product in cardiac regenerative medicine, so to provide cardioprotection following drug-derived injury or an ischemic insult, and improve cardiac repair while restoring the endogenous regenerative program within the heart.

INDEX

INTRODUCTION

Despite significant recent improvement of interventional medicine, cardiovascular disease (CD) and heart failure (HF) still represent the major cause of mortality and morbidity in the Western countries (Nichols et al.). Cardiac disease can arise from several conditions affecting heart structure and function. Myocardial infarction (MI), resulting from coronary artery disease(Laflamme and Murry, 2011), chemotherapy-derived cardiotoxicity (Molinaro et al., 2015), and congenital heart defects (Hanley et al., 1993) may all affect cardiac function and progressively lead to HF. In particular, CD pathogenesis is related to the very limited heart ability to withstand injury and aging, mainly due to insufficient cardio-protection along with inefficient repair and almost total lack of myocardial renewal. Hence, following CD and/or HF, cardiac transplantation still represents the ultimate therapeutic option, although severely hindered by the short supply of available donor hearts. This also translates into an economic burden for national health institutions, as more than 1 million of hospitalizations due to HF are annually reported in EU alone (Mozaffarian et al., 2015) and, despite the improvements in care, 1-year mortality rates for HF patients remains very high with 1 out of 4 patients dying within one year from diagnosis (Levy et al., 2002). Therefore, an innovative working strategy is strongly needed to counteract the development of CD and HF and open new frontiers in cardiac medicine.

Recently, increasing interest has been focused in exploiting the cardiovascular potential of autologous or allogeneic stem cells transplanted into the injured heart, with particular attention and promising results obtained by bone marrow mesenchymal stem cells (BM-MSC) (López et al., 2013). Nevertheless, several independent studies have demonstrated that injection of MSC into the damaged cardiac tissue results in limited differentiation - mainly into vascular lineages - while providing significant improvement in heart function

(Tao et al., 2016). Therefore stem cell-derived paracrine effect has emerged as a very promising strategy for the reactivation of endogenous mechanisms of repair and regeneration in several disease models (Gnecchi et al., 2008)(Mirotsou et al., 2011)(Bollini et al., 2013). Following transplantation, stem cells have been demonstrated in several studies to contribute to tissue regeneration mostly by modulatory effects rather than direct differentiation into new functional tissue; indeed, mounting evidence has shown that transplanted stem cells can release trophic signals to influence the surrounding microenvironment; this has led to a significant paradigm shift: from exploring the stem cell genome to analysing the stem cell "secretome" as the whole of growth factors and chemo-attractant molecules produced by paracrine secretion.

In light of such considerations, the search is now on identifying the suitable stem cell candidate to obtain the most cardio-active secretome to be exploited for future therapy. The more recent characterization of both fetal and perinatal MSC, with proprieties intermediate between embryonic and adult stem cells, has significantly broadened the stem cell scenario. Indeed, fetal stem cells isolated either from amniotic fluid fluid (AF)(De Coppi et al., 2007) or villi (Poloni et al., 2008) can be easily collected from leftover sample obtained during routine prenatal screening. Fetal and perinatal stem cells can offer specific advantages over adult MSC, since they are endowed with ES-like properties - such as remarkable self-renewal and expression of pluripotency to some extension - and a putative higher paracrine potential than the adult ones, being developmentally more immature. Moreover, they can easily overcome some of the classical drawbacks of adult stem cells, like BM-MSC that are obtained by invasive sampling associated with substantial morbidity, low yield and limited proliferative potential as often influenced by the donor age.

Human amniotic fluid-derived stem cells (hAFS) are broadly multipotent mesenchymal progenitors expressing pluripotency markers and high

self-renewal potential similar to embryonic stem cells, without being tumorigenic or causing any ethical concern (De Coppi et al., 2007). Because of their fetal, but non-embryonic origin, hAFS overcome many ethical concerns and can be easily obtained upon the expression of the stem marker c-KIT from leftover or discarded amniotic fluid samples collected during either amniocentesis (De Coppi et al., 2007)(Pozzobon et al., 2013) or eligible caesarean delivery (Schiavo et al., 2015).Thus they may represent an easy accessible source for future therapeutic applications. As a matter of fact, it has been previously demonstrated that c-KIT^{+} hAFS exert remarkable cardioprotective paracrine effects reducing the infarct size by about 14% in a rat acute model of MI (Bollini et al., 2011), possibly via the secretion of the cardioactive peptide thymosin beta 4, which, in turn, can reactivate epicardial progenitor cells to give rise de novo to fully mature cardiomyocytes (Smart et al., 2011). Moreover, rodent c-Kit^{+} AFS have showed to improve rat survival and clinical status, while maintaining the gut structure and function via the paracrine modulation of resident stromal cells expressing cyclooxygenase 2 (COX2), when injected in an established model of necrotising enterocolitis (Zani et al., 2014). Similar remarkable results have been also obtained in a model of skeletal muscle atrophy (HSA-Cre, Smn$^{F7/F7}$ mice), where transplantation of mouse c-Kit^{+} AFS showed to provide significant improvement in muscle strength and in the survival rate of the affected animals, together with the replenishment of the depleted skeletal muscle niche (Piccoli et al., 2012).

Within the stem cell paracrine scenario, growing interest has also been lately focused on the characterization of cell-secreted extracellular vesicles (EV). EV are membrane-bound cellular components enriched with soluble bioactive factors (proteins, lipids, etc) and RNA (mainly regulatory microRNA – miRNA - and mRNA) eliciting wide-ranging effects while mediating horizontal inter-cellular transfer of genetic information on the responder cells and modulating their function. EV

are secreted as micro-sized (microvesicles: 200-1000 nm) and nano-sized (exosomes: 40-150 nm) particles, thus acting as key biological effectors of paracrine signalling (Tetta et al., 2013). Microvesicles are released as shedding vesicles by direct budding of the plasma membrane, while exosomes are produced in endosomal multivesicular compartments (MVB, Multi-Vesicular Body) and secreted as the MVB fuses with the plasma membrane (Lötvall et al., 2014). Recent studies have shown that the beneficial effects observed in several preclinical model of experimental ischemic disease and injury following stem cell transplantation might be mainly mediated by the stem cell-EV. These include the activation of anti-apoptotic and pro-survival pathways eliciting angiogenic, anti-inflammatory and anti-fibrotic responses and the stimulation of resident endogenous progenitors, overall enhancing organ function (Rani et al., 2015). In particular, many studies have reported the potential efficacy of EV from adult mesenchymal stem cells (MSC) in providing cardioprotection against acute myocardial infarction (MI) (Arslan et al., 2013)(Lai et al., 2010)(Bian et al.), enhancing wound healing (Xu et al.), counteracting graft-versus-host-disease (GVHD) (Kordelas et al., 2014), reducing renal injury (Bruno et al., 2012), mediating liver regeneration (Tan et al., 2014) and stimulating neural plasticity following stroke (Xin et al., 2012). Since cell-free delivery of bioactive cargos by EV recapitulates the same beneficial responses of stem cell transplantation, they offer remarkable benefits over conventional cell therapy as immunologically-unresponsive agents (Bobis-Wozowicz et al., 2015). Despite the c-KIT^{+} AFS paracrine potential and distinct proteomic profile being confirmed by different independent studies (Bollini et al., 2011)(Mirabella et al., 2012)(Mirabella et al., 2011), at present the detailed composition and functional properties of both the hAFS conditioned media (hAFS-CM) and their secreted EV (hAFS-EV) on the injured cardiac tissue have not been elucidated yet.

AIM OF THE PROJECT and EXPERIMENTAL DESIGN

The aim of this PhD project has been providing detailed insights on the cardioactive paracrine potential of the hAFS secretome, by dissecting the specific contribution of hAFS-CM and hAFS-EV, so to suggest it as future advanced medicinal product for novel therapeutic approach in cardiac regenerative medicine.

I first investigated the hAFS-CM potential to provide efficient cardioprotection in a chemotherapy-derived cardiotoxicity *in vitro* model. Then, I characterised the hAFS-EV as biologically active carrier of regenerative paracrine effects both *in vitro* and *in vivo,* in a preclinical mouse model of skeletal muscle atrophy.
Finally, I translated the results obtained in the two previous part of my project into a preclinical mouse model of myocardial infarction (MI), so to define the precise role of the hAFS secretome components in both enhancing cardiac repair and unlocking endogenous regenerative mechanisms from within the injured tissue.

Therefore, the following tesis will be subdivided into 3 sections, according to the different specific studies I have performed to investigate the cardio-active paracrine potential of the hAFS secretome:

i) The cardioprotective potential of the hAFS secretome in a doxorubicin-derived cardiotoxicity model;

ii) First characterisation of hAFS extracellular vesicles as carrier of paracrine effects;

iii) Re-Activation of endogenous mechanism of cardiac repair and regeneration by the hAFS secretome in a preclinical mouse model of myocardial infarction.

i) THE CARDIOPROTECTIVE POTENTIAL OF THE hAFS SECRETOME IN A DOXORUBICIN-DERIVED CARDIOTOXICITY MODEL.

Since the hAFS-CM has been previously shown to mediate prompt cardioprotection by decreasing the infarct size in a rat model of acute myocardial ischemia and reperfusion injury in the short time (Bollini et al., 2011), here I further evaluated whether the hAFS-CM could also mediate pro-survival effect on cardiomyocyte and cardiac progenitor cells challenged by chemotherapy-derived cardiotoxicity *in vitro*.

As recent advance in diagnosis and therapy have made cancer curable in a substantial proportion of patients, the long-term side effect of oncological treatments may become a major health issue for cancer survivors once the tumour has been eliminated. In this scenario, anthracyclines, especially doxorubicin (Dox), are the mainstay of treatment for several types of cancer. Their main side effect is cardiotoxicity, which most often presents as left ventricular dysfunction or heart failure with delayed onset (Molinaro et al., 2015)(Octavia et al., 2012). In fact, many years can elapse between anthracycline administration and the appearance of anthracycline-related cardiomyopathy. Unfortunately, to date no effective mean of prevention of anthracycline cardiotoxicity exists (Huang et al., 2010).

Specifically, Dox use is hampered by cumulative and dose-related toxic effect causing cardiomyocyte and cardiac progenitor cells (CPC) premature senescence and apoptosis and leading to the development of severe cardiomyopathy and heart failure (Molinaro et al., 2015)(Octavia et al., 2012). Therefore, an ideal intervention to prevent Dox cardiotoxicity should limit DNA damage and elicit anti-senescent and anti-apoptotic pathways in cardiomyocytes and CPC. Here I am showing that the hAFS secretome has such profile of activity, since demonstrating the paracrine cardioprotective role of the hAFS-CM in antagonizing Dox-induced senescence and apoptosis on cardiac cells

in vitro by instructing target cells to limit DNA damage response, to increase Dox extrusion from the cells and to promptly activate pro-survival pathways via the PI3K/Akt signalling axis.

This specific study has been carried out in close collaboration with Dr. Pietro Ameri and his colleagues from the Cardiovascular Biology Laboratory, Department of Internal Medicine (DiMI) of University of Genova, who have major expertise on Dox-induced cardiotoxicity. The results I have significantly contributed to produce, which are reported here, have been recently published in Scientific Reports (joint first authorship).

Methods

Cell culture

hAFS were sorted for c-kit expression (CD117 MicroBead Kit, Miltenyi Biotechnology, Bergisch Gladbach, Germany) within the cells isolated from left over samples of II trimester amniotic fluid, collected via prenatal screening amniocentesis, with informed consent from donors and proved negative for disease (De Coppi et al., 2007; Pozzobon et al.; Schiavo et al., 2015). The protocol complied with the Helsinki Declaration and was approved by the local ethical committee Comitato Etico Regionale IRCCS AOU San Martino – IST (protocol 0036463/15 P.R. 428REG2015). Cells were cultured in Minimal Essential Medium (MEM) alpha with 15% fetal bovine serum (FBS), 1% L-glutamine, 1% penicillin/streptomycin, (Gibco-Thermo Fisher Scientific, Waltham, Massachusetts), 18% Chang B, and 2% Chang C (Irvine Scientific, Santa Ana, California) at sub-confluence. To limit the intrinsic variability of primary cultures, which might be influenced by the donors different age (samples were obtained by women from 25 up to 46 years old, mean: 38.4±3.3 years old), 3 different human amniotic fluid samples were pooled together to isolate hAFS for each experiment.

The NCTC 2544 cell line was purchased from the Interlab Cell Line Collection (Genova, Italy) and cultured in MEM/Earl's Balanced Salt Solution (MEM/EBSS) with 10% FBS, 1% non-essential aminoacids, 1% L-glutamine, and 1% penicillin/streptomycin (all EuroClone, Milano, Italy).

The H9c2 cell line was bought from the European Collection of Authenticated Cell Cultures (Salisbury, UK) and cultured as already described(Altieri et al., 2016; Fabbi et al., 2015).

mNVCM were isolated via enzymatic digestion from 2-day-old C57/Bl6 mouse heart by multiple digestions in a collagenase II solution (300U/ml, Worthington Biochemicals, Lakewood, New Jersey), according to(Radisic et al., 2003),and seeded on gelatin (1% solution,

Sigma-Aldrich, St.Louis, Missouri) coating at 10^5 cells/cm^2 in culture medium (69% Dulbecco's Modified Eagle Medium, DMEM, 15% M199, 10% horse serum, 5% FBS, 1% penicillin/streptomycin and 1% L-glutammine, Gibco-Thermo Fisher Scientific, Waltham, Massachusetts). All animal procedures were carried out in compliance with national and international laws and specific authorisation (protocol 792/2015-PR from Animal Facility of IRCCS AOU San Martino-IST).
hCPC were isolated as previously described(Gambini et al., 2011) from human auricolae fragments, obtained following written informed consent from patients, in compliance with the Helsinki Declaration and upon approval of the local ethical committee IRCCS Istituto Europeo di Oncologia and Centro Cardiologico Monzino (protocol CCFM C9/607). Briefly, the myocardial tissue was repeatedly digested at 37°C in a 3 mg/ml collagenase solution (Serva, Heidelberg, Germany), cells were FACS-sorted (FACSAria, Beckton-Dickinson, Brea, California) for c-kit expression using an APC-conjugated antibody (anti-CD117, clone YB5.B8; BD Biosciences, Franklin Lake, New Jersey) and cultured in Ham's F12 medium (Lonza, Basel, Switzerland) with 10% FBS (Gibco-Thermo Fisher Scientific, Waltham, Massachusetts), 2 mM L-glutathione and $5x10^{-3}$U/mL human erythropoietin (both Sigma-Aldrich), 10 ng/mL bFGF (Peprotech, Rocky Hill, New Jersey), and antibiotics (Lonza, Basel, Switzerland).

Characterization of hAFS after Hypoxic Preconditioning

The expression of specific stem cell markers was assessed by immunostaining using an anti-SSEA4 antibody (Abcam, Cambridge, United Kingdom) and an anti-NANOG antibody (Epitomics, Burlingame, California). *NANOG* mRNA levels were also evaluated by both qualitative RT-PCR (Forward: GCTGAGATGCCTCACACGGAG; Reverse: TCTGTTTCTTGACTGGGACCTTGTC) and real time qRT-PCR (Forward: TCCAGCAGATGCAAGAACTCTCCA; Reverse: CACACCATTGCTATTCTTCGGCCA). hAFS protein content was

analyzed by Western Blot (WB) for human HIF-1α (Hypoxia Inducible Factor-1 alpha, BD Bioscience, Brea, California) and βACTIN (Santa Cruz Biotechnology, Dallas, Texas). For hAFS immunophenotype, cells were incubated with PE- or FITC-conjugated antibodies against CD45, CD34, CD146, CD31, CD73, CD90, CD44, CD105 (eBioscience, San Diego, California), HLA-DR, DP, DQ and HLA-A,B,C (BD Pharmingen, Franklin Lake, New Jersey). Cell apoptosis was assessed using a FITC Annexin V Apoptosis Detection Kit (BD Pharmingen, Franklin Lake, New Jersey). hAFS were analyzed on a CyAn ADP analyzer equipped with 405nm, 488nm and 635nm lasers. Data was acquired with Summit 4.3 software (Beckmann Coulter, Brea, California).

Collection of hAFS-CM and hNCTC-CM

hAFS and NCTC 2544 cells were cultured for 24 hours in serum-free medium (SF: MEM alpha medium for hAFS and MEM/EBSS for NCTC 2544, both with 1% L-glutamine and 1% penicillin/streptomycin) in normoxia (20% O_2 and 5% CO_2 at 37°C) or hypoxia (1% O_2 and 5% CO_2 at 37°C in an hypoxic incubator, Eppendorf, Hamburg, Germany). The hAFS-CM_{Normo}, hAFS-CM_{Hypo}, hNCTC-CM_{Normo} and hNCTC-CM_{Hypo} were concentrated 20 times using ultrafiltration membranes with a 3kDa selective cut-off (Amicon Ultra-15, Millipore, Burlington, Massachusetts). Protein concentration was measured by Bradford assay. Samples were stored at – 80°C until use. At least 3 different batches of hAFS-CM and hNCTC-CM were used for each experiment.

Experiment outline

hAFS-CM was used at 40µg/ml, this concentration being the most protective in preliminary experiments with H9c2 cardiomyoblasts. The hNCTC-CM was employed at the same concentration. Cells were pre-incubated with hAFS-CM or hNCTC-CM for 3 hours prior to exposure to Dox. Apoptosis and cell viability were measured after Dox treatment (1µM) for 21 hours. Blocking experiments were performed by adding

0.025 µg/ml anti-IL-6 and/or 0.25 µg/ml anti-CXCL1 antibodies (clone MP5-20F3 and 48415, respectively, R&D Systems, Minneapolis, Minnesota) at the end of the 3 hour-incubation with the hAFS-CM when Dox treatment began, or 9 hours after hAFS-CM incubation, i.e. 6 hours after starting Dox treatment. Apoptosis was then evaluated 21 hours after Dox exposure. Senescence was examined after 3 hours of Dox exposure (H9c2: 0.1µM, mNVCM and hCPC: 0.2µM) followed by 42 hours in complete medium. DNA damage and gene expression profile were evaluated 6 hours after treatment with Dox (1µM), whereas nuclear translocation of NF-κB was assessed after Dox (1µM) incubation for 1.5 hours. To determine the acute effect on Akt phosphorylation, mNVCM were treated for 10 minutes with the hAFS-CM_{Hypo}, with or without pre-treatment with LY-294002 (20µM, Sigma-Aldrich, St.Louis, Missouri) for 1 hour. Before every experiment, cells were incubated in low-serum culture medium (DMEM low-glucose with 0.5% FBS, 1% L-glutamine, and 1% penicillin-streptomycin) for 1 hour.

Evaluation of senescence and apoptosis

To reveal SA β-galactosidase activity, cells were fixed in glutaraldehyde (0.5%) and incubated overnight at 37°C in a solution containing citric acid (10mM), potassium ferricyanide (5mM), NaCl (150mM), $MgCl_2$ (2mM), and 5-bromo-4-chloro-3-indolyl-beta-d-galactopyranoside (1mg/ml, all Sigma Aldrich, St.Louis, Missouri)(Itahana et al., 2013). Senescence of mNVCM was also revealed by immunostaining using a primary rabbit polyclonal antibody against $p16^{INK4a}$ (Proteintech, Manchester, UK), followed by Vectastain secondary antibody, horseradish peroxidase (HRP)-streptavidin, and 3,3`-diaminobenzidine (all from Vector Laboratories, Burlingame, California) as detection system. Apoptosis was assessed by immunocytochemistry, using a rabbit monoclonal anti-cleaved caspase-3 antibody (clone 5A1E, Cell Signaling Technologies, Danvers, Massachusetts). The percentage of SA β-galactosidase, $p16^{INK4a}$ and cleaved caspase-3 positive cells was

evaluated considering six random fields (20x), taken with the Leica Q500 MC Image Analysis System (Leica, Wetzlar, Germany).

Cell viability assay

Following Dox exposure with or withour hAFS-CM or hNCTC-CM pre-incubation, MTT solution (250µg/ml; Sigma-Aldrich, St.Louis, Missouri) was added to the cells for 4 hours and absorbance
read at 570nm on a VersaMax (GE Intelligent Platforms, Boston, Massachusetts) plate reader.

Assessment of DNA damage

After exposure to Dox (1µM) with or without pre-treatment with the hAFS-CM_{Hypo}, mNVCM were fixed in paraformaldehyde solution (4%, Sigma Aldrich, St.Louis, Missouri) and incubated with a rabbit monoclonal antibody against γH2aX (Ser139, clone 20E3, Cell Signalling Technologies, Danvers, Massachusetts) followed by Alexa Fluor488-conjugated secondary antibody (Gibco-Thermo Fisher Scientific, Waltham, Massachusetts). Fluorescence emission was quantified using an Infinite 200 PRO plate reader (Tecan, Männedorf, Switzerland). Immunocytochemistry, immunofluorescence and cell culture images were acquired with an Axiovert microscope equipped with Axiovision software (Carl Zeiss, Oberkochen, Germany).

Gene expression profiling

The gene expression profile of mNVCM treated with Dox (1µM) with or without pre-incubation with the hAFS-CM_{Hypo}, was analysed by Affymetrix MG 430.2 microarray technology. Total RNA was extracted using the RNeasy Micro Kit (Qiagen, Hilden, Germany). cRNA for hybridization was prepared using the GeneChip® 3' IVT PLUS Reagent Kit following the instructions provided by Affymetrix. Hybridisation and scanning were performed by standard procedures, as recommended by Affymetrix. Data were deposited in the Gene Expression Omnibus

repository (www.ncbi.nlm.nih.gov/geo/, accession number: GSE74513) and pre-processed using the RMA algorithm with quantile normalization(Irizarry et al., 2003). Differentially expressed genes were identified applying a threshold of two-fold increase or decrease of the expression values when comparing the two conditions. Enrichment of functional categories of genes was analyzed by EnrichR Gene Set Enrichment Analysis (http://amp.pharm.mssm.edu/Enrichr/)(Chen et al., 2013).

Real-time quantitative RT-PCR analysis

Total RNA from mNVCM cells was extracted using Qiazol Lysis Reagent (Qiagen, Hilden, Germany) and cDNA obtained using the iScriptTM cDNA Syntesis Kit (Bio-Rad, Hercules, California). Real-time qRT-PCR was carried out on a 7500 Fast Real-Time PCR System (Applied Biosystems, Forest City, California) using Syber Green Master Mix (Gibco-Thermo Fisher Scientific, Waltham, Massachusetts). Primer sequences for mouse *Il6* (Forward: TCGTGGAAATGAGAAAAGAGTTGTG; Reverse: CCAGTTTGGTAGCATCCATCATTT), *Cxcl1* (Forward: ACTTGGGGACACCTTTTAGCA; Reverse: ACTCAAGAATGGTCGCGAGG), *Abcb1b* (Forward: AAACTCCATCACCACCTCACG, Reverse: ATCTTCTGAGGTTCCGCTCAA) and *Hprt* (Forward: CCCCAAAATGGTTAAGGTTGC, Reverse: CCAACAAAGTCTGGCCTGTAT*)* were designed using the NCBI Primer-Blast tool (http://www.ncbi.nlm.nih.gov/tools/primer-blast/.Gene expression levels were normalized using *Hprt* or *GAPDH* as endogenous control by applying the 2^{-ddCt} method.

Western blot

Whole cell lysates were separated on a tris-glycine gel (8-16%, Gibco-Thermo Fisher Scientific, Waltham, Massachusetts), transferred onto a poly-vinylidene difluoride membrane (Bio-Rad, Hercules, California),

and incubated overnight with the following primary antibodies: anti-phosphorylated AKT (Ser^{473} rabbit monoclonal, clone D9E; Cell Signaling Technologies, Danvers, Massachusetts); anti-Akt (rabbit polyclonal, cone 11e7 Cell Signalling Technologies, Danvers, Massachusetts); anti-phosphorylated IκBα (Ser$^{32/36}$ mouse monoclonal, clone 5A5, Cell Signalling Technologies, Danvers, Massachusetts); anti total-IκBα (mouse monoclonal, clone 112B2, Cell Signalling Technologies, Danvers, Massachusetts); and anti-p16^{INK4a} (rabbit polyclonal, Proteintech, Manchester, UK). The membrane was incubated with goat anti-rabbit or anti-mouse HRP-conjugated secondary antibodies (sc-2030 and sc-2005, respectively; Santa Cruz Biotechnology, Dallas, Texas). Bands were detected by Clarity Western ECL Substrate (Bio-Rad, Hercules, California), imaged using Alliance LD2 system and software (UVItec, Cambridge, UK), and quantified by densitometry analysis with ImageJ software (NCBI, Bethesda, Maryland). Values were normalized against those of GAPDH, as revealed by a primary antibody directly conjugated to HRP (clone D16H11, Cell Signalling Technologies, Danvers, Massachusetts).

Quantification of nuclear levels of NF-κB

Cells were first lysed in an hypotonic solution containing Tris-HCl (20mM), NaCl (10mM), $MgCl_2$ (3mM), PMSF (1 mM), and 1x PIC (all Gibco-Thermo Fisher Scientific, Waltham, Massachusetts) in order to separate the cytoplasmic and nuclear fractions. Nuclear proteins were then retrieved by disrupting the nuclear fraction in an extraction buffer (1 mM Tris pH 7.4, 2mM Na_3VO_4, 100mM NaCl, 1mM EDTA, 10% glycerol, 1mM NaF, 0.5% deoxycholate, 20mM $Na_4P_2O_7$, and 0,5% NP40), and quantified by means of Bio-Rad protein assay (Bio-Rad, Hercules, California). Levels of nuclear p65 were assessed using a NF-κB p65 ELISA kit (Gibco-Thermo Fisher Scientific, Waltham, Massachusetts).

Measurement of Dox fluorescence in culture medium

mNVCM and cells were treated as described above. Their conditioned medium was collected at 0.5, 2, 4, 8, 16 and 24h after Dox administration and immediately evaluated for fluorescence emission on a Infinite reader M200 (Tecan, Männedorf, Switzerland) equipped with a 530/25nm excitation and a 590/20nm emission filter (Dox excitation/emission peak).

Statistical analyses

Results are presented as mean ± s.e.m. of at least three (n=3) independent replicated experiments. Comparisons were drawn by two-way ANOVA (fluorescence intensity of the mNVCM- and MDA-MB-231-conditioned medium after exposure to Dox with or without pre-incubation with the hAFS-CM_{Hypo}) or one-way ANOVA followed by post-hoc Tukey's multiple comparisons test (all other data). Statistical analysis was performed using GraphPad Prism Version 6.0a (GraphPad Software) with statistical significance set at $p<0.05$.

Results

Hypoxic preconditioning does not significantly affect hAFS stemness.

hAFS viability, phenotype and stemness were analyzed under the following conditions: (a) control normoxic (20% O_2, 5% CO_2 at 37°C in complete medium, CTRL); (b) SF normoxic (20% O_2, 5% CO_2 at 37°C in SF medium, SF); (c) control hypoxic (1% O_2, 5% CO_2 at 37°C in complete medium, CTRL) and (d) SF hypoxic (1% O_2, 5% CO_2 at 37°C in SF medium, SF). hAFS did not show any significant morphological alteration under hypoxic versus normoxic condition, both in CTRL and SF culture [Fig.1A]. The expression of specific stem markers, such as SSEA4 and Nanog was maintained in all conditions [Fig.1B-D]. WB for HIF-1α confirmed that 24h treatment was sufficient for the hAFS to become responsive to the hypoxic microenvironment [Fig.1C]. While hAFS viability in the different settings was not statistically different with their immunophenotype unaltered, hypoxic preconditioning [Fig.1E-F] significantly influenced the protein concentration of the hAFS-CM;

hAFS viability, phenotype and stemness were analyzed under the following conditions: (a) control normoxic (20% O_2 in complete medium, CTRL); (b) SF normoxic (20% O_2 in SF medium, SF); (c) control hypoxic (1% O_2 in complete medium, CTRL) and (d) SF hypoxic (1% O_2 in SF medium, SF). hAFS did not show any substantial morphological alteration under hypoxic versus normoxic conditions, both in CTRL and SF culture [Fig.1A]. Also, the expression of the stem markers SSEA4 and NANOG [Fig.1A] was not significantly altered. SSEA4 was consistently expressed by more than 83% of hAFS, regardless of the culture settings [Fig.1C]. While *NANOG* mRNA was not significantly affected by preconditioning [Fig.1D], protein expression was heterogeneously distributed in hAFS, yet without any evident difference compared to the control condition [Fig. 1A]. HIF-1α expression confirmed that 24h treatment was sufficient for the hAFS to

become responsive to the hypoxic microenvironment [Fig.1B]. hAFS immunophenotype remained unaltered, lacking expression for hematopoietic and mature lineage antigens - such as CD45, CD34, HLA Class II and CD31 – and showing reasonably high to medium-high expression of the canonical mesenchymal markers CD73, CD90, CD44 and CD105. A small, but non-significant decrease in CD73 and CD105 expression was detected in hypoxic and SF conditions. hAFS cells showed variable CD146 expression, as previously reported (Bottai et al., 2012; Chiavegato et al., 2007), while they maintained robust expression of HLA Class I [Fig.1E]. hAFS viability was variable: although the SF condition affected hAFS more than hypoxic stimulation, this was not statistically significant and likely dependent on hAFS donor variation [Fig.1F]. Indeed, hAFS-CM_{Hypo} showed an almost two-fold increase in protein concentration compared to hAFS-CM_{Normo}, (*$p<0.05$) [Fig1G].

The hAFS secretome rescues H9c2 cells from Dox-induced senescence and apoptosis.

An established *in vitro* model of Dox cardiotoxicity (Altieri et al., 2016; Fabbi et al., 2015) was initially used to screen the effects of the hAFS-CM. H9c2 rat embryonic cardiomyoblasts were exposed to Dox with or without prior incubation with the hAFS-CM_{Normo} and hAFS-CM_{Hypo}. Since we previously observed that hAFS are activated by the ischemic environment and promote cardiomyocyte survival in a paracrine manner (Bollini et al., 2011), hypoxic preconditioning was used as a working strategy to enrich hAFS-CM for cardioprotective factors. As shown in Fig.2, the percentage of cells stained for senescence associated (SA) β-galactosidase (Altieri et al., 2016) [Fig.2A-B] and cleaved caspase-3 [Fig.2C-D] dramatically rose with Dox to values similar to those found previously (Altieri et al., 2016; Fabbi et al., 2015) and was significantly reduced by 35% and 26%, respectively, by pre-treatment with hAFS-CM_{Normo} (46.5±1.7% vs 30.4±4.5% of SA β-

galactosidase positive cells and 25.0±1.0% vs 18.5±0.8% cleaved caspase-3 positive cells). The hAFS-CM_{Hypo} was even more protective, the number of senescent and apoptotic cells being decreased by 49% and 43% respectively (46.5±1.7% vs 23.7±1.8% of β-galactosidase positive cells and 25.0±1.0% vs 14.2±1.4% cleaved caspase-3 positive cells).

By contrast, Dox-elicited senescence and apoptosis were not reduced by pre-incubation with the conditioned medium from the human keratinocyte cell line, NCTC 2544 (hNCTC-CM_{Normo} and hNCTC-CM_{Hypo}), used as an internal control [Fig.2B-C].

hAFS-CM_{Hypo} effectively protects mouse neonatal cardiomyocytes against Dox.

Next, the cardioprotective potential of hAFS-CM_{Hypo} - which had proved to be the most effective form of hAFS-CM to prevent Dox toxicity in the experiments with H9c2 cardiomyoblasts - was confirmed on primary mouse neonatal ventricular cardiomyocytes (mNVCM). Consistent with earlier studies (Altieri et al., 2016), SA β-galactosidase positive mNVCM were about 45% after Dox treatment. Pre-incubation with hAFS-CM_{Hypo} diminished the frequency of senescent cells by 47% (Fig.3A-B: upper panel; 44.7±2.9% vs 23.6±2.4% of SA β-galactosidase positive cells). Similar results were obtained by immunostaining for $p16^{INK4a}$, with the hAFS-CM_{Hypo} decreasing the pro-senescent effect of Dox by 35% (Fig.3B lower panel; 48.8±1.8% vs 31.8±1.5% of $p16^{INK4a}$ positive cells). Moreover, there were twice as many cleaved caspase-3 positive cells with Dox as without treatment, and this increase in apoptosis was also reduced by the hAFS-CM_{Hypo} by 41% (Fig.3C and 3E: 41.6±2.1% vs 24.7±1.1% cleaved caspase-3 positive cells). Correspondingly, cell viability, as measured by MTT assay, was increased by 10.5% by pre-incubation with hAFS-CM_{Hypo} [Fig.3D and 3F]. Importantly, hNCTC-CM did not prevent Dox-initiated senescence and apoptosis of mNVCM [Fig.3B, 3E-F], nor were these

cell responses significantly modified by hAFS-CM_{Hypo} or hAFS-CM_{Normo} alone.

Immunoreactivity for phosphorylated H2AX (γH2AX), a sensitive indicator of DNA double-strand breaks and damage(El-Awady et al., 2015), was much more widespread and intense following exposure to Dox, than in untreated mNVCM [Fig.3G]. Mean fluorescence intensity for γH2AX was increased by about 4-fold by Dox compared to untreated cells, but limited to a 2.4 fold change, corresponding to a 37% reduction, by pre-incubation with the hAFS-CM [Fig.3G, right panel].

hAFS-CM_{Hypo} acts through the NFkB-controlled pro-survival genes Il6 and Cxcl1 and the PI3K/Akt pathway.

To identify the pathways responsible for hAFS-CM_{Hypo} antagonism of Dox cardiotoxicity, gene expression profiles were compared between mNVCM treated with Dox or incubated with hAFS-CM_{Hypo} followed by Dox exposure. Microarray analysis using Affymetrix technology revealed that pre-treatment with hAFS-CM_{Hypo} led to the up-regulation of genes coding for cytokines, chemokines, growth factors, and chemokine and cytokine receptor binding proteins [Fig.4A]. In particular, *Il6* and *Cxcl1* were highly expressed. Confirmatory real time qRT-PCR at 6 hours after Dox treatment demonstrated that these two genes were up-regulated by 7 and 29 fold compared to untreated cells and by 17- and 59 fold compared to Dox treatment, respectively, when the hAFS-CM_{Hypo} preceded Dox exposure [Fig. 4B]. Since IL-6 and CXCL-1 have been shown to be involved in mNVCM survival (Craig et al., 2000),(Bachmaier et al., 2014), we investigated whether blockade of these two cytokines might influence the protective effects of hAFS-CM_{Hypo}. The decrease in apoptosis attained with hAFS-CM_{Hypo} was significantly blunted when pre-incubation with hAFS-CM_{Hypo} was followed by treatment with Dox, along with antibodies against IL-6 or IL-6 as well as CXCL-1 (either soon after or after 6 hours post Dox

administration, Fig.4C), thus indicating that hAFS-CM_{Hypo} inhibits Dox-induced apoptosis via IL-6 and, to a lesser extent, CXCL-1.
Il6 and *Cxcl1* are controlled by nuclear factor kappa-light-chain-enhancer of activated B cells (NF-κB). Under basal conditions, the latter is kept inactive in the cytoplasm by inhibitor of κB alpha (IκBα). Phosphorylation of IκBα at critical serine residues leads to its degradation and relieves NF-κB, which can localize to the nucleus and modulate the transcription of target genes. Consistently, pre-incubation of mNVCM with hAFS-CM_{Hypo} before Dox treatment enhanced IκBα phosphorylation [Fig.5A] and increased the amount of NF-κB in the nuclear compartment, as assessed by ELISA for the p65 subunit [Fig.5B], although not to a statistically significant extent. Since the phosphoinositide 3-kinase (PI3K)/Akt cascade is a main trigger of IκBα degradation, we sought to determine whether this pathway lies upstream of the activation of NF-κB, the induction of *Il6* and *Cxcl1*, and the protection against Dox toxicity by the hAFS-CM_{Hypo}. The PI3K inhibitor, LY-294002, reduced the phosphorylation of IκBα [Fig.5A], prevented the nuclear accumulation of NF-κB [Fig.5B], and attenuated the increase in *Il6* and *Cxcl1* [Fig.5C]. Furthermore, it abolished the inhibition of Dox-triggered senescence and apoptosis attained with the hAFS-CM_{Hypo} [Fig.5D], indicating that hAFS-CM_{Hypo} up-regulates the NF-κB-dependent pro-survival genes, *Il6* and *Cxcl1*, and counteracts Dox cardiotoxicity at least in part via PI3K/Akt. In fact, hAFS-CM_{Hypo} potently stimulated the phosphorylation of Akt twice as much compared to Dox treatment alone, an effect which was abrogated by LY-294002 [Fig.5E].

hAFS-CM_{Hypo} promotes Dox efflux from mouse neonatal cardiomyocytes.

Since pre-incubation with the hAFS-CM_{Hypo} substantially reduced DNA damage by Dox treatment, we wondered whether the hAFS-CM_{Hypo} might also affect the retention of the drug by mNVCM besides activating

protective pathways. As experimental studies have shown that the transmembrane pump ABCB1B extrudes Dox from cells and is critical to determine its toxic effects (Krishnamurthy et al., 2012), we examined the levels of this transporter in mNVCM. Pre-incubation with the hAFS-CM_{Hypo} led to a sharp increase in *Abcb1b* expression of about 3-fold and 2-fold, respectively, compared to Dox treatment alone or to untreated cells and this was prevented by LY-294002 [Fig.6A]. Since Dox is autofluorescent, the fluorescence in culture medium after treatment with the drug is a function of its efflux from cells. This feature was exploited to determine whether *Abcb1b* modulation reduced Dox accumulation in mNVCM. As shown in Figure 6B, fluorescence in culture medium was significantly higher at 8, 16 and 24 hours after exposure to Dox, when cells were pre-incubated with hAFS-CM_{Hypo} than when they were not [Fig.6B].

hAFS-CM_{Hypo} antagonizes Dox toxicity on human cardiac progenitor cells.

Damage, senescence and depletion of human endogenous cardiac progenitor cells (hCPC) are thought to be critical for the pathogenesis of Dox cardiomyopathy (Piegari et al., 2013),(Huang et al., 2010). Therefore, we assessed whether hAFS-CM_{Hypo} may also protect hCPC against Dox. hCPC were isolated from human atrial samples as previously described (Gambini et al., 2011) and treated with Dox with or without prior incubation with hAFS-CM_{Hypo} or hNCTC-CM_{Hypo}. The frequency of SA β-galactosidase positive cells was significantly increased by Dox, as expected, and reduced by 51% by pre-incubation with hAFS-CM_{Hypo} (50.1±6.4% vs 24.5±1.9% of SA β-galactosidase positive cells), whilst hNCTC-CM_{Hypo} was not effective [Fig.7A-B]. The same trend was observed when senescence was evaluated by analysing the expression of $p16^{INK4a}$, with hAFS-CM_{Hypo} decreasing $p16^{INK4a}$ levels by 30% (2.3-fold increase vs 1.6-fold increase compared to untreated cells, Fig.7C and 7D). In agreement with the results of

previous, similar *in vitro* studies (Huang et al., 2010)·(De Angelis et al., 2010), Dox induced hCPC apoptosis, as assessed by staining for activated caspase-3, to a limited extent (4.5±0.6% vs 0.9±0.1% cleaved caspase-3 positive cells, Fig.7E-F). The rate of apoptosis was even lower when cells were pre-incubated with hAFS-CM_{Hypo} before exposure to Dox, although not significantly (4.5±0.6% vs 3.8±0.5% cleaved caspase-3 positive cells with Dox alone vs hAFS-CM_{Hypo} + Dox, respectively; Fig.7E-F).

Figures

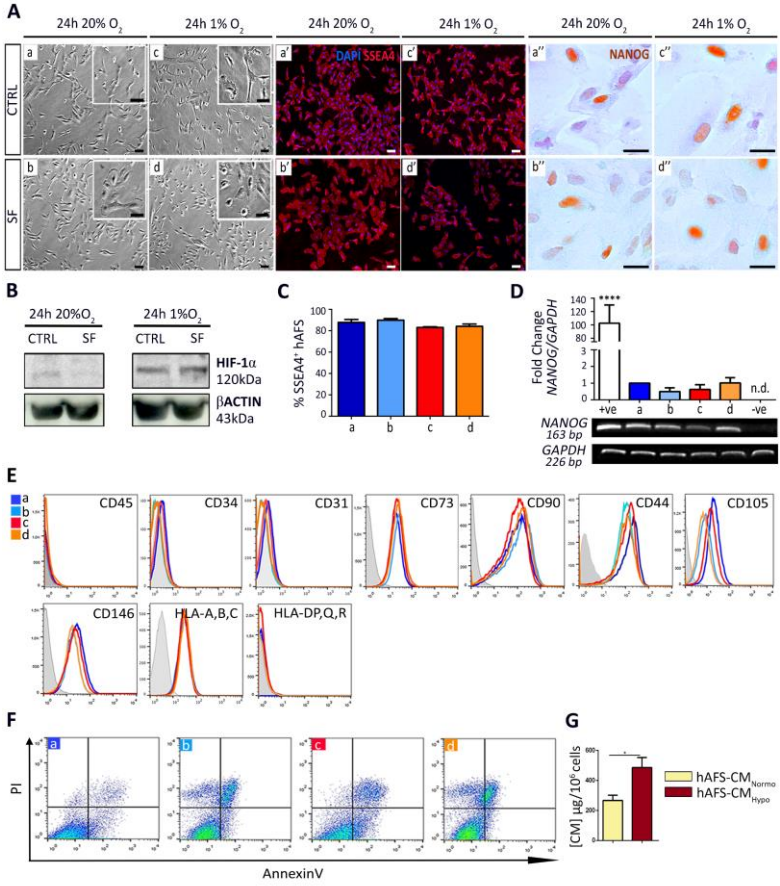

Figure 1 A) Bright field, SSEA4 and NANOG immunostaining images of hAFS under: (a), (a') and (a'') 24h 20% O_2 CTRL conditions; (b), (b') and (b'') 24h 20%O_2 SF conditions; (c), (c') and (c'') 24h 1% O_2 preconditioning in CTRL medium; (d), (d') and (d'') 24h 1% O_2 preconditioning in SF condition; scale bar 50µm. **B)** WB for HIF-1α expression by hAFS after 24h of 20% O_2 or 1% O_2 preconditioning in complete (CTRL) or SF medium. **C)** SSEA4⁺ hAFS under: (a) 24h 20% O_2 CTRL condition: 87.8 ± 2.8%; (b) 24h 20%O_2 SF condition: 89.9 ±

1.5%; (c) 24h 1% O_2 preconditioning in CTRL medium: 83.0 ± 0.7% and (d) 24h 1% O_2 preconditioning in SF condition: 84.1 ± 2.2%; values expressed as mean ± s.e.m. **D)** Real time qRT-PCR and qualitative RT-PCR analysis for *NANOG* and *GAPDH* expression of hAFS under 24h: (a) 20% O_2 CTRL and (b) 20% O_2 SF conditions, (c) 1% O_2 CTRL and (d) 1% O_2 SF conditions; +ve: positive control, human embryonic stem cells (hES) (****p<0.0001); -ve: negative control: HDF; n.d.: not determined. **E)** hAFS immunophenotype under 24h 20% O_2 in CTRL (a) or SF conditions (b) or under 24h 1% O_2 preconditioning, in either CTRL (c) or SF conditions (d). **F)** Apoptosis analysis by Annexin V and PI of hAFS under 24h: (a) 20% O_2 CTRL and (b) 20% O_2 SF conditions, (c) 1% O_2 CTRL and (d) 1% O_2 SF conditions. **G)** Bradford assay to determine protein concentration in hAFS-CM_{Normo} and hAFS-CM_{Hypo}

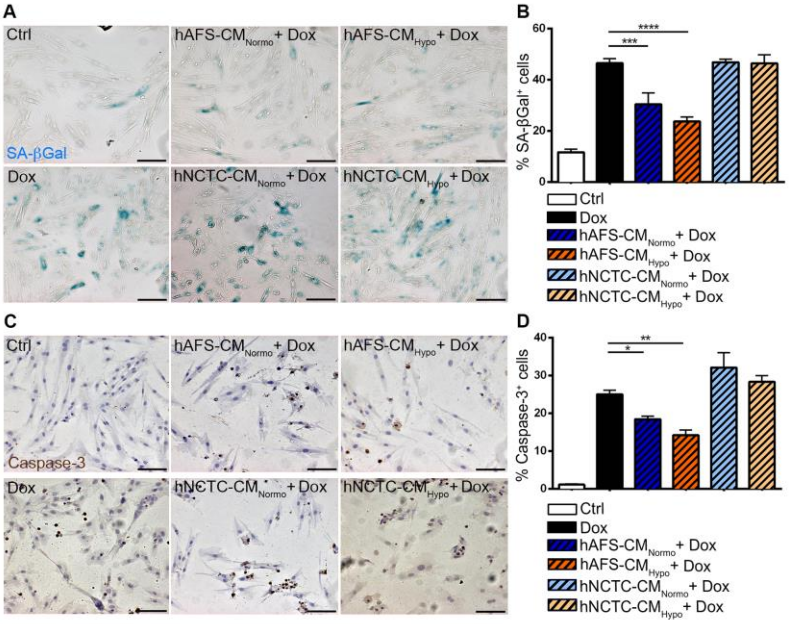

Figure 2 A) Representative images of rat H9c2 cardiomyoblasts stained for senescence associated (SA) β-galactosidase: untreated cells (*Ctrl*), cells exposed to 0.1µM Dox (*Dox*), and cells pre-incubated

with 40µg/ml of: the hAFS-CM_{Normo} (*hAFS-CM_{Normo}* + *Dox*), the hAFS-CM_{Hypo} (*hAFS-CM_{Hypo}* + *Dox*), the hNCTC-CM_{Normo} (*hNCTC-CM_{Normo}* + *Dox*), or the hNCTC-CM_{Hypo} (*hNCTC-CM_{Normo}* + *Dox*) prior to Dox treatment. Scale bar 100µm. **B**) Percentage of H9c2 cells expressing SA β-galactosidase after exposure to Dox with or without pre-incubation with 40µg/ml of the hAFS-CM or hNCTC-CM (mean ± s.e.m.). Ctrl: 11.7±1.2%, Dox: 46.5±1.7%, hAFS-CM_{Normo} + Dox: 30.4±4.5%, hAFS-CM_{Hypo} + Dox: 23.7±1.8%, hNCTC-CM_{Normo} + Dox: 46.9±1.2%, and hNCTC-CM_{Hypo} + Dox: 46.4±3.3%; *** $p<0.001$ ($p=0.0004$), **** $p<0.0001$. **C**) Representative images of H9c2 cardiomyoblasts stained for cleaved caspase-3 (Caspase-3): untreated cells (*Ctrl*), cells exposed to 1µM Dox (*Dox*), and cells pre-incubated with 40µg/ml of: the hAFS-CM_{Normo} (*hAFS-CM_{Normo}* + *Dox*), the hAFS-CM_{Hypo} (*hAFS-CM_{Hypo}* + *Dox*), the hNCTC-CM_{Normo} (*hNCTC-CM_{Normo}* + *Dox*), or the hNCTC-CM_{Hypo} (*hNCTC-CM_{Normo}* + *Dox*) prior to Dox treatment. Scale bar 100µm. **D**) Percentage of H9c2 cells expressing cleaved caspase-3 (% Caspase-3^+ cells) after exposure to Dox with or without pre-incubation with 40µg/ml of the hAFS-CM or hNCTC-CM (mean ± s.e.m.). Ctrl: 1.1±0.2%, Dox: 25.0±1.1%, hAFS-CM_{Normo} + Dox: 18.5±0.8%, hAFS-CM_{Hypo} + Dox: 14.2±1.4%, hNCTC-CM_{Normo} + Dox: 32.0±3.9%, and hNCTC-CM_{Hypo} + Dox: 28.3±1.7%; * $p<0.05$ ($p=0.0433$), ** $p<0.01$ ($p=0.0014$).

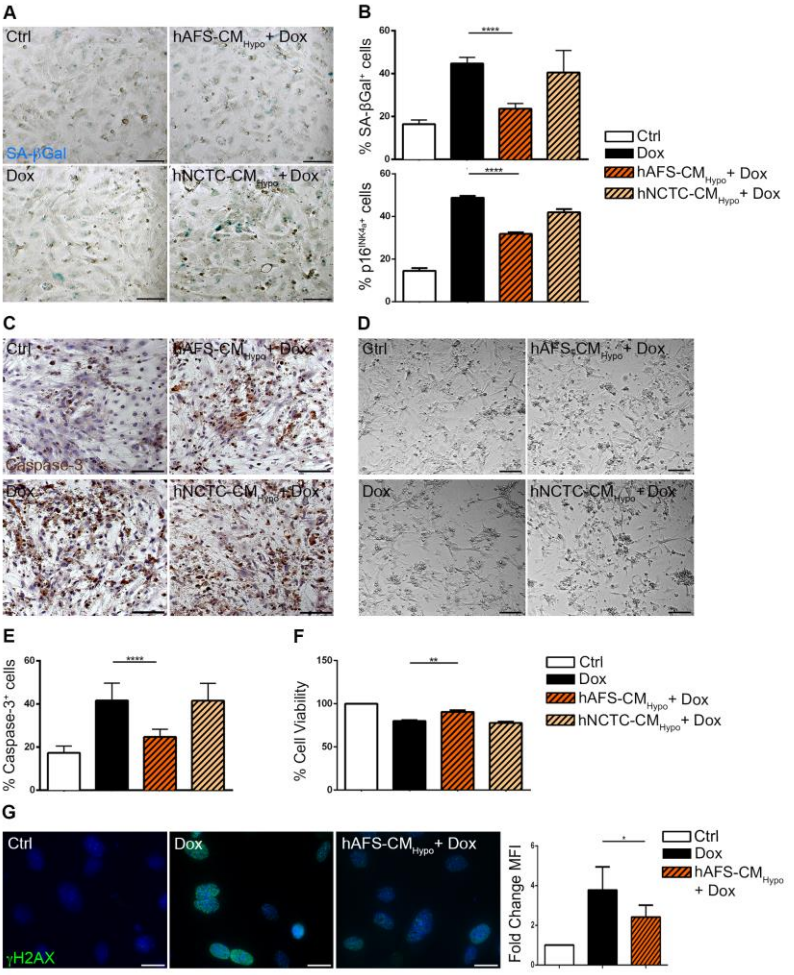

Figure 3 A) Representative images of mNVCM stained for senescence associated (SA) β-galactosidase: untreated cells (*Ctrl*), cells exposed to 0.2µM Dox (*Dox*), and cells pre-incubated with 40µg/ml of hAFS-CM$_{Hypo}$ (*hAFS-CM$_{Hypo}$* + *Dox*) or hNCTC-CM$_{Hypo}$ (*hNCTC-CM$_{Normo}$* + *Dox*). Scale bar 100µm. **B**) Upper panel: mNVCM expressing SA β-galactosidase after Dox exposure with or without pre-incubation with 40µg/ml of the hAFS-CM$_{Hypo}$ or the hNCTC-CM$_{Hypo}$ (mean ± s.e.m.). Ctrl: 16.4±1.9%, Dox: 44.7±2.9%, hAFS-CM$_{Hypo}$ + Dox: 23.6±2.4%, and hNCTC-CM$_{Hypo}$ + Dox: 40.5±10.2%; **** p<0.0001. Lower panel:

mNVCM expressing $p16^{INK4a}$ after Dox treatment with or without pre-incubation with 40µg/ml of the hAFS-CM_{Hypo} or the hNCTC-CM_{Hypo} (mean ± s.e.m.). Ctrl: 14.5±2.9%, Dox: 48.8±1.8%, hAFS-CM_{Hypo} + Dox: 31.8±1.5%, and hNCTC-CM_{Hypo} + Dox: 41.9±3.0%; **** p<0.0001. **C**) Representative images of mNVCM stained for cleaved caspase-3 (Caspase-3): untreated cells (*Ctrl*), cells exposed to 1µM Dox (*Dox*), and cells pre-incubated with the hAFS-CM_{Hypo} (*hAFS-CM_{Hypo}* + *Dox*) or the hNCTC-CM_{Hypo} (*hNCTC-CM_{Normo}* + *Dox*). Scale bar 100µm. **D**) Representative images of viable mNVCM by MTT assay: untreated cells (*Ctrl*), cells exposed to 1µM Dox (*Dox*), and cells pre-incubated with the hAFS-CM_{Hypo} (*hAFS-CM_{Hypo}* + *Dox*) or the hNCTC-CM_{Hypo} (*hNCTC-CM_{Normo}* + *Dox*) prior to Dox. Scale bar 100µm. **E**) mNVCM expressing cleaved-caspase-3 (% Caspase-3^+ cells) after exposure to Dox with or without pre-incubation with 40µg/ml of the hAFS-CM_{Hypo} or the hNCTC-CM_{Hypo} (mean ± s.e.m.). Ctrl: 17.3±0.8%, Dox: 41.6±2.1%, hAFS-CM_{Hypo} + Dox: 24.7±1.1%, and hNCTC-CM_{Hypo} + Dox: 41.5±4.1%; **** p<0.0001. **F)** Percentage of viable mNVCM by MTT assay, after exposure to Dox with or without pre-incubation with 40µg/ml of the hAFS-CM_{Hypo} or hNCTC-CM_{Hypo}, compared to untreated cells (mean ± s.e.m.). Ctrl: 100%, Dox: 80.0±0.8%, hAFS-CM_{Hypo} + Dox: 90.5±2.1%, and hNCTC-CM_{Hypo} + Dox: 77.8±1.4%; ** p< 0.01 (p=0.006). **G**) Representative images of mNVCM stained for γH2AX: untreated cells (*Ctrl*), cells exposed to 1µM Dox (*Dox*), and cells pre-incubated with 40µg/ml of the hAFS-CM_{Hypo} (*hAFS-CM_{Hypo}* + *Dox*). Scale bar 20µm. The graph on the right shows the mean fluorescence intensity (MFI) fold change after exposure to Dox, with or without pre-incubation with the hAFS-CM_{Hypo}; * p<0.05 (p=0.0114).

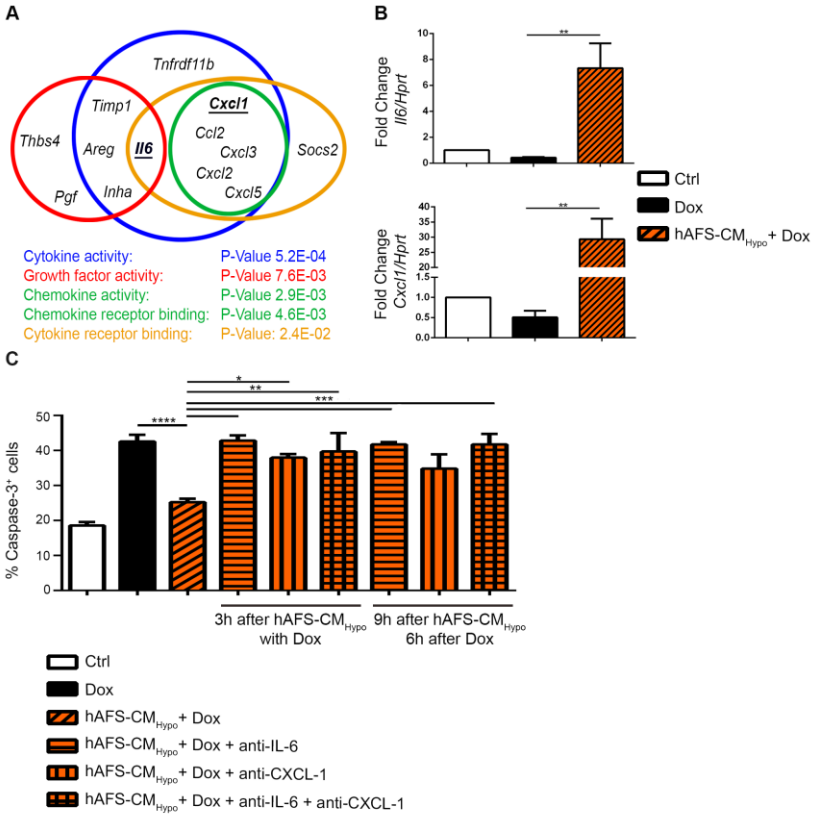

Figure 4 A) Schematic illustrating the cluster of genes coding for cytokines, chemokines, growth factors, and chemokine and cytokine receptor-binding proteins up-regulated by incubation with 40µg/ml of hAFS-CM_{Hypo} prior to exposure to 1µM Dox, according to microarray analysis. **B)** Real time qRT-PCR showing significant up-regulation of the NF-κB-controlled pro-survival genes *Il6* and *Cxcl1* in mNVCM incubated with 40ug/ml of hAFS-CM_{Hypo} prior to treatment with 1µM Dox; ** $p<0.01$ ($p=0.0015$ and $p=0.0020$, respectively). **C**) Percentage of mNVCM expressing cleaved caspase-3 (% Caspase-3^+ cells) after exposure to Dox, with or without pre-incubation with 40µg/ml of the hAFS-CM_{Hypo} and with blocking antibodies against IL-6 (anti-IL6) and/or CXCL-1 (anti-CXCL1) added to the culture medium (mean ± s.e.m.).

Ctrl: 18.55±4.0%, Dox: 42.57±7.7%, hAFS-CM_{Hypo} + Dox: 25.25±3.5%, The following values refer to results obtained adding blocking antibodies when Dox treatment began, after 3 hours of incubation with the hAFS-CM: hAFS-CM_{Hypo} + Dox + anti-IL-6: 42.79±2.7%, hAFS-CM_{Hypo} + Dox + anti-CXCL-1: 37.94±1.8%, hAFS-CM_{Hypo} + Dox + anti-IL-6 and+ anti-CXCL-1: 39.68±9.1%, **** $p<0.0001$, *** $p<0.001$ ($p=0.0002$), ** $p<0.01$ ($p=0.0041$) * $p<0.05$ ($p=0.0181$). The following values refer to results obtained adding blocking antibodies 6 and 9 hours after Dox treatment and hAFS-CM incubation, respectively: hAFS-CM_{Hypo} + Dox + anti-IL-6: 41.75±1.1%, hAFS-CM_{Hypo} + Dox + anti-CXCL-1: 34.83±7.1%, hAFS-CM_{Hypo} + Dox + anti-IL-6 + anti-CXCL-1: 41.75±5.1%; *** $p<0.001$ ($p=0.0006$).

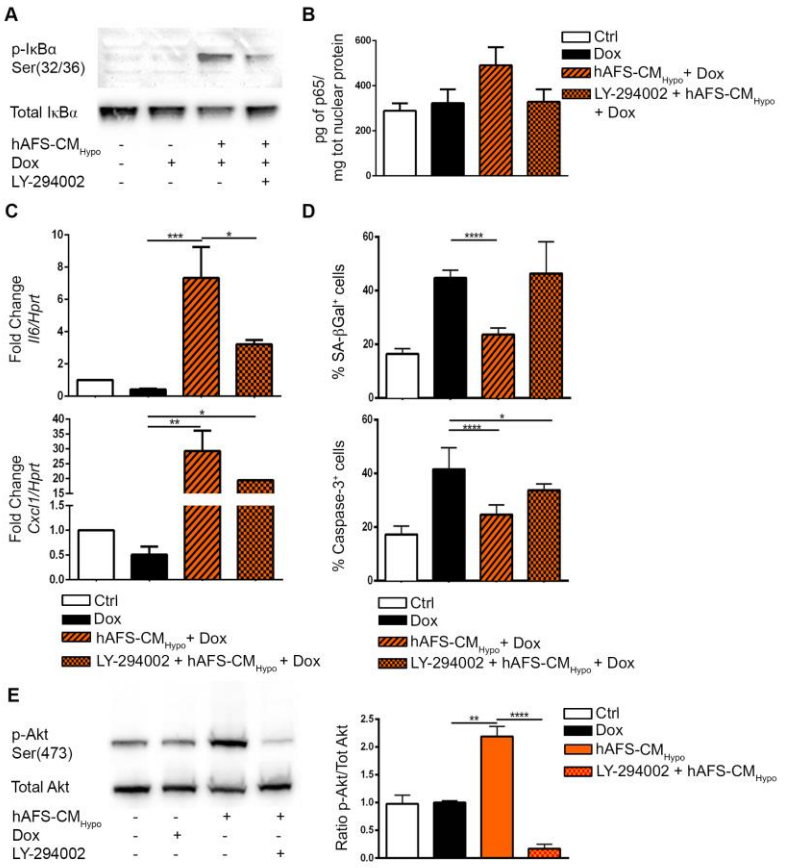

Figure 5 A) Western blot analysis for the expression of phosphorylated IκBα (Ser$^{32/36}$ p-IκBα, 40kDa) in untreated mNVCM or mNVCM treated with 1μM Dox, with 40μg/ml hAFS-CM$_{Hypo}$ prior to exposure to 1μM Dox, or with 20μM LY-294002 (PI3K inhibitor) followed by 40μg/ml hAFS-CM$_{Hypo}$ and 1μM Dox. **B)** ELISA analysis for nuclear expression of the p65 subunit of the NF-kB complex in untreated mNVCM (*Ctrl*) or mNVCM treated with 1μM Dox (*Dox*), with 40μg/ml hAFS-CM$_{Hypo}$ followed by 1μM Dox (*hAFS-CM$_{Hypo}$ + Dox*), or with 40μg/ml hAFS-CM$_{Hypo}$ followed by 1μM Dox after pre-incubation with 20μM LY-294002 (*LY-294002 + hAFS-CM$_{Hypo}$ + Dox*). *Pg*: picogram; *μg*: microgram. **C)** Real time qRT-PCR showing that treatment of mNVCM with 20μM LY-294002 (*LY-294002 + hAFS-CM$_{Hypo}$ + Dox*) also

abrogated the upregulation of *Il6* and decreased that of *Cxcl1* attained by pre-incubation with 40µg/ml hAFS-CM_{Hypo} prior to exposure to 1µM Dox (*hAFS-CM_{Hypo}* + *Dox*). * p< 0.05 (p=0.0309 and p=0.0324, for *Il6* and *Cxcl1* respectively), ** p<0.01 (p=0.0015), *** p<0.001 (p=0.0006). **D**) Percentage of mNVCM expressing SA β-galactosidase (upper panel) and cleaved caspase-3 (% Caspase-3^+ cells, lower panel): untreated cells (*Ctrl*), cells exposed to 1µM Dox (*Dox*), and cells treated with µg/ml hAFS-CM_{Hypo} followed by 1µM Dox (*hAFS-CM_{Hypo}* + *Dox*) or with 40µg/ml hAFS-CM_{Hypo} followed by 1µM Dox after pre-incubation with 20µM LY-294002 (*LY-294002* + *hAFS-CM_{Hypo}* + *Dox*). Note the reversion of the cardioprotective effects of the hAFS secretome with LY-294002 (LY-294002 + hAFS-CM_{Hypo} + Dox: 46.37±6.84% of SA β-galactosidase positive cells and 33.80±0.94% of cleaved caspase-3 positive cells, values expressed as mean ± s.e.m.; * p< 0.05 (p=0.0208), **** p<0.0001. **E)** Western blot analysis (left panel) and corresponding densitometry (right panel) for phosphorylated Akt (Ser^{473} p-Akt, 60kDa) in untreated mNVCM (*Ctrl*) or mNVCM treated with 1µM Dox (*Dox*), with 40µg/ml hAFS-CM_{Hypo} (*hAFS-CM_{Hypo}*), or with 20µM LY-294002 (PI3K inhibitor) followed by 40µg/ml hAFS-CM_{Hypo} (*LY-294002* + *hAFS-CM_{Hypo}*). ** p<0.01 (p=0.0011), **** p<0.0001.

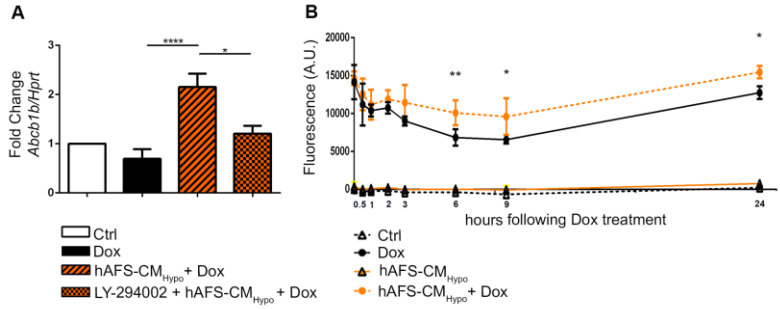

Figure 6 A) Real time qRT-PCR showing significant up-regulation of the *Abcb1b* gene in mNVCM incubated with 40µg/ml hAFS-CM_{Hypo} prior to exposure to 1µM Dox (*hAFS-CM_{Hypo}* + *Dox*) compared to untreated mNVCM (*Ctrl*) and mNVCM exposed to Dox (*Dox*); this effect was significantly reduced when cells were treated with the PI3K

inhibitor, LY-294002 (*LY-294002* + *hAFS-CM$_{Hypo}$* + *Dox)*; * p<0.05 (p=0.0232), **** p<0.0001. **B**) Quantification of Dox fluorescence in the mNVCM-conditioned medium at 0.5, 1, 2, 3, 6, 9 and 24h following incubation with 40ug/ml hAFS-CM$_{Hypo}$ and/or exposure to 1µM Dox (mean ± s.e.m.). ** p<0.01 (p=0.0058), * p<0.05 (p=0.0110 and p=0.0292 for the 9h and 24h time point respectively). *A.U.*: Arbitrary Unit.

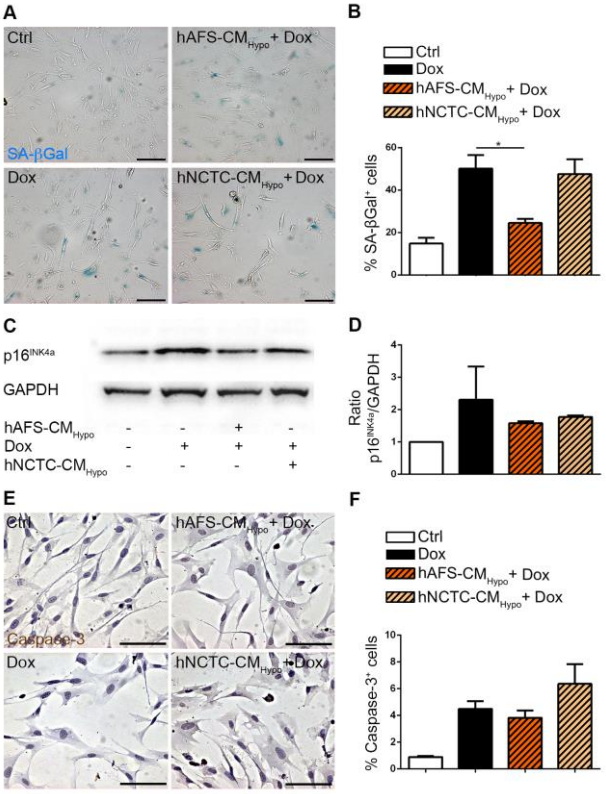

Figure 7 A) Representative images of human c-kit+ CPC (hCPC) stained for senescence associated (SA) β-galactosidase: untreated cells (*Ctrl*), cells exposed to 0.2µM Dox (*Dox*), and cells incubated with 40µg/ml of the hAFS-CM$_{Hypo}$ (*hAFS-CM$_{Hypo}$* + *Dox*) or with the hNCTC-CM$_{Hypo}$ (*hNCTC-CM$_{Normo}$* + *Dox*) prior to Dox treatment. Scale bar 100µm. **B**) Percentage of hCPC expressing SA β-galactosidase (mean

± s.e.m.). Ctrl: 14.8±2.7%, Dox: 50.1±6.4%, hAFS-CM_{Hypo} + Dox: 24.6±1.9%, and hNCTC-CM_{Hypo} + Dox: 47.5±7.0%; *p< 0.05 (p=0.0285). **C**) Representative western blot for the expression of the senescence marker $p16^{INK4a}$ (17kDa; housekeeping GAPDH, 37kDa) after exposure to 0.2µM Dox with or without pre-incubation with 40µg/ml of the hAFS-CM_{Hypo} or with hNCTC-$CM_{Hypo.}$ **D**) Densitometry of the western blot for $p16^{INK4a}$ with same conditions as in (c). **E**) Representative images of hCPC stained for cleaved-caspase-3 (Caspase-3): untreated cells (*Ctrl*), cells exposed to 1µM Dox (*Dox*), and cells incubated with 40µg/ml of the hAFS-CM_{Hypo} (*hAFS-CM_{Hypo}* + *Dox*) or with the hNCTC-CM_{Hypo} (*hNCTC-CM_{Normo}* + *Dox*) prior to Dox treatment. Scale bar 100µm. **F**) Percentage of hCPC expressing cleaved caspase-3 (% Caspase-3^{+} cells, mean ± s.e.m.). Ctrl: 0.90±0.1%, Dox: 4.5±0.6%, hAFS-CM_{Hypo} + Dox: 3.8±0.5%, and hNCTC-CM_{Hypo} + Dox: 6.4±1.5%.

ii) FIRST CHARACTERISATION OF hAFS-EXTRACELLULAR VESICLES AS CARRIER OF PARACRINE EFFECTS.

Given the encouraging results obtained on the hAFS-CM cardioprotective and stimulatory potential, I moved forward to determine whether the extracellular vesicle (EV) contained in the hAFS secretome could play a pivotal role as pro-active mediators of specific paracrine effects. Thus, in order to answer this question I've been working on the comprehensive description and characterisation of the hAFS-EV, which has been an unexplored field within the hAFS biology so far.

hAFS secreted EV ranged from 50 up to 1000nm in size. *In vitro* analysis defined their role as biological mediators of regenerative, paracrine effects while their modulatory role in decreasing skeletal muscle inflammation *in vivo* was shown for the first time. Hypoxic preconditioning significantly induced the enrichment of exosomes endowed with regenerative microRNAs within the hAFS-EV. The results produced have been published in Stem Cell Translational Medicine (first authorship). Pictures from this work have also been selected for the front cover of the May issue. Please refer to: http://stemcellsjournals.onlinelibrary.wiley.com/hub/issue/10.1002/sct3.2017.6.issue-5/

Part of the *in vivo* experiments of this study on the skeletal muscle atrophy mouse model (HSA-Cre, $Smn^{F7/F7}$ mice), have been performed in collaboration with Dr. Martina Piccoli and Dr. Michela Pozzobon from the Stem Cells and Regenerative Medicine Laboratory, Fondazione Istituto di Ricerca Pediatrica Città della Speranza, Department of Women and Children Health, University of Padova, Padova, Italy. Some other *in vitro* experiments have been done in collaboration with PhD students and colleagues from the Regenerative Medicine Laboratory (i.e. Dr. Andrea Papit and Miss Elisa Principi).

Methods

Cell Culture

hAFS were cultures as described in the previous section. HDF (Gibco-Thermo Fisher Scientific, Waltham, Massachusetts) were kindly provided by Dr. Renata Bocciardi and Prof. Roberto Ravazzolo (IRCCS Giannina Gaslini, Genova, Italy) and cultured in RPMI medium with 16% FBS, 1% L-glutamine, and 1% penicillin/streptomycin (all EuroClone, Milano, Italy); C2C12 cells were purchased from Interlab Cell Line Collection (ICLC, Genova, Italy) and cultured in low glucose Dulbecco's Modified Essential Medium (DMEM) medium with 10% FBS, 1% L-glutamine and 1% penicillin/streptomycin (all EuroClone, Milano, Italy). hPBMC were isolated from buffy coat samples of leftover heparinized whole blood supplied by the Blood Transfusion Center IRCCS AOU San Martino -IST, Genova, following written informed consent, according to Helsinki declaration and in compliance with authorization from the local ethical committee. hPBMCs were isolated by Ficoll (Cedarlane, Burlington, Canada) gradient centrifugation. Cells were seeded at 10^5 cells/well density in 96 well-culture dish (Costar, Washington, D.C) in RPMI medium (Gibco-Thermo Fisher Scientific, Waltham, Massachusetts) with 10% FBS (Sigma-Aldrich, St. Louis, Missouri), 1% penicillin/streptomycin and 1% L-Glutamine (both Euroclone, Milano, Italy), as previously described [1].

hAFS Preconditioning

hAFS were cultured for 24 hours in serum-free (SF) medium (Minimum Essential Medium Eagle *alpha*, with 1% L-glutamine and 1% penicillin/streptomycin) under normoxic (20% O_2 and 5% CO_2 at 37°C) or hypoxic (1% O_2 and 5% CO_2 at 37°C in a hypoxic incubator, Eppendorf, Hamburg, Germany) conditions. The hAFS-conditioned medium (hAFS-CM) was collected as described in the previous section and processed for hAFS-EV isolation.

Isolation and Characterization of hAFS-EV

hAFS-EV were isolated by ultracentrifugation [5] from hAFS-CM obtained from cells cultured for 24h under SF normoxic (hAFS-CM_{Normo}) or hypoxic (hAFS-CM_{Hypo}) conditions.

hAFS-CM was collected and centrifuged at +4°C at 3,000*g* for 20' and 10,000*g* for 15' to remove cell debris. hAFS-CM was then processed by ultracentrifugation in a Optima L-90K (Beckmann Coulter, Brea, California) at 100,000*g* for 90'. The pellets containing hAFS-EV (hAFS-EV_{Normo} or hAFS-EV_{Hypo}, respectively) were washed in 1X PBS by a final step at 100,000*g* for 70' and then resuspended in PBS 1X. Samples were then stored at – 80°C until use. At least 3 different batches of hAFS-EV_{Normo} and hAFS-EV_{Hypo} were used for every experiment.

hAFS and hAFS-EV were analyzed by transmission electron microscopy (TEM) under a Philips EM 208 microscope with a digital camera (University Centre for Electron Microscopy, CUME, Perugia, Italy). hAFS were fixed with 2.5% glutaraldehyde (Sigma-Aldrich, St. Louis, Missouri), in 0.1 M pH 7.3 phosphate buffer (PB), for 1h. The pellet was post-fixed in 2% osmium tetroxide, dehydrated in a graded series of ethanol, pre-infiltrated in propylene oxide and embedded in Epoxy resin (Epon 812). 90 nm-thick sections were mounted on 200-mesh copper grids, stained with uranyl acetate and lead citrate. For hAFS-EV analysis, a formvar coated copper grid (Electron Microscopy Sciences, Hatfield, Pennsylvania) was placed on the top of a drop of EV suspension. Grids were fixed for 10' with 2.5% glutaraldehyde in PB and contrasted with 2% uranyl acetate and air-dried. hAFS-EV were also characterized by nanoparticle tracking technology using a NanoSight LM10 (Malvern Instruments, Malvern, UK) to analyze particles released by 10^6 cells. The concentration of membrane-bound protein on the surface of freshly isolated, intact hAFS-EV was measured using BCA assay (Gibco-Thermo Fisher Scientific, Waltham,

Massachusetts). WB on hAFS and hAFS-EV was performed for the expression of TSG101 (Abcam, Cambridge, UK), ALIX (Santa Cruz Biotechnology, Dallas, Texas) GRP94 (Abcam, Cambridge, UK) and human βACTIN (Santa Cruz Biotechnlology, Dallas, Texas) as previously described. hAFS-EV were also evaluated by FACS for the presence on their surface of the mesenchymal stem cell antigen CD105 (eBioscience, San Diego, California), the conventional exosomal markers CD81, CD9, CD63, Annexin V (AnnV) and the co-stimulatory molecules CD80 and CD86 (all BD Bioscience, Franklin Lake, New Jersey).

Uptake Analysis of hAFS-EV by Target Cells and Functional In Vitro Studies

hAFS-EV were labeled with the PKH67 Green Fluorescent Cell Linker (Sigma-Aldrich, St. Louis, Missouri), following manufacturer's instructions. 1µg/10^4 cells (for HDF and C2C12 cells) and 1µg/10^5 cells (for hPBMC) $PKH67^+$ hAFS-EV_{Normo} and $PKH67^+$ hAFS-EV_{Hypo} were incubated for 3h with the target cells in SF medium and analyzed on a CyAn ADP analyzer. Data was acquired with Summit 4.3 software and analysed by FlowJo software. To assess the biological effects driven by hAFS-EV on HDF and C2C12 cells, three different concentrations (1µg-, 2µg- and 4µg/10^4 cells) of either hAFS-EV_{Normo} or hAFS-EV_{Hypo} were used. To analyze cell proliferation, HDF were primed with hAFS-EV and then analyzed by BrdU colorimetric assay (Roche, Basel, Switzerland) according to the manufacturer's instructions. To define the anti-apoptotic effect of hAFS-EV, C2C12 were incubated with hAFS-EV and exposed to oxidative damage. Cell viability was measured by MTT assay using a 150µg/ml MTT solution (Sigma-Aldrich, St. Louis, Missouri).

Data were acquired on a VersaMax (GE Intelligent Platforms, Boston, Massachusetts) plate reader.

The immunomodulatory potential of hAFS-EV was evaluated on hPBMC stimulated with 5µg/ml phytohemagglutinin (PHA, Sigma-Aldrich, St. Louis, Missouri) and 5µg/ml pokeweed mitogen (PWM, Sigma-Aldrich, St. Louis, Missouri) for 1h, to induce T- and B-lymphocytes expansion, followed by incubation with 1µg/10^5 cells of hAFS-EV_{Normo} or hAFS-EV_{Hypo} for 5 days.
Regulatory T cells (T reg) activation was evaluated by flow cytometry using FITC- or PE-conjugated antibodies against human CD4 and CD25 (BD Biosciences, Franklin Lake, New Jersey). To evaluate B-cell maturation, cells were stained against PE-conjugated anti-human CD19 and APC-conjugated anti-human CD27 (BD Biosciences, Franklin Lake, New Jersey). Cells were acquired by a CyAn ADP analyzer with Summit 4.3 software and analyzed using FlowJo software.

In Vivo Angiogenic Matrigel Plug Assay
Adult C57Bl/6J male mice were subcutaneously injected with ice-cold un-polymerized Matrigel (Corning, Corning, New York) solution containing 10µg of either hAFS-EV_{Normo} or hAFS-EV_{Hypo}. All the animal work was performed in compliance with ethical national and international (EU Directive 2010/63/EU) standards and according to institutional guidelines from the Animal Facility of IRCCS AOU San Martino-IST, Genova. Mice were sacrificed 3 weeks after injection and Matrigel plugs were collected for histological evaluation by hematoxylin and eosin staining and immunohistochemistry for CD31 expression. The blood hemoglobin content of each plug was evaluated using the Drabkin's Reagent (Sigma-Aldrich, St. Louis, Missouri). Samples were minced, dispersed in water to lyse erythrocytes and centrifuged, according to the manufacturer's instructions. Recovered supernatants were analyzed on a Biophotometer Plus (Eppendorf, Hamburg, Germany) reader at 540 nm wavelength.

Real time qRT-PCR was also performed for the expression of *VegfA* (Forward: CAAACCTCACCAAAGCCAGC; Reverse: GCGCTTTCGTTTTTGACCCT), *Pecam1* (Forward: GGAAGTGTCCTCCCTTGAGC; Reverse: GCCTTCCGTTCTTAGGGTCG), *Cdh5 (VE-Cadherin)* (Forward: CCTGAGGCAATCAACTGTGC; Reverse: GGAGGAAGCTGATCTTGTCCG) and *beta-2-microglobulin (B2M)* (Forward: GCTTCAGTCGTCAGCATGG; Reverse: CAGTTCAGTATGTTCGGCTTCC) genes.

Mouse Model of Muscular Atrophy

Twelve week-old *HSA-Cre, Smn$^{F7/F7}$* mice (Piccoli et al., 2012) (n=8 per time point analysis) were randomized to receive either control (PBS) or hAFS-EV, as represented in Fig. 11A. 1µg of hAFS-EV$_{Normo}$ and hAFS-EV$_{Hypo}$ was injected in the right and left *Tibialis Anterior* (TA) muscles, respectively. Mice were sacrificed 1 and 7 days after treatment and muscle tissue processed for immunostaining and real time qRT-PCR.

8 µm-thick cryosections of treated TA muscles fixed in 4% PFA were stained with Alexa Fluor 594-conjugated goat anti-mouse IgG antibody (A-11005, Gibco-Thermo Fisher Scientific, Waltham, Massachusetts) and anti-LAMININ (Sigma-Aldrich, St.Louis, Missuri) and anti-CD68 (ab125212 Abcam, Cambridge, UK) primary antibodies followed by anti-rabbit Alexa Fluor® 594- and anti-rat Alexa Fluor® 488-conjugated secondary antibodies. Nuclei were counterstained with DAPI (Sigma-Aldrich, St.Louis, Missuri). Images were acquired by DMI 6000B microscope with LAS AF software (Leica, Wetzlar, Germany). IgG infiltrated and central nucleated fibers were counted on 6 random pictures per sample (8 animals per time point), and data was expressed as the percentage on the total number of fibers per picture (all pictures were taken with the same magnification). The area covered by IgG infiltration in each treated muscle was also expressed in terms of percentage of mean fluorescent area using ImageJ software

(https://imagej.nih.gov/ij/) by measuring the fluorescent area of 6 random pictures in each sample and calculating the percentage over the picture area (all pictures were taken with the same magnification).
For real time qRT-PCR RNA was extracted using RNeasy Plus Mini kit (Qiagen, Hilden, Germany) and 1µg used for cDNA synthesis by iScriptTM cDNA Syntesis Kit (Bio-Rad, Hercules, California). Real-time qRT-PCR was carried out for the *Nos2* (Forward: GCAGGTCTTTGACGCTCGGA; Reverse: ATGGCCGACCTGATGTTGCC), *Arg1* (Forward: AGGGAGTCAACTCATTGGCG; Reverse: AGGTTGCCCATGCAGATTCCC), *Il-1α* (Forward: AGGGAGTCAACTCATTGGCG; Reverse: TGGCAGAACTGTAGTCTTCGT), *Il-10* (Forward: CCAGTTTTACCTGGTAGAAGTGATG; Reverse: TGTCTAGGTCCTGGAGTCCAGCAGACTC), *Il-4* (Forward: AGATGGATGTGCCAAACGTCCTCA; Reverse: AATATGCGAAGCACCTTGGAAGCC), *Il-6* (Forward: CTCTGCAAGAGACTTCCATCCAGT; Reverse: AGTAGGGAAGGCCGTGGTTGTCA), *Ptgs2* (Forward: ATGAGTACCGCAAACGCT; Reverse: TGTAGAGGGCTTTCAATTCTGC) and *beta-2-microglobulin (B2M)* (Forward: GCTTCAGTCGTCAGCATGG; Reverse: CAGTTCAGTATGTTCGGCTTCC) genes on a 7500 Fast Real-Time PCR System (Applied Biosystems, Forest City, California) using Syber Green Master Mix (Gibco-Thermo Fisher Scientific, Waltham, Massachusetts).Gene expression levels were normalized using B2M as endogenous controls by applying the 2^{-ddCt} method.
All the animal work was performed in compliance with ethical national and international (EU Directive 2010/63/EU) standards according to institutional guidelines from the University of Padova Animal Care and Use Committee (CEASA, protocol 67/2011).

Small Non-Coding RNA Profiling of hAFS-EV

Total hAFS-EV RNA was extracted using Qiazol Lysis Reagent (Qiagen, Hilden, Germany). Analysis of the small non-coding RNA content was performed on a 2100 Bioanalyzer using the Small RNA Kit and the Agilent 2100 expert software (all from Agilent Technologies, Santa Clara, California).

Real Time qRT-PCR Analysis of the hAFS-EV microRNA Content.

Total RNA from hAFS and hAFS-EV was extracted using miRNAeasy Mini Kit following the manufacturer's instructions. miScript II RT Kit was used for cDNA synthesis and selected miScript Primer Assay and miScript SYBR® Green PCR Kits were used for quantitative RT-PCR analysis on a 7500 Fast Real-Time PCR System (Gibco-Thermo Fisher Scientific, Waltham, Massachusetts). The following human miRNAs (all from Qiagen, Hilden, Germany) were evaluated: miR-223, miR-146a, miR-let7c, miR-21, miR-126, miR-146b, miR-199a-3p and miR-210. Gene expression levels were normalized to the corresponding miRNA expression in hAFS using the 2^{-ddCt} method.

Analysis of Direct Transfer of Exosomal RNA from the hAFS-EV into Target Cells

RNA content in hAFS-EV was labeled using the SYTO® RNASelect™ Green Fluorescent Nucleic Acid Stain (Gibco-Thermo Fisher Scientific, Waltham, Massachusetts) following the manufacturer's instructions. 1 µg of SYTO®+ hAFS-EV_{Normo} or SYTO®RNASelect+ hAFS-EV_{Hypo} was incubated for 3h with 10^4 HDF or C2C12 cells in SF medium and analyzed after 1h by FACS.

Real time qRT-PCR Evaluation of Specific miRNA Enrichment and their Target Genes in the Target Cells

HDF and C2C12 cells were incubated with 4µg/10^4 cells of either hAFS-EV_{Normo} or hAFS-EV_{Hypo} in SF medium, following the same

protocol used for cell proliferation and viability assays. After 1 hour incubation in complete medium, total RNA from HDF and C2C12 cells was isolated using Qiazol Lysis Reagent (Qiagen, Hilden, Germany). Analysis of selected miRNAs was performed as described above; the miRNA target genes *MNT* (Forward: CAACGTGGATGACAAGAAGACG; Reverse: TCAGGGACTGGATGTACCGC) (HDF) and *Casp8ap2* (Forward: CATGGAGAGCTCATGTGCA; Reverse: TGGGAACTGGTTTTTCATTTTCCT) (C2C12) were analyzed by real time qRT-PCR as mentioned before. Gene expression levels were normalized to *GAPDH* (Forward: ATGGCACCGTCAAGGCTGAGAA Reverse: CCAGCATCGCCCCACTTGATT) (HDF) and *beta-2-microglobulin (B2M)* (Forward: GCTTCAGTCGTCAGCATGG; Reverse: CAGTTCAGTATGTTCGGCTTCC) (C2C12) as endogenous controls using the 2^{-ddCt} method.

Proteomic Comparative Profiling of hAFS-EV

hAFS-EV_{Normo} and hAFS-EV_{Hypo} protein content was isotopically labeled using the TMT Duplex kit protocol (Gibco-Thermo Fisher Scientific, Waltham, Massachusetts (Rauniyar et al., 2013)). Samples were dried under nitrogen steam then re-dissolved with 50µl of 3% acetonitrile with 0.1% formic acid (Qiagen, Hilden, Germany) for further LC-MS/MS analysis. The peptide mixture was analyzed using a Synapt G2 QToF instrument equipped with nanoACQUITY liquid chromatography system and a nanoSpray ion source (Waters Inc., Milford, Massachusetts). Raw data processing was done using PLGS software (Waters Inc., Milford, Massachusetts). Protein identification and quantification was performed by interrogating the SwissProt database using MASCOT Server software (Matrixscience (Perkins et al., 1999)). Enrichment analysis was performed with FunRich 3.0 (http://www.funrich.org/) on Biological Pathway using FunRich as reference database.

Statistical Analysis

Results are presented as mean ± s.e.m. (standard error of mean) of at least three (n=3) independent experiments. Analyses were performed using GraphPad Prism Version 6.0a (GraphPad Software); p values < 0.05 were considered statistically significant. Furthermore
statistical analysis was performed by unpaired t-test (for analysis comparing hAFS-EV in control condition versus preconditioning), by hypergeometric test followed by Bonferroni correction (for proteomic data analyzed by FunRich 3.0), and by one-way ANOVA followed by post-hoc Tukey's multiple comparisons test (for all remaining data).

Results

hAFS Secrete EV in Their Conditioned Medium

TEM analysis revealed that hAFS can actively secrete EV ranging in size from 50 to 1000 nm (Fig.8A). We further investigated hAFS-EV secretion for 24h under SF conditions to avoid any contamination by FBS-EV (1% O_2 hypoxic versus 20% O_2 normoxic) (Lötvall et al., 2014). The hAFS-CM ultracentrifuged pellet contained hAFS-EV between 50 and 200 nm (Fig.8B); furthermore the vesicle electron density and the absence of nuclear or cytoplasmic residues in both the EV released in situ by the cells (Fig.8A), and the hAFS-EV isolated by ultracentrifugation (Fig.8B), demonstrated that apoptotic bodies were not significantly present. Nanoparticle tracking (Fig.8C) showed a reasonably high number of particle in both hAFS-EV_{Normo} and hAFS-EV_{Hypo} (283.33 ± 64.75*10^6 particle/ml and 283.83 ± 79.85*10^6 particle/ml, respectively, p=0.65); both hAFS-EV_{Normo} and hAFS-EV_{Hypo} particle dimension showed average size of 180nm. BCA assay was performed to evaluate the protein content on the EV surface. Hypoxic preconditioning led to a significant enrichment of proteins on the hAFS-EV surface (4.19 ± 0.43 µg/10^6 cells) with almost 2-fold increase compared to normoxic cells (2.35±0.26 µg/10^6 cells, Fig.8D, ***p<0.001). WB confirmed the expression of the microvesicle and exosome canonical markers TSG101 and ALIX (Lötvall et al., 2014) on the hAFS-EV (Fig.8E). Notably, hAFS-EV did not express GRP94, indicating no contamination from the endoplasmic reticulum associated with apoptotic blebs (Caradec et al., 2014) (Fig.8E). FACS analysis revealed a significant exosomal subpopulation expressing the markers CD81, CD9, AnnV, and CD63 within the hAFS-EV (Fig. 8F and 9B). In particular, hypoxic preconditioning led to a significant enrichment of $CD81^+$, $CD9^+$ and $CD63^+$ exosomes in hAFS-EV_{Hypo} compared to the hAFS-EV_{Normo}, (1.5-, 1.3-, and 2.4-fold, *p<0.05 and **p<0.01, respectively), despite similar total secreted particle content. We also

labeled hAFS-EV using the CellTrace Far Red DDAO-SE kit to distinguish intact vesicles from cell debris, as recently described by others (Grisendi et al., 2015). CellTrace-positive hAFS-EV were further analyzed for the expression of the mesenchymal stem cell antigen CD105, showing that about 60% of them maintained this marker (Pozzobon et al., 2013) (61.3±2.3% and 59.4±12.3% in hAFS-EV_{Normo} and hAFS-EV_{Hypo}, respectively, p=0.8985, Fig. 9A). hAFS-EV did not express co-stimulatory molecules CD80 and CD86 (Judge et al., 1999), suggesting immune tolerance (Fig. 9B).

Analysis of hAFS-EV Biological Effects on Target Cells.

The role of both hAFS-EV_{Hypo} and hAFS-EV_{Normo} as biological mediators of paracrine effects was assessed on different target cells. Analyses on HDF, C2C12, and hPBMC incubated for 3h with either $PKH67^+$ hAFS-EV_{Normo} or hAFS-EV_{Hypo} showed similar internalization efficiency (65.4±4.4% and 63.5±5.6% $PKH67^+$HDF, p=0.94; 75.9±3.4% and 83.7±1.1% $PKH67^+$ C2C12, p=0.11, and 9.3±2.6% and 12.5±2.5% $PKH67^+$ hPBMC, p=0.54, respectively Fig.10A). Following 4h incubation with 1-2-4 μg/10^4 cells hAFS-EV_{Normo}, proliferation of BrDU-labeled HDF showed a dose-dependent, 2- to almost 3.5-fold increase, compared to untreated cells (****p<0.0001). hAFS-EV_{Hypo} treatment further stimulated HDF proliferation by 2.5- to 4.3-fold change compared to untreated cells (****p<0.0001), and with higher dose-effect response compared to hAFS-EV_{Nomro} ($^{\#\#}$p<0.01; $^{\#}$p<0.5 and $^{\#\#\#}$p<0.001, Fig.10B). C2C12 mouse myoblast cell line underwent oxidative stress by treatment with 1mM H_2O_2 for 2h in the presence of hAFS-EV. MTT analysis showed that cells exposed to H_2O_2 had 65% lower cell viability (****p<0.0001). Following 3h of pre-treatment with hAFS-EV, C2C12 cells significantly recovered from injury, with improved cell viability and increased proliferation (Fig.10C). hAFS-EV_{Normo} mediated remarkable dose-dependent anti-apoptotic effects enhancing cell survival up to 2- and 6-fold compared to control

cells and to cells not receiving any treatment before undergoing oxidative stress, respectively (****p<0.0001). hAFS-EV_{Hypo} exerted an even more effective cytoprotective role by increasing cell viability in a dose-dependent manner up to 3- and 8-fold (Fig.10C, ****p<0.0001). Moreover, the pro-survival influence exerted by hAFS-EV_{Hypo} was significantly more effective than that observed with hAFS-EV_{Normo} (####p<0.0001).

To understand the immunomodulatory potential of hAFS-EV, hPBMC were stimulated by PHA (Mirebella et al., 2011) and PWM (Bekeredjian-Ding et al., 2012) in order to activate T- and B-lymphocytes, followed by incubation with either hAFS-EV_{Normo} or hAFS-EV_{Hypo}. The target cell response was evaluated by analyzing cell proliferation and selective maturation into T reg and memory B cells by the expression of CD4/CD25 (high) (Mareschi et al., 2016) and CD19/CD27 (de Masson et al., 2014), respectively. hAFS-EV were internalized by hPBMC with lower efficiency compared to other target cells used in this study (Fig.10A). Both hAFS-EV_{Normo} and hAFS-EV_{Hypo} did not significantly affect hPBMC proliferation in control conditions (naïve hPBMC, p=0.6417), or after stimulation (PHA and PWM, p=0.3632 and p=0.5120, Fig. 10D). hAFS-EV did not influence the polarization of T reg (data not shown). However, both hAFS-EV_{Normo} and hAFS-EV_{Hypo} exerted significant modulatory effect by reducing the maturation of $CD27^{+}CD19^{+}$ memory B cell in response to PWM (*p<0.05, Fig.10E).

A mouse Matrigel plug assay was used to determine the pro-angiogenic effect of hAFS-EV_{Normo} and hAFS-EV_{Hypo} *in vivo*. Histological analysis and CD31 immunostaining revealed that in the hAFS-EV-loaded Matrigel plugs infiltrating host cells were detectable (Fig.11A and 11D). Real time qRT-PCR analysis suggested a certain degree of angiogenic potential of hAFS-EV compared to vehicle-loaded (PBS) control plugs, as shown by up-regulation of the vascular marker *Cdh5*, *Pecam1* and *VegfA* on the cells colonizing the plug (Fig.11C), although not in a

significant manner. Nevertheless, the evaluation of hemoglobin content showed a 2.6-fold increase in the hAFS-EV_{Hypo}-treated plugs (33.73 ± 7.97 μg/μl) compared to the control (13.06 ± 1.04 μg/μl, *p<0.05) and the hAFS-EV_{Normo} ones (14.63 ± 1.79 μg/μl, Fig.11B). Hence, hAFS-EV_{Hypo} were able to, at least to some extent, attract and stimulate host endothelial cells.

Regenerative Paracrine Potential of hAFS-EV in a Mouse Model of Skeletal Muscle Atrophy.

TA muscle fibers of *HSA-Cre, $Smn^{F7/F7}$* mice treated with hAFS-EV_{Normo} and hAFS-EV_{Hypo} showed remarkable decrease of immunoglobulin (IgG) and $CD68^+$ cell infiltration compared to control animals, 1 and 7 days after injection (Fig.12B). This effect correlated with a drastic reduction of damaged infiltrated fibers (approximately 80% and 89% in the first 24 hours after hAFS-EV_{Normo} and hAFS-EV_{Hypo} administration, *p<0.05, Fig.12C). In mice treated with hAFS-EV_{Hypo}, this effect was maintained up to 7 days after injection by a 79% decrease of the IgG-damaged fibers (*p<0.05, Fig.12C). This trend was further confirmed by the evaluation of the percentage of the infiltrated fiber mean fluorescent area. Indeed, hAFS-EV_{Normo} and hAFS-EV_{Hypo} treatments were equally effective in reducing the extension of the IgG-infiltrated area within the muscle fibers by 91.5% and 95% respectively (**p<0.01) at day 1 post injection, and by 80.25% and 91% at day 7 post injection (**p<0.01, Fig.12C). Compared to controls, the number of central nucleated TA fibers was significantly reduced by 72% 1 day after receiving intramuscular injection of hAFS-EV_{Hypo} (*p<0.05, Fig.12D). This effect was no longer observed after 7 days, although hAFS-EV_{Hypo} mantained a significant lower amount of central nucleated fibers compared to hAFS-EV_{Normo} (71% less, #p<0.05, Fig.12D). Real time qRT-PCR of the ratio between the inflammatory markers *Nos2* and *Arg1* (Heredia et al., 2013) showed a substantial decrease in the activation of pro-inflammatory M1 macrophages (ratio *Nos2/Arg1*>1),

in favor of pro-resolving M2 phenotype (ratio *Nos2/Arg1*<1). After 1 day, both hAFS-EV_{Normo} and hAFS-EV_{Hypo} induced macrophage polarization by decreasing the *Nos2/Arg1* ratio by about 4-fold compared to untreated animals (*p<0.05, Fig.12E). This effect began to decrease 7 days after hAFS-EV injection. Pro-inflammatory cytokines followed a similar pattern of expression. Following hAFS-EV injection, the expression of the pro-inflammatory *Il-1α* (Shamim et al., 2000) decreased by almost 50% at 1 day (***p<0.001) and 7 days (*p<0.05) after treatment, with similar effects between hAFS-EV_{Normo} and hAFS-EV_{Hypo} (Fig.12F). Likewise, *Il-6* (Fish et al., 2008) levels dropped significantly by 87% and 65% (***p<0.001 and **p<0.01, respectively) within the first 24h after hAFS-EV administration. hAFS-EV_{Hypo} was more effective (*p<0.05) as maintaining this modulation for up to 7 days after treatment (Fig.13A). Pro-inflammatory *Il-4* (Deyhle et al., 2016) expression decreased by 37% 1 day after hAFS-EV_{Hypo} treatment (*p<0.05). At the same time, within the first 24h after treatment, there was a significant upregulation of the pro-resolving *Il-10*, typically released by M2 macrophages (Tidball and Villalta, 2010), (1.6-fold, **p<0.01 and 2.8-fold, ****p<0.0001, respectively) with hypoxic EV exerting a stronger effect compared to normoxic ones (1.8-fold increase, ****p<0.0001, Fig.12F). This trend was maintained also after a few days, although without reaching statistical significance. hAFS-EV were also able to modulate the expression of the *Pstg2* gene, encoding for the COX2 enzyme, in host cells. hAFS-EV_{Normo} and the hAFS-EV_{Hypo} induced a significant down regulation of *Pstg2* in mice 1 day (67% and 56%, respectively, **p<0.01 and *p<0.05), and 7 days (86% and 87% respectively, ****p<0.0001, Fig.13A) after treatment.

MicroRNA Profiling of the hAFS-EV.

hAFS-EV_{Normo} and hAFS-EV_{Hypo} showed to contain small non-coding RNAs and miRNAs (20 to 40 nucleotides, Fig.14A). In particular, hAFS-EV_{Hypo} showed significant enrichment over the hAFS-EV_{Normo} of the

following miRNAs (Fig. 14B): miR-223 (***p<0.001, 1.3-fold), miR-146a (**p<0.01, 1.6-fold), miR-let7c (***p<0.001, 2-fold), miR-21 (***p<0.001, 2-fold), miR-126 (****p<0.0001, 2.5-fold), miR-146b (****p<0.0001, almost 3-fold), miR-199a-3p (**p<0.01, almost 3-fold), miR-210 (****p<0.0001, 3.6-fold).

Mechanism Insights of the hAFS-EV Regenerative Potential via Direct Transfer of Exosomal miRNAs into the Target Cells

To assess whether direct transfer of their nucleic acid cargo could drive the hAFS-EV paracrine effect, we analyzed the uptake of fluorescently labeled exosomal RNA by target cells *in vitro*. Following incubation with SYTO®RNASelect^{+} hAFS-EV_{Normo} and SYTO®RNASelect^{+} hAFS-EV_{Hypo}, we observed acquisition of fluorescence by 88.67±4.21% and 86.73±4.46% of HDF cells (****p<0.0001 compared to untreated cells), and by 91.5±3.38% and 85.97±5.51% of C2C12 cells (****p<0.0001 compared to untreated ones), respectively (Fig.14C). This result indicates that hAFS-EV can actively release their RNA content into the target cells in the very short time. Real time qRT-PCR analysis on the responder HDF and C2C12 cells revealed significant enrichment of some of the 8 regenerative miRNAs carried by hAFS-EV (Fig.14D-E). Following incubation with hAFS-EV_{Hypo}, HDF cells showed a significant enrichment of 4 out of the 8 miRNAs analyzed (Fig. 14D): miR-146a (3.5-fold, **p<0.01), miR-126 (4.6-fold, *p<0.05), miR-199a-3p (5.2-fold, *p<0.05) and miR-210 (5.1-fold, *p<0.05); all remaining miRNAs (miR-223, miR-let7c, miR-21, miR-146b) were enhanced in the cells primed with the hAFS-EV, although this increase was not significant (Fig.15A). C2C12 cells primed with the hAFS-EV_{Hypo} and exposed to H_2O_2, when compared to untreated cells, with or without oxidative damage, revealed higher amount of miR-let7c (3.4- and 2.0-fold, **p<0.01 and *p<0.05, respectively), miR-21 (4.7- and 6.0-fold, **p<0.01), miR-146b (2.6- and 2.9-fold, *p<0.05), miR-199a-3p, (2.7- and 3.0-fold, *p<0.05 and **p<0.01) and miR-210 (7.0- and 3.5-fold,

**p<0.01 and *p<0.05 respectively) (Fig. 14E). Similar to HDF, all other miRNAs (miR-223, miR-146a, miR-126) were enhanced in the cells primed with the hAFS-EV, although this increase was not significant (Fig.15B). Since miR-210 was one of the mostly enriched miRNA following hAFS-EV_{Hypo} uptake, we evaluated whether its target genes were modulated. Expression of MNT, an antagonist of the cell-cycle promoter c-MYC (Zhang et al., 2009), and *Casp8ap2*, a pro-apoptotic gene (Won Kim et al., 2009), was analyzed in HDF and C2C12 cells, respectively, following treatment with hAFS-EV_{Hypo}. While HDF cells reduced MNT expression by almost 60%, this decrease was not statistically significant. On the other hand, C2C12 cells were able to significantly decrease *Casp8ap2* expression of about 83% (*p<0.05 Fig.15C), altogether supporting a substantial, functional role of the transferred miR-210 in mediating anti-apoptotic effect.

Proteomic Profiling of the hAFS-EV.

The proteomic characterization of both hAFS-EV_{Normo} and hAFS-EV_{Hypo} allowed the identification of 498 proteins, some of which (74 out of 100) among those most expressed by exosomes, according to ExoCarta (http://www.exocarta.org, a dedicated database of exosomal proteins, RNA and lipids (Keerthikumar et al., 2015)). 84 proteins out of the total 498 were enriched within the hAFS-EV_{Hypo} compared to the hAFS-EV_{Normo} and significantly involved in biological pathways (****p<0.0001, Fig.16A) including metabolism of protein and RNA, including mRNA, gene expression and translation, metabolism and peptide chain elongation.

Figures

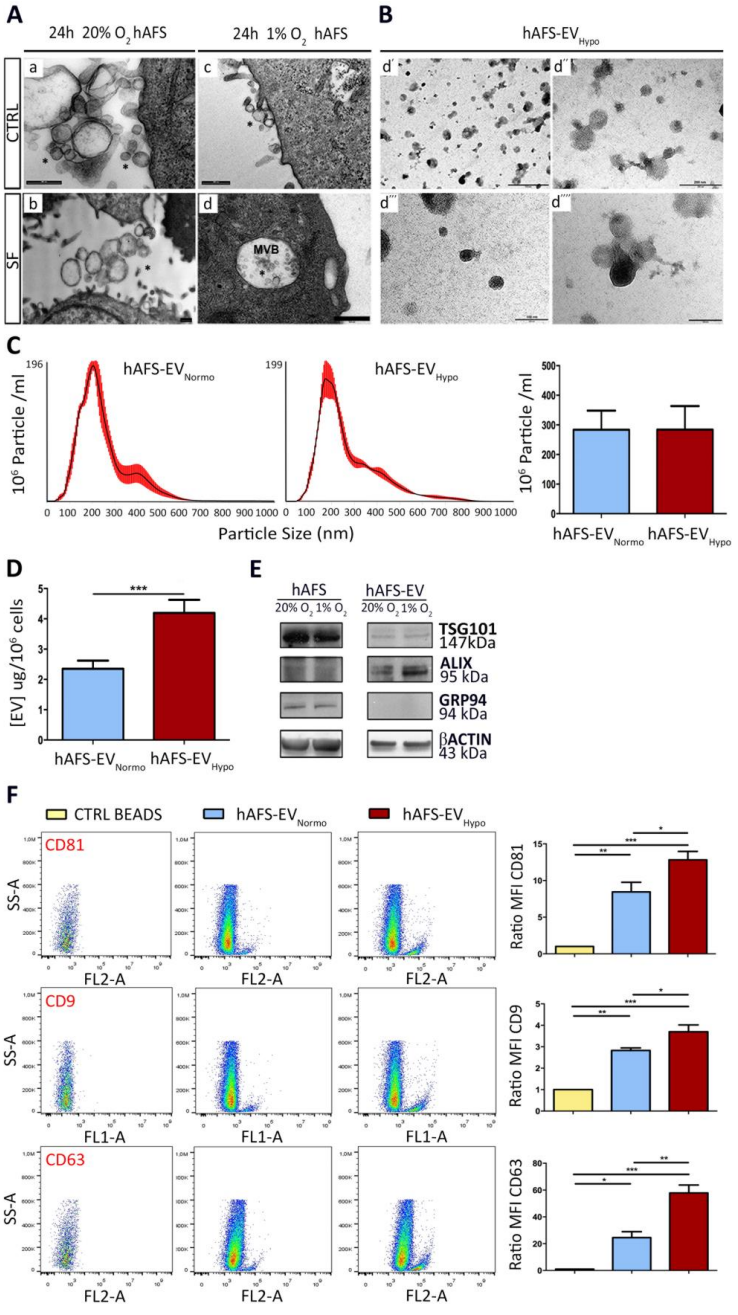
A
24h 20% O2 hAFS
24h 1% O2 hAFS
B
hAFS-EVHypo
CTRL
SF
a
b
c
d
MVB
d'
d''
d'''
d''''
C
hAFS-EVNormo
hAFS-EVHypo
10^6 Particle /ml
Particle Size (nm)
D
[EV] ug/10^6 cells
***
E
hAFS
hAFS-EV
20% O2 1% O2
TSG101 147kDa
ALIX 95 kDa
GRP94 94 kDa
βACTIN 43 kDa
F
CTRL BEADS
CD81
CD9
CD63
SS-A
FL2-A
FL1-A
Ratio MFI CD81
Ratio MFI CD9
Ratio MFI CD63

Figure 8 A) TEM analysis of hAFS under 24h 20% O_2 CTRL (a) or 20% O_2 SF conditions (b) and 1% O_2 CTRL (c) or 1% O_2 SF (d) conditions; scale bars 500nm. **B)** TEM Analysis of 1% O_2 hAFS-EV (hAFS-EV_{Hypo}); scale bar 500nm in (d'); 200nm in (d'') and 100nm (d''' and d''''). **C)** Nanosight analysis measuring the amount of particles within hAFS-EV_{Normo} (283.3 ± 64.8*10^6 particle/ml) and hAFS-EV_{Hypo} (283.8 ± 79.9*10^6 particle/ml) released by 10^6 cells (right panel); values are expressed as mean ± s.e.m. Representative images of the graphical output are reported in the left panel. **D)** BCA assay of the protein concentration of hAFS-EV_{Hypo} (4.2 ± 0.4 μg/10^6 cells, ***p<0.001, p=0.0005) over hAFS-EV_{Normo} (2.4 ± 0.3 μg/10^6 cells) released by 10^6 cells. **E)** Western Blot analysis of TSG101, ALIX, GRP94 and βACTIN by hAFS and hAFS-EV, both under 20% O_2 and 1% O_2 SF conditions. **F)** FACS Analysis of hAFS-EV_{Normo} and hAFS-EV_{Hypo} bound to the ExoCap™ Capture Beads compared to control empty beads (CTRL BEADS) for the exosomal markers CD81 (*p<0.05, p=0.049; **p<0.01, p= 0.005, ***p<0.001, p=0.0004), CD9 (*p<0.05, p=0.047; **p<0.01, p= 0.0015, ***p<0.001, p=0.0002) and CD63 (*p<0.05, p=0.02; **p<0.01, p= 0.004, ***p<0.001, p=0.0002). Representative dot plots are illustrated in the left panel, the evaluation of the MFI ratio on the right panels; *MFI: Mean Fluorescent Intensity.*

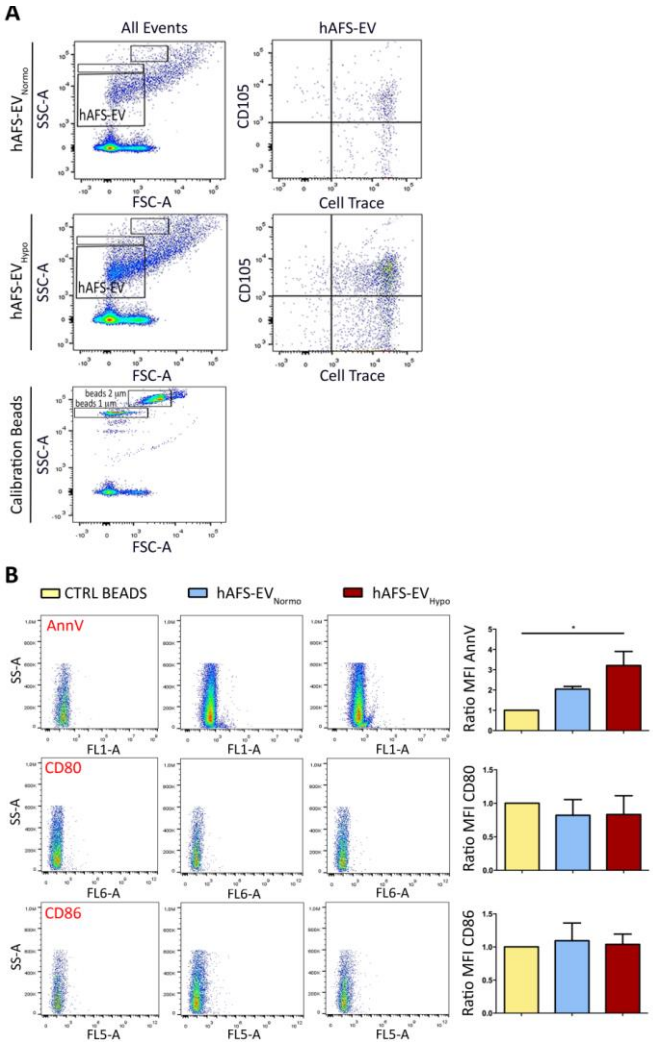

Figure 9. A) FACS analysis of hAFS-EV$_{Normo}$ (upper panel) and hAFS-EV$_{Hypo}$ (middle panel) for the mesenchymal stem cell marker CD105 and the CellTrace Far Red DDAO-SE dye. The dimensional gates were set according to 1- and 2µm calibration beads (lower panel). **B)** FACS analysis of hAFS-EV$_{Normo}$ and hAFS-EV$_{Hypo}$ using the ExoCap™ Capture Beads compared to control empty beads (CTRL BEADS) for the expression of Annexin V (*p<0.05, p=0.019), CD80 and CD86.

AnnV: Annexin V; MFI: Mean Fluorescent Intensity.

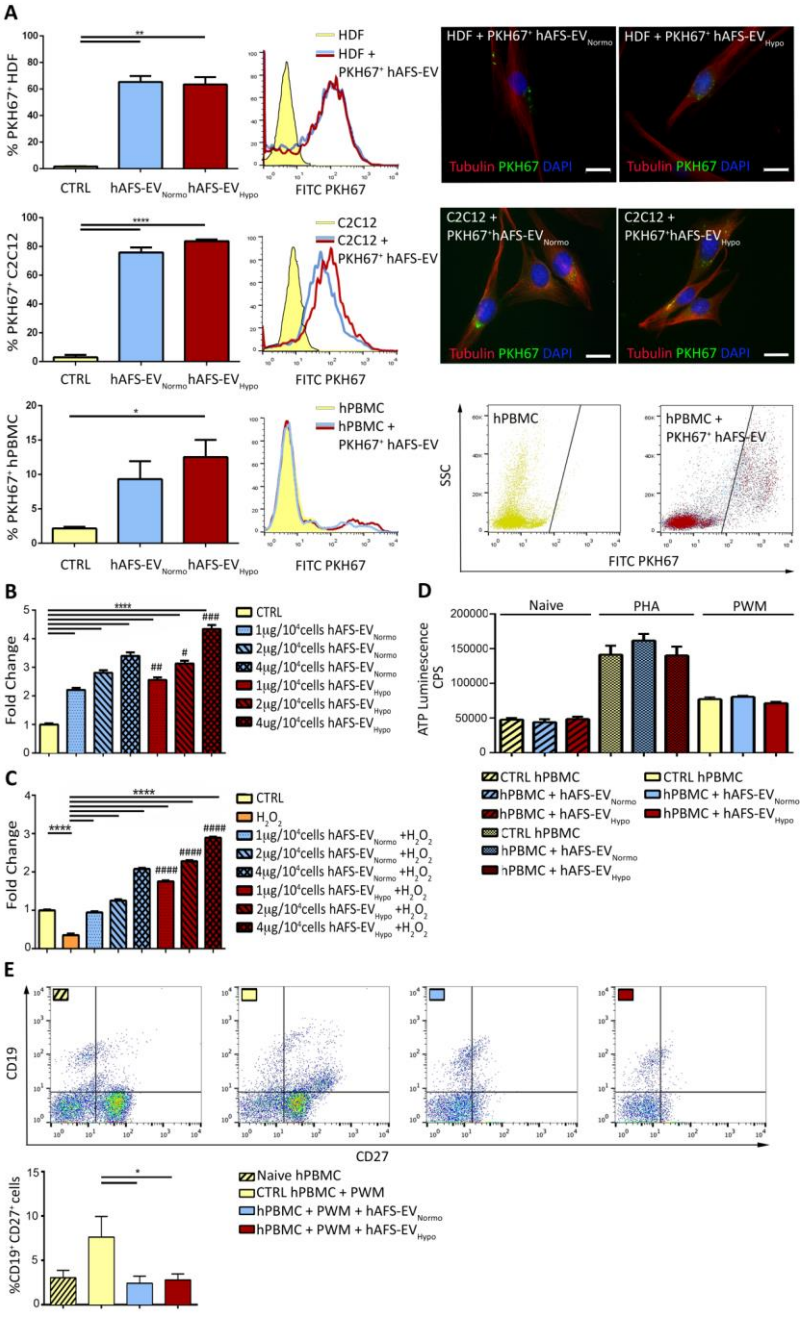

Figure 10. A) PKH67^{+} hAFS-EV uptake by HDF, C2C12 and hPBMC by FACS (values normalized to mode on the y-axis) and immunostaining (scale bar: 20µm). PKH67^{+} cells after treatment with hAFS-EV$_{Normo}$ and hAFS-EV$_{Hypo}$ were: 65.4 ± 4.4% and 63.5 ± 5.6% HDF (**p<0.01, p=0.0033 and p=0.0036 respectively); 75.9 ± 3.4% and 83.7 ± 1.1% C2C12 (****p<0.0001); 9.3 ± 2.6% and 12.5 ± 2.5% hPBMC (*p<0.05, p=0.017). **B)** BrdU ELISA on HDF treated with 1-2-4 µg/10^4 cells of hAFS-EV$_{Normo}$ and hAFS-EV$_{Hypo}$ versus untreated cells (*CTRL*); **** p<0.0001; $^{\#}$p referring to hAFS-EV$_{Hypo}$ versus hAFS-EV$_{Normo}$: $^{\#}$p<0.05 (p=0.033), $^{\#\#}$p<0.01 (p=0.0077), $^{\#\#\#}$p<0.001 (p=0.0002). Values expressed as the fold change of sample absorbance read at 370nm (reference wavelength approx. 492nm). **C)** MTT assay on C2C12 primed with 1-2-4 µg/10^4 cells of hAFS-EV$_{Normo}$ or hAFS-EV$_{Hypo}$ and exposed to oxidative stress versus untreated cells (*CTRL*) or damaged cells without hAFS-EV stimulation (H_2O_2). **** p<0.0001; $^{\#}$p referring to hAFS-EV$_{Hypo}$ versus hAFS-EV$_{Normo}$: $^{\#\#\#\#}$p<0.0001. Values expressed as the fold change of the sample absorbance read at 560nm and 670nm. **D)** hPBMC proliferation under un-stimulated (*Naive*) and activating (*PHA or PWM*) conditions with 1 µg/10^5 cells of hAFS-EV$_{Normo}$ and hAFS-EV$_{Hypo}$ versus untreated cells (*CTRL hPBMC*); *CPS*: Counts Per Second. **E)** FACS analysis of mature CD19^{+}CD27^{+} B cells treated with 1µg/10^5 cells of hAFS-EV$_{Normo}$ or hAFS-EV$_{Hypo}$. *Naïve hPBMC*: 3.48 ± 0.86%; *CTRL hPBMC + PWM*: 8.48 ± 2.63%; *hPBMC + PWM + hAFS-EV$_{Normo}$*: 2.32±0.96%; *hPBMC + PWM + hAFS-EV$_{Hypo}$*: 2.36 ± 0.62%. *p<0.05 (p=0.045 and p=0.047).

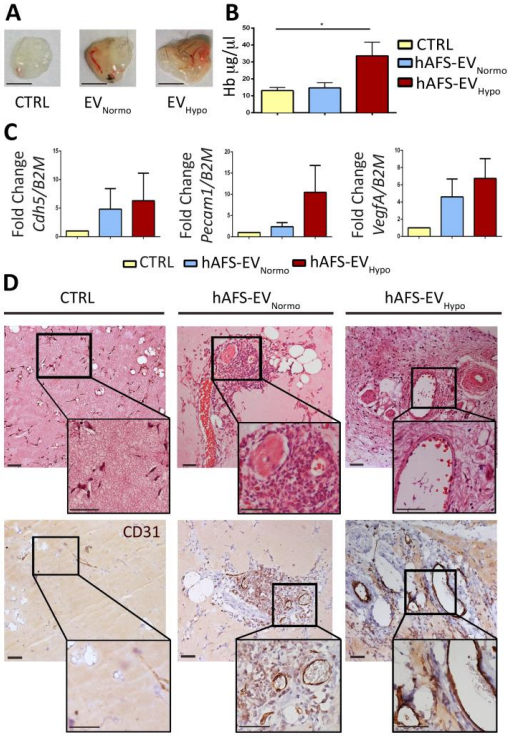

Figure 11. A) Representative images of Matrigel plugs loaded with 10µg of hAFS-EV_{Normo} or hAFS-EV_{Hypo} and recovered after 3 weeks from C57Bl/6J mice; scale bar 5mm. **B)** Evaluation of blood hemoglobin content on the Matrigel plugs loaded with 10 µg of hAFS-EV_{Normo} or hAFS-EV_{Hypo} versus the PBS control *p<0.05 (p=0.04). **C)** Real time qRT-PCR analysis on the recovered plugs for *Cdh5, VegfA* and *Pecam1* expression as normalized to *B2M* expression. **D)** Representative images of histological evaluation of vessel formation within the Matrigel plug by infiltrating host cells via hematoxylin and eosin and CD31 staining, scale bar: 50µm. *CTRL*: vehicle loaded (PBS) Matrigel plug; *hAFS-EV_{Normo}*: hAFS-EV_{Normo} loaded Matrigel plug*;* *hAFS-EV_{Hypo}*: hAFS-EV_{Hypo} loaded Matrigel plug.

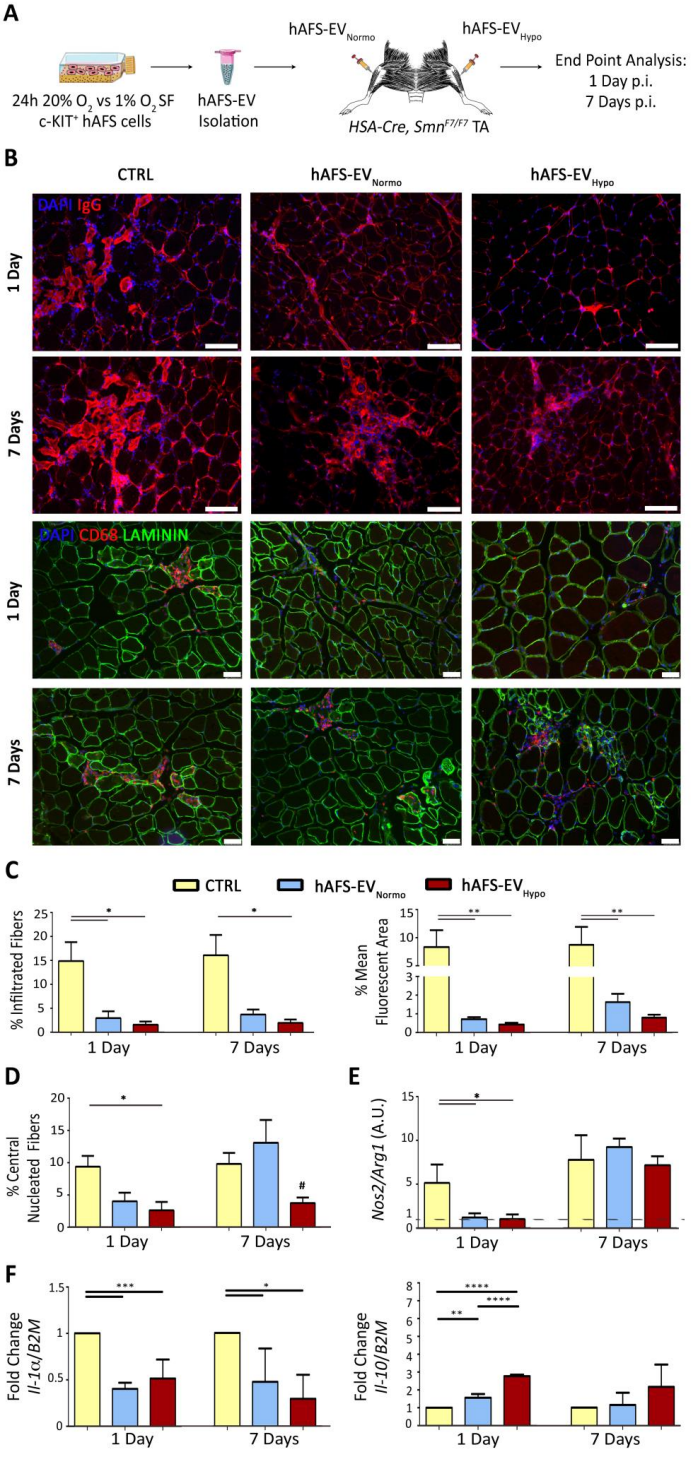
A
hAFS-EV Normo
hAFS-EV Hypo
24h 20% O2 vs 1% O2 SF
c-KIT+ hAFS cells
hAFS-EV Isolation
HSA-Cre, Smn F7/F7 TA
End Point Analysis:
1 Day p.i.
7 Days p.i.
B
CTRL
hAFS-EV Normo
hAFS-EV Hypo
1 Day
7 Days
DAPI IgG
DAPI CD68 LAMININ
C
CTRL
hAFS-EV Normo
hAFS-EV Hypo
% Infiltrated Fibers
% Mean Fluorescent Area
1 Day
7 Days
D
% Central Nucleated Fibers
E
Nos2/Arg1 (A.U.)
F
Fold Change Il-1α/B2M
Fold Change Il-10/B2M

Figure 12 A) *In vivo* procedure. **B)** IgG (red), CD68 (red) and LAMININ (green) expression in the TA muscle of untreated (*CTRL*) and 1µg hAFS-EV$_{Normo}$- and hAFS-EV$_{Hypo}$-treated mice at 1 and 7 days post injection (p.i.); scale bar: 100µm and 50µm, respectively. **C)** IgG-infiltrated fibers at 1- and 7 days p.i. (*CTRL 1 Day*: 14.9 ± 3.9%; *hAFS-EV$_{Normo}$ 1 Day*: 2.9 ± 1.4%; *hAFS-EV$_{Hypo}$ 1 Day*: 1.6 ± 0.7%; *p<0.05 p=0.031 and p=0.016; *CTRL 7 Days*: 16.1 ± 4.3%; *hAFS-EV$_{Normo}$ 7 Days*: 3.8 ± 1.0%; *hAFS-EV$_{Hypo}$ 7 Days*: 2.0 ± 0.7%; *p<0.05, p=0.035) and corresponding mean fluorescent area (*CTRL 1 Day*: 8.33 ± 3.0%; *hAFS-EV$_{Normo}$ 1 Day*: 0.71 ± 0.11%; *hAFS-EV$_{Hypo}$ 1 Day*: 0.42 ± 0.1%; **p<0.01, p=0.002; *CTRL 7 Days*: 8.90 ± 3.2%; *hAFS-EV$_{Normo}$ 7 Days*: 1.64 ± 0.44%; *hAFS-EV$_{Hypo}$ 7 Days*: 0.80 ± 0.15%; **p<0.01, p=0.006 and p=0.003). **D)** Central nucleated fibers at 1- and 7 days p.i.: *CTRL 1 Day*: 9.4 ± 1.6%; *hAFS-EV$_{Normo}$ 1 Day*: 4.0 ± 1.3%; *hAFS-EV$_{Hypo}$ 1 Day*: 2.6 ± 1.3%, *p<0.05, p=0.015; *CTRL 7 Days*: 9.8 ± 1.7%; *hAFS-EV$_{Normo}$ 7 Days*: 13.1 ± 3.5%; *hAFS-EV$_{Hypo}$ 7 Days*: 3.7 ± 0.9%; $^{\#}$p<0.05, p=0.033, as hAFS-EV$_{Hypo}$ versus hAFS-EV$_{Normo}$. **E)** Ratio of *Nos2* over *Arg2* by real time qRT-PCR; *p<0.05, p=0.045 and p=0.036 for hAFS-EV$_{Normo}$ and hAFS-EV$_{Hypo}$; *A.U. Arbitrary Units.* **F)** Real time qRT-PCR for *Il-1α* (***p<0.001, p=0.0002 and p=0.001; *p<0.05, p=0.046 and p=0.0163, for hAFS-EV$_{Normo}$ and hAFS-EV$_{Hypo}$) and *Il-10* (****p<0.0001, **p<0.01, p=0.004*)*.

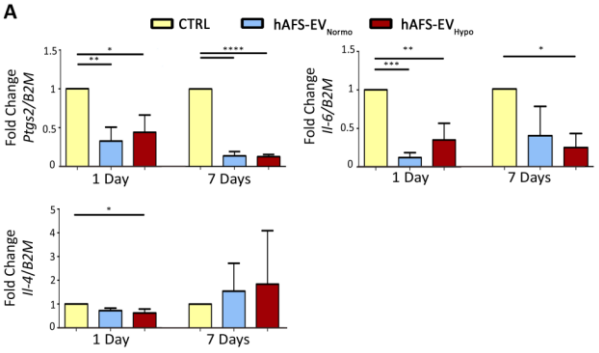

Fig. 13 A) Real time qRT-PCR analysis for the expression of the *Ptgs2* gene encoding for the COX2 enzyme (upper left panel, *p<0.05, p=0.019; **p<0.01, p=0.007; ****p<0.0001), for the *Il-6* (upper right panel, *p<0.05, p=0.021; **p<0.01, p=0.002; ***p<0.001, p=0.0004) and *Il-4* (lower left panel, *p<0.05, p=0.015) genes. Gene expression was normalized using the *B2M* gene as internal control.

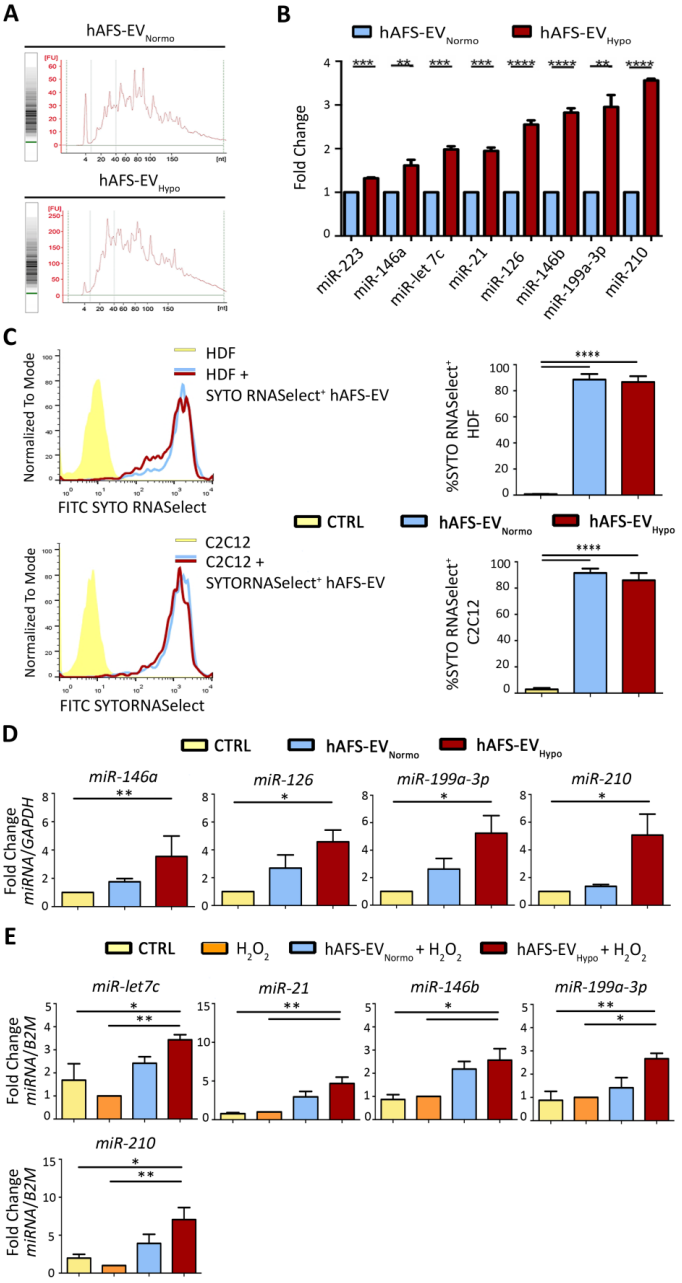

Fig. 14 A) Analysis of hAFS-EV small non-coding RNA content by Agilent technology. **B)** Real time qRT-PCR of hAFS-EV$_{Hypo}$ versus

hAFS-EV_{Normo} showing significant enrichment of the following regenerative miRNAs: miR-223 (***p<0.001, p=0.0001), miR-146a (**p<0.01, p=0.009), miR-let7c (***p<0.001, p=0.0002), miR-21 (***p<0.001, p=0.0003), miR-199a-3p (**p<0.01, p=0.002), miR-126, miR-146b and miR-210 (****p<0.0001). **C)** Uptake analysis of hAFS-EV fluorescently labeled RNA by HDF (upper panel) and C2C12 (lower panel) via FACS (on the left representative histogram graphs with corresponding values in the graphs on the right). 88.67 ± 4.21% and 86.73 ± 4.46% of HDF (****p<0.0001) and 91.5 ± 3.38% and 85.97 ± 5.51% of C2C12 cells (****p<0.0001) became fluorescent following incubation with 1μg/10^4 cells of SYTO®RNASelect$^+$ hAFS-EV_{Normo} and hAFS-EV_{Hypo}, showing direct uptake of the marked RNA cargo. **D)** Real time qRT-PCR analysis for the enrichment of specific hAFS-EV-delivered miRNAs in the target proliferative HDF: miRNA-146a, **p<0.01, p=0.006; miRNA-126 and miR-199a-3p (*p<0.05, p=0.03), miR-210 (*p<0.05, p=0.04). **E)** Real time qRT-PCR analysis for the enrichment of specific hAFS-EV-delivered miRNAs in the target C2C12 with or without H_2O_2 treatment: miR-let7c (**p<0.01, p=0.005 and *p<0.05, p=0.04); miR-21 (**p<0.01, p=0.002 and p=0.001 respectively); miRNA-146b (*p<0.05, p=0.020 and p=0.012); miRNA-199a-3p (*p<0.05, p=0.013 and **p<0.01 p=0.008) and miRNA-210 (**p<0.01, p=0.006 and *p<0.05 p=0.02). Gene expression was normalized to human *GAPDH* and to mouse *B2M* as internal controls in the HDF and C2C12 cells, respectively.

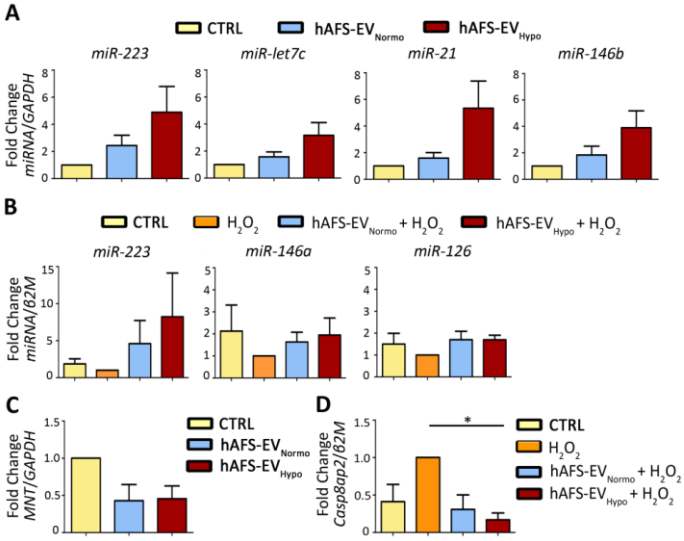

Fig. 15 A) Real time qRT-PCR analysis for the enrichment of the hAFS-EV-delivered miR-223, miR-let7c, miR-21 and miR-146b delivered by hAFS-EV within the target HDF undergoing cell proliferation assay. **B)** Real time qRT-PCR analysis for the enrichment of the hAFS-EV-delivered miR-223, miR-146a and miR-126 within the target C2C12 cell undergoing cell viability assay. **C)** Real time qRT-PCR analysis for the miR-210 target gene MNT within the responder HDF undergoing cell proliferation assay. **D)** Real time qRT-PCR analysis for the miR-210 target gene *Casp8ap2* within the responder C2C12 undergoing cell viability assay (*p<0.05, p=0.023). Gene expression was normalized using the human *GAPDH* and the mouse *B2M* gene as internal control in the HDF and C2C12 cells, respectively.

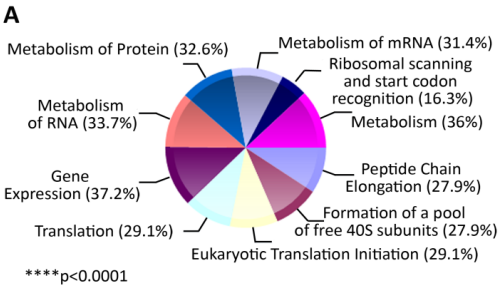

Fig. 16 A) Pecentages of protein significantly enriched in the hAFS-EV_{Hypo} over the hAFS-EV_{Normo} and considerably involved in the indicated biological pathways (****p<0.0001): metabolism of protein and RNA, including mRNA; gene expression and translation; metabolism; eukaryotic translation initiation; formation of pool of 40s subunits, peptide chain elongation; ribosomal scanning and start codon recognition.

iii) RE-ACTIVATION OF ENDOGENOUS MECHANISM OF CARDIAC REPAIR AND REGENERATION BY THE hAFS SECRETOME IN A PRECLINICAL MOUSE MODEL OF MYOCARDIAL INFARCTION.

In this last part of my research activity, I have been analysing the hAFS secretome potential in both enhancing cardiac repair, but also in trigger cardiac regeneration by acting on epicardial CPC and resident cardiomyocyte, following a myocardial infarction (MI). As a matter of fact, so far the cardiac regenerative potential of the hAFS secretome has been investigated only in an acute model of MI by a rat ischemia/reperfusion injury model, where the cardioprotective effect of the hAFS-CM was assessed within 2 hours from administration by Bollini et al. in 2011(Bollini et al., 2011). Therefore, a more comprehensive analysis of the stimulatory effect of the hAFS secretome on the specific key mechanisms of both cardiac repair and regeneration is needed.

Optimal restoration of the injured heart should be provided by efficiently tackling two specific aspects: i) defective cardiac repair and ii) lack of myocardial renewal, following significant loss of cardiomyocytes. As a matter of fact, the heart responds to an ischemic injury - such as the occlusion of a coronary artery causing the death of a consistent amount of cardiomyocytes - by promptly activating a wound healing process, involving the activation of the inflammatory response and of myofibroblasts that rapidly lay down a collagen-enriched scar tissue to compensate the cardiomyocyte loss, thus sustaining mechanical strength and preventing ventricular rupture, overall avoiding sudden death. Despite such repair mechanism represents an emergency plan, it may have detrimental consequences in the long term, representing an initial life-saving mechanism turning into a paradigm of failed repair.

On top of this, cardiomyocyte renewal deficiency further worsens the pathological scenario.

Nevertheless, recent evidences have highlighted that the adult mammalian heart harbours an endogenous restorative programme based on resident cardiac progenitor cells (CPC) improving cardiomyocyte survival, angiogenesis and cardiac function following MI (Cahill et al., 2017). Several kinds of CPC have been described, with recently growing interest dedicated to the epicardium-derived progenitor cells (EPDC) that contribute to coronary vessels and possibly to ventricular cardiomyocytes during development (Smart et al., 2007)(Zhou et al., 2008), while also maintaining some regenerative potential in the adult injured heart (Zhou and Pu, 2012), after specific paracrine priming (Smart et al., 2011). Furthermore, the long-held dogma that mammalian cardiomyocytes have completely withdrawn from the cell cycle has been recently rejected, although the number of mitotic cardiomyocytes drops precipitously within the first week of life, with cardiomyocyte renewal rate at 0.5 - 1% per year in adult humans (Bergmann et al., 2009)(Senyo et al., 2013). Interestingly, these two mechanisms are widely responsive in the neonate for a limited time. In this scenario growing interest has been driven to exploiting stem cell paracrine biology, in order to efficiently unlock and restore such regenerative programme.

Therefore, in this section I have been working on addressing crucial aspects related to the profiling of the cardioactive modulatory potential of the hAFS secretome in triggering:

(1) the improvement of cardiac repair mechanisms, including modulation of inflammation, angiogenesis and inhibition of chronic fibrosis and excessive scarring;

(2) the activation of the cardiac endogenous regenerative programme based on both restoration of the epicardial CPC potential and the proliferation of surviving resident cardiomyocytes.

hAFS-CM exerted significant anti-apoptotic effect on mouse neonatal cardiomyocyte undergoing oxidative and hypoxic damage, with the hypoxic hAFS-CM being particularly cardioprotective under ischemic condition. hAFS-CM was also able to induce to trigger the proliferation of rat neonatal cardiomyocytes, and of several subpopulation of human CPC. Profiling of the the hypoxic hAFS-CM highlighted the enrichment of regenerative cytokines. *In vivo* data showed that intra-myocardial injection of hAFS-CM soon after MI provided substantial acute cardioprotection, curbed down inflammation in the short term, while also sustaining angiogenesis, boosting cardiomyocyte proliferation after 4 weeks. the hAFS secretome also induced the increase of endogenous EPDC within a week from MI. Some of the *in vivo* work presented here has been performed at the Dept. of Molecular Cell Biology, Leiden University Medical Centre (LUMC), Leiden, The Netherlands, under the supervision of Prof. Marie-Josè Goumans and Dr. Anke Smits.

Notably, in this last section I've also aimed to pinpoint the therapeutic role of the secretome soluble fraction versus the extracellular vesicle (EV) component, in a preclinical mouse model of myocardial infarction (MI) by administrating either total hAFS-CM, the conditioned medium depleted by EV (hAFS-DM), and the hAFS-EV.

Methods

Cell Culture

hAFS and human keratinocyte NCTC 2544 were cultures as described in the previous section. Human adult cardiac progenitor cell (hCPC) were obtained from atrial appendage specimens obtained during heart valve surgery procedure as clinical waste, at the San Martino Hospital (Genova, Italy) following written informed consent and according to the Helsinki Declaration and to the local ethical committee authorization (P.R.007REG2013). Cells were isolated as previously described (Messina et al., 2004)(Barile et al., 2014) and cultured in Iscove Modified Dulbecco's Medium (EuroClone, Milano, Italy) with 20% fetal bovine serum (FBS), 1% L-glutamine, 1% penicillin/streptomycin, (all Thermo Fisher Scientific, Waltham, Massachusetts). Human foetal Sca-1+ cardiac progenitor cells (fSca-1+ hCPC) were obtained from human foetal heart tissue, aged, collected after elective abortion without medical indication from 10 to 22 weeks of gestation, following written informed consent. Experiments were performed according to the official guidelines of the Leiden University Medical Center and approved by the local Medical Ethics Committee. Cells were sorted for Sca-1 expression (MACS MicroBead Kit, Miltenyi Biotechnology, Bergisch Gladbach, Germany) as previously described (van Vliet et al., 2008) and cultured on 0.1% gelatin-coated dishes in M199 (Gibco-Thermo Fisher Scientific, Waltham, Massachusetts)/EGM (3:1) supplemented with 10% FCS (Gibco-Thermo Fisher Scientific, Waltham, Massachusetts), 10 ng/ml basic fibroblast growth factor (bFGF), 5 ng/ml epithelial growth factor (EGF), 5 ng/ml insulin-like growth factor (IGF-1) and 5 ng/ml hepatocyte growth factor (HGF). Human adult epicardium derived progenitor cells (hEPDC) were obtained from human atrial samples obtained during cardiac surgery for extracorporeal bypass and anonymously collected as surgical waste under general informed consent. Experiments were performed

according to the official guidelines of the Leiden University Medical Center and approved by the local Medical Ethics Committee. Cells were isolated by separating the epicardium from the underlying myocardium as previously described (Moerkamp et al., 2016). Briefly, the tissue was processed into small pieces and digested in a 0.25% Trypsin/EDTA solution (Serva, Heidelberg, Germany). Cells were cultured in 1:1 Dulbecco's modified Eagle's medium (DMEM-glucose low; Invitrogen, Carlsbad, California) and Medium 199 (M199; Invitrogen, Carlsbad, California) supplemented with 10% heat-inactivated FCS (Gibco-Thermo Fisher Scientific, Waltham, Massachusetts), and 100 U/ml penicillin/streptomycin (Gibco-Thermo Fisher Scientific, Waltham, Massachusetts). To avoid hEPDC undergoing epithelial-to-mesenchymal transition (EMT) while maintaining cobble-like morphology (hEPDCc), the ALK5-kinase inhibitor SB431542 (5–10 µm; Tocris Bioscience, Bristol, UK) was added to the culture medium. hEPDC activating the EMT process as not treated with such inhibitor, acquired a more elongated, fibroblast-like, spindle morphology (hEPDCs).

Mouse and rat neonatal ventricular cardiomyocytes (mNVCM and rNVCM) were isolated via enzymatic digestion from 2- (C57/Bl6 mouse and Wistar rat) and 5-days-old (Wistar rat) rodent heart as previously described (Lazzarini et al., 2016)(Eulalio et al., 2012b). Cells were seeded on 1% gelatin solution, (Sigma-Aldrich, St.Louis, Missuri) in complete plating medium (69% Dulbecco's Modified Eagle Medium, DMEM, 15% M199, 10% horse serum, 5% FBS, 1% penicillin/streptomycin and 1% L-glutammine and 4.5g/l glucose DMEM with 5% FBS, 20mg/ml vitamin B12 and with 100U/ml of penicillin and 100mg/ml of streptomycin (all Gibco-Thermo Fisher Scientific, Waltham, Massachusetts and Sigma-Aldrich, St.Louis, Missuri). Rat ventricular cardiomyocytes (rNVCM) were also used as isolated from 5-days-old Wistar rats by enzimatic digestion in a 0.25mg/ml of pancreatin (Sigma-Aldrich, St.Louis, Missuri), 0.125 mg/ml collagenase

type II (WorthingtonBiochemicals, Lakewood, New Jersey) and 10 mg/ml DNaseII (Sigma-Aldrich, St.Louis, Missuri) digestive buffer under costant stirring. Cell isolation was performed in compliance with national and international laws and specific authorisation (protocol 384/2016-PR and EEC Council Directive 86/609, OJL 358, 12 December 1987).

Human circulating endothelial colony-forming cells (hECFC) were obtained as previously described (Dragoni et al., 2015); briefly, mononuclear cells (MNC) were separated by density gradient centrifugation from peripheral blood samples obtained from healthy donors (protocol n.20110004143, IRCCS Policlinico San Matteo Foundation, Pavia) and plated on collagen-coated culture dishes (BD Bioscience, Franklin Lake, New Jersey) in growth medium (EGM-2 MV, Lonza, Basel, Switzerland) supplemented with endothelial basal medium (EBM-2), 5% FBS, recombinant human (rh) epithelial growth factor (rhEGF), rh vascular endothelial growth factor (rhVEGF), rh fibroblast growth factor-basic (rhFGF-B), rh insulin-like growth factor 1 (rfIGF-1), ascorbic acid and heparin. Outgrowth of hECFC from adherent MNC was characterised by the formation of a cluster of cobblestone-shaped cells that was previously demonstrated to belong to the endothelial lineage (Moccia and Poletto, 2015).

HUVEC (Human Umbilical Vein Endothelial Cells) were isolated as previously described (Tersteeg et al., 2012) and cultured in endothelial EGM-2 cultured medium (Lonza, Basel, Switzerland).

Collection of cell-conditioned medium and EV isolation

hAFS- and hNCTC-conditioned medium (hAFS-CM and hNCTC-CM, respectively) were produced and collected as previously described (Lazzarini et al., 2016). Briefly, cells were washed with PBS solution and incubated for 24h in serum-free medium (4.5g/l glucose DMEM, 1% L-glutamine, and 1% penicillin/streptomycin) under hypoxic

condition (1% O_2, 5% CO_2 at 37°C in a hypoxic incubator, Eppendorf, Hamburg, Germany).
hAFS-extracellular vesicles (hAFS-EV) were produced by ultracentrifugation in a Optima L-90K (Beckman Coulter, Brea, California) from hAFS-CM as previously described (Balbi et al., 2017). hAFS-CM depleted of hAFS-EV, here defined as hAFS-depleted medium (hAFS-DM), was obtained as the remaining surnatant after hAFS-CM ultracentrifugation and hAFS-EV isolation. hAFS-CM, hAFS-DM and hNCTC-CM were further concentrated using ultrafiltration membranes with a 3kDa selective cut-off (Amicon Ultra-15, Millipore, Burlington, Massachusetts). hAFS-EV were resuspended in PBS solution and stored at -80 °C until use. For the assessment of hAFS-EV uptake by the myocardial tissue in the preclinical mouse model of MI, vesicles were labelled with the FITC-conjugated lipophilic dye PKH67 as previously described (Balbi et al., 2017).

In vitro evaluation of the hAFS secretome paracrine potential
The paracrine potential of the hAFS secretome was evaluated on different target cells, by treating them with 80ug/ml of hAFS-CM or hNCTC-CM in serum-free condition (SF). hNCTC-CM was used as negative control.

Cardioprotective Potential
To assess hAFS-CM pro-survival effect, mNVCM were primed in SF with the hAFS-CM versus hNCTC-CM for 3h, then exposed for 4h to oxidative stress and to hypoxic conditions by incubating them with 150 µM H_2O_2 solution and under 1% O_2 atmosphere, respectively, and then cultured in complete medium for the following 24h. Cell viability was assessed by MTT assay using a 150µg/ml MTT solution (Sigma-Aldrich, St.Louis, Missouri).

Angiogenic Effect

The hAFS-CM angiogenic potential was evaluated through measurement of Ca^{2+} signalling generated in hECFC and by in vitro tube formation assay [25,36]. For Ca^{2+} signalling, hECFC cultured on a coverslip were loaded with 4μM fura-2 acetoxymethyl ester (fura-2/AM; 1 mM stock in dimethyl sulfoxide) in physiological salt solution (PSS) for 1 hour at room temperature. PSS had the following composition (in mM): 150 NaCl, 6 KCl, 1.5 CaCl2, 1 MgCl2, 10 Glucose, 10 Hepes. This solution was titrated to pH 7.4 with NaOH. After washing in PSS, cells were observed by an upright epifluorescence Axiolab microscope (Carl Zeiss, Oberkochen, Germany, with a Zeiss ×40 Achroplan objective). hECFC were excited alternately at 340 and 380 nm, and the emitted light detected at 510 nm. Custom software, working in the LINUX environment, was used to drive the camera (Extended-ISIS Camera, Photonic Science, Millham, UK) and the filter wheel, and to measure and plot on-line the fluorescence from 10 up to 50 rectangular "regions of interest" (ROI). Each ROI was identified by a number. Since cell borders were not clearly identifiable, a ROI may not include the whole cell or may include part of an adjacent cell. Adjacent ROIs never superimposed. $[Ca^{2+}]_i$ was monitored by measuring, for each ROI, the ratio of the mean fluorescence emitted at 510 nm when exciting alternatively at 340 and 380 nm (shortly termed "ratio"). An increase in $[Ca^{2+}]_i$ causes an increase in the ratio (Dragoni et al., 2015). Ratio measurements were performed and plotted on-line every 3 s. The experiments were performed at room temperature (22°C).

The tube formation assay was carried out as previously shown (Dragoni et al., 2015)(Lodola et al., 2017). To evaluate the angiogenic effect of hAFS-CM versus hNCTC-CM, early passage (P2-P3) hECFC were cultured in basal medium EBM-2 supplemented with 2% FBS in Cultrex (Trevigen, Gaithersburg, Maryland)-coated 96 well plates, in the presence of either hAFS-CM or hNCTC-CM for 24 hours. Capillary network formation was assessed starting from 4 up to 24 hours later. Three different sets of experiments, each performed in duplicate, were

carried out. To evaluate the effect of Ca^{2+} signalling, the same protocol was repeated by priming hECFC with hAFS-CM in the presence of BAPTA (30 μM, 2 hours), a membrane-permeable chelator used to prevent Ca^{2+}-dependent processes (Dragoni et al., 2015)·(Lodola et al., 2017).

Likewise, angiogenic potential of the conditioned medium of human EPDC (hEPDC) primed with total hAFS-CM was assessed on HUVEC in vitro. hEPDC were cultured over-night with 80μg/ml of hAFS-CM. The following day hEPDC were cultured in fresh culture medium supplemented with 1% of heat-inactivated FCS (Gibco-Thermo Fisher Scientific, Waltham, Massachusetts); hEPDC-CM was collected 5 days later as described above. HUVEC were cultured for 24 hours in either positive control medium (EGM-2 medium), negative control medium (hEPDC culture medium with 1% FBS), un-primed hEPDC-CM or hAFS-CM-primed hEPDC-CM (here indicated as $^{\text{hAFS-CM primed}}$hEPDC-CM). Capillary network formation was assessed starting from 4 up to 24 hours later. Experiments were repeated a minimum of three times and the vasculogenic response was measured by evaluating both dimensional and topological parameters. As previously illustrated (Dragoni et al., 2015)(Lodola et al., 2017), we analyzed length of endothelial tube-like structures (TLS), the number of polygon structures established by TLS, referred to as complex meshes as indicative of endothelial cell migration and number of junctions by using the Angiogenesis Analyzer plugin of ImageJ (Gilles Carpentier, Faculte´ des Sciences et Technologie, Universite´ Paris Est, Creteil Val de Marne, France).

Proliferative Potential on NVCM and CPC

rNVCM proliferation was assessed by incubating cells with hAFS-CM versus hNCTC-CM over-night together with 5μM EdU (Life Technology, Carlsbad, California) solution for the following 24h. Cells were fixed with 4% PFA and stained by rabbit anti-rat cardiac αActin

(Abcam) and Click-IT EdU-555 Imaging kit to reveal EdU incorporation (Life Technology, Carlsbad, California). Images were acquired and computed at the ICGEB High-Throughput Screening Facility, Trieste, Italy. (http://www.icgeb.org/high-throughput-screening.html).
The proliferative effect of hAFS-CM was also evaluated on different CPC populations. Human adult CPC, human fetal Sca-1+ CPC, hEPDCc and hEPDCs were primed with hAFS-CM versus hNCTC-CM over-night. All CPC populations were then incubated for the following 24h in complete medium supplemented with 10μM bromodeoxyuridine (BrdU). BrdU colorimetric assay (Roche, Basel, Switzerland) was performed according to the manufacturer's instructions. CPC were also treated with hAFS-CM versus hNCTC-CM for 3h, then fixed with 4% PFA and processed by using a rabbit anti-human Ki67 (Millipore, Burlington, Massachusetts) antibody and phalloidin solution (LifeTechnology, Carlsbad, California). Images were acquired on a Axiovert microscope equipped with Axiovision software (Carl Zeiss, Oberkochen, Germany).

Cytokine and Chemokine Profiling of Cell Secretome
The cytokine and chemokine profile of hEPDCs-CM, hAFS-CM primed hEPDCs-CM was analysed using a cytokine array assay (Proteome Profiler™ Human XL Cytokine Array kit; R&D System, Minneapolis, Minnesota) following the manufacture's instructions. Analysis was performed on 2.5μg of total protein images of spotted array membranes acquired on X-ray film exposed for 6 minutes. Images were analysed by ImageJ (https://imagej.nih.gov/ij/) with the protein Array Analyzer Plug-in. The same analysis was applied to evaluate the cytokine and chemokine profile of the whole hypoxic hAFS secretome (hypoxic hAFS-CM) as compared to control normoxic one (ctrl hAFS-CM)

In vivo assessment of the hAFS secretome cardioactive potential

Mouse preclinical model of myocardial infarction (MI).

C57Bl6/J wild type mice (n=45) and inducible $Wt1^{CreERT2/+}$;$R26R^{mTmG/+}$ mice (n=46) were housed and treated within the Animal Facilities of San Martino Hospital (Ospedale Policlinico San Martino, IRCCS per Oncologia, Genova, Italy) and Leiden University Medical Center (Leiden, The Netherlands), in compliance with national and European international standards of animal care and according to required authorisation from the Italian Ministry of Health (n.384/2016-PR) and the Committee on Animal Welfare of Leiden University Medical Center (PE.13353001). $Wt1^{CreERT2/+}$;$R26R^{mTmG/+}$ heterozygous transgenic mice were used as inducible lineage trace system to label in vivo epicardial EPDC (Zhou et al., 2012).

The preclinical model of myocardial infarction (MI) was obtained as previously described by permanent occlusion of the left anterior descending (LAD) coronary artery (Smart et al., 2011)(Bollini et al., 2011). All animals undergoing surgical procedure received appropriate analgesic administration (buprenorphine, 0.1-1 mg/kg) 100µg of either hAFS-CM, hAFS-DM or 4.5µg of hAFS-EV solution versus control vehicle serum-free medium were injected in the myocardium within the peri-infarct area into two different sites with a 30G needle insulin syringe (about 20 µL volume in total) soon after performing LAD ligation; chest was then closed and the mouse allowed to fully recover. On recovery, mice received intra-peritoneal injection of bromodeoxyuridine solution (BrdU, 80 mg/kg; Invitrogen, Carlsbad, California) if required. Further injections were administered at 1, 2 and 7 days post-surgery. Activation of the inducible genetic labelling in inducible $Wt1^{CreERT2/+}$;$R26R^{mTmG/+}$ mice was achieved through intra-peritoneal tamoxifen (20mg/kg, Sigma-Aldrich, St.Louis, Missuri) injections, as previously defined (Balmer et al., 2014). Control sham animals for functional ultrasound analysis underwent the same surgical procedure, but without LAD ligation.

Cardiac function analysis by echocardiography

Functional ultrasounds analysis by echocardiography was performed on isofluorane-anaesthetized C57/Bl6 mice at 7 days and 28 days after MI. Echocardiography was performed on a Vevo 770 High-Resolution In Vivo Micro-Imaging System (VisualSonic, Toronto, Canada) and analysed with Vevo 770 v3.0.0 software to evaluate the percentage of left ventricle ejection fraction (% LVEF) in each animal.

Histological Analysis

Hearts were harvested at 24h, 7 days, and 28 days following MI; for evaluation of the hAFS-EV uptake from the myocardial tissue, hearts were harvested after 3 hours from MI and treatment. Hearts were bisected transversely midway through the scar, fixed in 4% PFA and snap-frozen (wild type samples) or paraffin-embedded (transgenic samples) for further sectioning and immunofluorescence or histochemical analyses. Paraffin embedding masked the endogenous red fluorescence signal of $WT1^{CreERT2/+}$;$R26R^{mTmG/+}$ mice, as well as the GFP fluorescence in the Cre-recombinant epicardial cells, which was detected via immunostaining with a specific anti-GFP antibody. Apoptosis was evaluated by TUNEL (Terminal deoxynucleotidyl transferase dUTP Nick End Labeling) In Situ Cell Death Detection Kit (Roche, Basel, Switzerland), while fibrosis and ventricular remodelling was assessed by Masson's Trichromic staining (Bio Optica, Milano, Italy), following the manufacturer's instructions. The following primary antibodies were used: goat anti-mouse cTnI (cardiac-troponin I, 4T21/2 HyTest, Turku, Finland), rabbit anti-mouse myeloperoxidase (MPO, ab9535 Abcam, Cambridge, UK), rat anti-mouse CD68 (MCA1957, Bio-Rad, Hercules, California), chicken anti-GFP (ad13970 Abcam, Cambridge, UK), rabbit anti-mouse Wilms' Tumor 1 (WT1, ab89901 Abcam, Cambridge, UK), rat anti-Brdu (Bromodeoxyuridine, clone BU1/75 (ICR1), Thermo Scientific, Waltham, Massachusetts), rabbit anti-mouse platelet endothelial cell adhesion molecule (PECAM-1,

sc1506-R M20 Santa Cruz Biotechnology, Dallas, Texas), mouse anti-mouse alpha smooth muscle actin (αSMA, A2547 Sigma-Aldrich, St.Louis, Missuri). AlexaFluor-488, -594, -647 conjugated secondary antibodies were used (Molecular Probes – Thermo Scientific, Waltham, Massachusetts). Images were acquired on a Pannoramic Slide Scanner (3dhistech, Budapest, Hungary). Confocal images were acquired on a Leica SP5 confocal microscopy (Leica, Wetzlar, Germany).

Real Time qRT-PCR Analysis

Total RNA was extracted from heart apex at 3h and 24h post MI. RNA extraction was performed with Qiazol Lysis Reagent (Qiagen, Hilden, Germany) and cDNA obtained from either mRNA or miRNA using the iScriptTM cDNA Syntesis Kit (Bio-Rad, Hercules, California) and the miScript II RT Kit (Qiagen, Hilden, Germany), according to manufacturer's instructions. Real-time qRT-PCR analysis was performed on a 7500 Fast Real-Time PCR System (Applied Biosystems, Forest City, California) using the SensiFAST SYBER Lo-ROX kit (Bioline, London, UK) to assess the expression profile of the following genes within the murine cardiac tissue: *Il1α* (Forward: AGGGAGTCAACTCATTGGCG; Reverse: TGGCAGAACTGTAGTCTTCGT), *Mpo* (Forward: AGGATAGGACTGGATTGCCTG; Reverse: GTGGTGATGCCAGTGTTGTCA), *Wt1* (Forward: TTCAAGGACTGCGAGAGAAG; Reverse: GGGAAAACTTTCGCTGACAA), and *Raldh2* (Forward: TGAGTTTTGGCTTACGGGAGT; Reverse: TTGTTGTGAGGCAAGAGTGG); the expression profile of the human miRNAs *miR-146a*, *miR-210* and *miR-199a-3p* (all from miScript Primer Assay Qiagen, Hilden, Germany) was evaluated using miScript SYBR® Green PCR Kits. *Beta-2-microglobulin (B2M)* (Forward: GCTTCAGTCGTCAGCATGG; Reverse:

CAGTTCAGTATGTTCGGCTTCC), was used as internal reference and house keeping control gene.

Statistical Analysis

Results are presented as mean ± s.e.m. (standard error of mean) of at least three (n = 3) independent replicated experiments. Comparisons were drawn by one-way ANOVA followed by post-hoc Tukey's multiple comparisons test (for all in vitro experiments) or by unpaired t-test (for all other tests and when comparing hAFS-CM vs hAFS-DM or hAFS-EV). Statistical analysis was performed using GraphPad Prism Version 6.0a (GraphPad Software) with statistical significance set at *p< 0.05.

Results

The human AFS secretome mediates pro-survival, angiogenic and stimulatory paracrine effects in vitro.

To assess the role of the hAFS secretome as source of therapeutic effects, we analysed the paracrine potential of hAFS-CM on target cells in vitro. hAFS hypoxic preconditioning was adopted as working strategy in order to enrich hAFS-CM with trophic factors, as we previously observed that hAFS can get activated by the ischemic environment (Bollini et al., 2011).

Primary mNVCM were pre-treated with hAFS-CM and exposed to either oxidative stress or hypoxia, so to reproduce an ischemic injury in vitro. MTT analysis revealed substantial decrease in cell viability by about 60% and 30% when mNVCM were exposed to oxidative and hypoxic damage, respectively (****$p<0.0001$) [Fig.17A-B]. hAFS-CM showed to remarkably counteract mNVCM apotosis, by rescuing cell survival almost completely under oxidative stress (by about 93%, [Fig.17A]) and entirely in hypoxic conditions (by about 104% [Fig.17B]), respectively (****$p<0.0001$). Notably, in both models, hAFS-CM was significantly more effective than hNCTC-CM, as protecting about 37% and 26% more cells, correspondingly (****$p<0.0001$).

hAFS-CM angiogenic potential was evaluated on hECFCs, which are recruited into peripheral blood after myocardial ischemia to restore the damaged vascular network by either providing the building blocks for neo-vessel formation or by stimulating local angiogenesis in a paracrine way (Massa et al., 2005)(Tasev et al., 2016) hECFCs formed noticeable bidimensional capillary-like networks under stimulation by hAFS-CM, while hNCTC-CM did not significantly triggered tube formation [Fig.17C]. Indeed, TLS value in hAFS-CM-exposed cells was more than 2-fold and almost 5-fold higher compared to control (basal medium) and hNCTC-CM conditions, respectively (****$p<0.0001$); meshes were similarly enriched in the hECFCs primed with hAFS-CM

compared to control sample (by 1.5-fold increase, *p<0.05) and hNCTC-CM treatment (by 4-fold increase, ****p<0.0001); likewise, the number of master junctions developed by hECFCs under the instruction of the hAFS secretome was improved by 3.5- and 9-fold and compared to standard and hNCTC-CM conditions (**p<0.01 and ***p<0.001, respectively).

Intracellular Ca^{2+} signalling has long been known to control angiogenesis (Moccia et al., 2014); recently, repetitive oscillations in intracellular Ca^{2+} concentration ($[Ca^{2+}]_i$) only have been shown to drive proliferation and tube formation in hECFCs (Dragoni et al., 2011)(Dragoni et al., 2015)(Lodola et al., 2017). Therefore, to further corroborate the different pro-angiogenic outcome of the distinct secretome preparations, we assessed whether hECFCs displayed diverse Ca^{2+} responses when exposed to either hAFS-CM or hNCTC-CM. In agreement with the tubulogenic assays, only hAFS-CM caused robust intracellular Ca^{2+} oscillations in the majority of hECFCs (****p<0.0001), while hNCTC-CM triggered a biphasic increase in $[Ca^{2+}]_i$ that is not able to control proliferation and tube formation in these cells [Fig.17D]. Of note, preventing the intracellular Ca^{2+} oscillations with BAPTA (30 μM, 2h), a membrane permeable buffer of intracellular Ca^{2+} levels (Dragoni et al., 2011)(Lodola et al., 2017), dramatically inhibited in vitro tubulogenesis in hECFCs challenged with hAFS-CM (****p<0,0001 and **p<0,001, [Fig.17C]).

hAFS-CM reactivating potential was assessed on different subpopulation of primary human cardiac progenitor cells, isolated from myocardial tissue. The hAFS secretome positively modulated all human CPC considered, by boosting their proliferation, as evaluated by BrdU incorporation and Ki67 staining. While treatment with hNCTC-CM did not influence cell replication compared to control condition, following 18h incubation, hAFS-CM significantly increased DNA replication by about 47% in adult hCPC (***p<0.001, [Fig.18A]), by 47% in fSca-1+ hCPC (****p<0.0001, [Fig.18B]) and by 50% and 70% in

hEPDCc and hEPDCs (***p<0.001, [Fig.18C-D]). These results were further confirmed by Ki67 staining, being increased by 62% in adult hCPC (****p<0.0001, [Supplementary Fig.1A]), by 50% in fSca-1+ hCPC (*p<0.05, [Supplementary Fig.1B]) and by 147% and 140% in hEPDCc (*p<0.05) and hEPDCs (**p<0.01, [Supplementary Fig.1C-D]).

Noteworthy enhancement of rNVCM proliferation following hAFS-CM priming was also reported. α-actinin-positive rNVCM actively cycling as incorporating EdU significantly increased by 4,6-fold following hAFS-CM paracrine modulation [Fig.18E], when compared to untreated control (****p<0.0001). On the contrary, the hNCTC secretome resulted in a smaller proliferative induction, which, although contributing to sustain cell cycle compared to control (mock) cells (2,6-fold increase, *p<0.05), resulted in limited effect compared to the hAFS secretome (1,8-fold decrease, **p<0.01). These results were further confirmed on less responsive rNVCM isolated from 5-day-old rat heart. Indeed, at this stage, cardiomyocyte proliferation was limited; however, the percentage of EdU+ rNCVM notably increased upon the treatment with hAFS-CM by about 43% (**p<0.01) compared to untreated cells (Ctrl), while hNCTC-CM did not significantly influence cardiomyocyte behaviour at this stage (p>0.05), [Fig. 18F].

The hAFS secretome enhances myocardial repair following MI in vivo.

Histological analysis on the cardiac tissue at 24h after MI and intra-myocardial injection of the whole hAFS secretome (hAFS-CM) in the infarct border area, showed a significant decrease in cell apoptosis by about 39% compared to vehicle-treated animals (***p<0.001, [Fig.19A]). Treatment with hAFS-CM further curbed down the acute inflammatory response as infiltrating MPO-positive neutrophils and CD68-positive macrophages were reduced by 40% (*p<0,05 [Fig.19B]) and 44% (*p<0.05, [Fig.19C]), respectively. Modulation of inflammation

by the hAFS secretome was further confirmed by the remarkable decreased of *Il1α* expression by 38% (*p<0.05) and *Mpo* expression by 60% (**p<0,01) via real time qRT-PCR [Supplementary Fig.1E].

The hAFS secretome is represented by hAFS-CM, which is the whole of soluble trophic paracrine factors and extracellular vesicles (EV) secreted by hAFS; in order to understand whether the soluble over the vesicular fraction within hAFS-CM is responsible of the regenerative effects observed, mice were also treated with hAFS-CM previously depleted of hAFS-EV, namely hAFS-DM.

The cardioprotective and anti-inflammatory effects driven by acute administration of the hAFS secretome also influenced pathological remodelling in the long term, as mice initially treated with hAFS-CM showed lower fibrosis compared to control animals, with a 41% smaller infarct size (*p<0.05) at 28 days following MI. On the contrary, hAFS-DM did not significantly inhibit ventricle remodelling, compared to vehicle-treated mice (p>0.05). Indeed, hAFS-DM treated mice developed a 1.5-fold larger infarct scar than in the hAFS-CM group (**p<0.01 [Fig.20A]). hAFS secretome exerted beneficial effect on cardiac function as early as 7 days post MI; ultrasounds analysis revealed significant recovery of cardiac function in the treated mice, with improvement of the left ventricle ejection fraction percentage (%LVEF, Supplementary Fig.1F). Sham animals showed about 60.73±4.06 %LVEF (data not shown), which dramatically dropped down to 10.99±1.13 %LVEF when mice experienced MI (***p<0.001), similarly to what previously reported by others (Van Den Borne et al., 2009). Acute administration of hAFS-CM soon after MI rescued cardiac function by significantly increasing the ejection fraction by almost 2-fold (20.02±1.66 %LVEF, ***p<0.001) compared to untreated animals. On the contrary, hAFS-DM did not significantly preseve LVEF; despite increasing it by almost 33% compared to control animals (p>0.05), yet it showed a relevant 38% decrease in efficacy compared to the whole secretome containing EV (*p<0.05). Outstandingly, restoration of

cardiac function was further preserved in the long term, at 28 days post-MI, following the initial treatment, with similar hemodynamic values: control MI mice showing an even worse and compromised ejection fraction (8.96±1.04 %LVEF); hAFS-CM treated ones supported improved function by 86% (16.69±1.92 %LVEF, **p<0.01), while hAFS-DM partially increased LVEF, but without statistically significant contribution (11.82±1.05 %LVEF, p>0.05), showing a 41% decrease compared to hAFS-CM (*p<0.05 [Fig.20B]).

Local angiogenesis was considerably increased by both hAFS-CM and hAFS-DM administration when evaluated 28 days post MI, with no meaningful difference between the two approaches [Fig.20C]; indeed PECAM-1-positive capillaries in the infarct and border zone area raised by about 57% and 27%, under the hAFS-CM and hAFS-DM influence, respectively (*p<0.05); similarly, αSMA-positive cells were significantly enhanced by 60% with hAFS-CM (**p<0.01) and 21% with hAFS-DM (*p<0.05).

Notably, the hAFS secretome also activated adult resident cardiomyocyte proliferation, as revealed by BrdU and cardiac Troponin I staining at 28 days post-MI, [Fig.20D]. BrdU-positive cardiomyocytes as found scattered within the myocardium in the peri-infarct zone, increased by 2.4-fold when primed with hAFS-CM compared to vehicle-treated mice (7.38±0.39 versus 3.03±0.42 cells/mm^2, respectively, ****p<0.0001) and by 1.7 fold related to hAFS-DM (7.38±0.39 versus 4.31±0.86 cells/mm^2 respectively, **p<0.01), which did not induce any relevant effect, compared to control animals (p>0.05).

The hAFS secretome triggers the reactivation of an endogenous regenerative programme from within the heart

We further investigated whether the paracrine beneficial effects exerted by the hAFS secretome on the injured myocardial tissue could also involve the reactivation of dormant adult endogenous CPC residing within the epicardium, the so-called epicardium-derived progenitor cells

(EPDC), so to reinstate a more specific regenerative cardiac response to myocardial infarction.

In vivo administration of hAFS-CM soon after LAD ligation resulted into a meaningful 2.3- and 1.7-fold increased and restored expression of the embryonic epicardial genes *Wt1* and *Raldh2*, in myocardial tissue 7 days after MI (**p<0.01 and ****p<0.0001, [Supplementary Fig.1G). In order to genetically label in vivo the reactivated adult EPDC re-expressing the key embryonic epicardial *Wt1* gene, otherwise down-regulated, we used inducible $Wt1^{CreERT2/+}$;$R26R^{mTmG/+}$ mice to pulse label responsive WT1+ EPDC via GFP expression, as previously shown(Zhou et al., 2012). To pin point the role of stem cell-secreted EV in driving regenerative paracrine effects from within the hAFS secretome, here we also considered mice injected with hAFS-EV soon after LAD ligation. hAFS-CM injection boosted the reactivation of adult WT1+ GFP+ EPDC by 2.3-fold, compared to control treated mice (***p<0.001), and by 2.1-fold compared to hAFS-DM (**p<0.01), which did not contribute significantly (p>0.05). hAFS-EV treatment mimicked the whole secretome effects, on WT1+ GFP+ EPDC, as increasing them by 2.2- and 2.1-fold related to control and hAFS-DM treated mice, respectively (*p<0.05 both), with no difference over hAFS-CM (p>0.05 [Fig.21A]).

BrdU-positive cycling cardiomyocytes were also found at 7 days post MI in control conditions as few scattered GFP-negative cells which doubled following either hAFS-CM or hAFS-EV stimulation (*p<0.05), with no considerable difference between the two treatments (p>0.05); in particular, hAFS-CM showed once more to be more effective than hAFS-DM (*p<0.05), which did not contribute significantly [Fig.21B].

Despite WT1+ GFP+ EPDC substantial reactivation driven by the hAFS secretome, histological analysis performed both at 7 and 28 days after MI on heart sections of inducible $Wt1^{CreERT2/+}$;$R26R^{mTmG/+}$ mice treated with either hAFS-CM, hAFS-DM or hAFS-EV over vehicle solution, revealed that the stimulated CPC did not mature into any

cardiovascular phenotype, but remained confined into the expanded subepicardial space. Indeed, GFP+ WT1+ EPDC decreased at 28 days after MI and we did not detect any PECAM-1- or αSMA- or cTnI-positive cell expressing GFP in the cardiac tissue [Fig.21C-D], suggesting that reactivation of quiescent adult EPDC by restoration of WT1 expression did not result into direct commitment into vascular or cardiomyocyte lineages.

The hAFS secretome might act via paracrine cascade on resident cardiac cells

In order to understand whether the hAFS secretome could act via the reactivation of resident EPDC, which in turn can modulate the cardiac microenvironment and contribute to the beneficial paracrine effects observed, we primed in vitro adult human EPDC with hAFS-CM and then used the resulting hEPDC-CM in a matrigel in vitro angiogenesis assay with HUVEC [Fig.22A]. hEPDC-CM obtained without any priming by the hAFS secretome was not particularly effective in sustaining HUVEC tubulogenesis in terms of TLS length and number of junctions developed, compared to cells grown in angiogenic medium (**$p<0.05$). $^{hAFS\text{-}CM\ primed}$hEPDC-CM increased HUVEC capillary TLS length; junctions and number of branches over unprimed hEPDC-CM treatment (*$p<0.05$; ****$p< 0.0001$; **$p<0.01$, respectively), with values comparable to those obtained in the positive control culture conditions ($p>0.05$). Then we analyzed the cytokine and chemokine profile of hAFS secretome-primed versus un-primed hEPDC-CM [Fig.22B]. Priming with the whole hAFS secretome resulted in a positive trend in the enrichment of plasminogen activator inhibitor-1 (PAI-1), interleukin-8 (IL-8), insulin like growth factor binding protein 2 (IGFBP-2), interleukin-4 (IL-4), interleukin-22 (IL-22), osteopontin (OPN), EMMPRIN, and to a less extent of stromal cell-derived factor 1-alpha (SDF-1α) angiopoietin-2 (ANGPT-2), monocyte chemotactic protein-1 (MCP-1), fibroblast growth factor-19 (FGF-19). hAFS-DM influenced

the hEPDC secretome comparably, but with higher enhancement of MCP-1 expression [Supplementary Table 1].

Since hAFS-CM treatment presented definite advantage over hAFS-DM in triggering resident cardiomyocyte proliferation at 7 and 28 days following injury, we further evaluated whether such influence could be mediated by hAFS-EV-dependent paracrine horizontal transfer of specific microRNAs (miRNA) into the target myocardial tissue. Indeed, a previous study from our group recently showed that hAFS-EV are loaded with regenerative miRNA(Balbi et al., 2017), including some regulating cell cycle re-entry of adult mature cardiomyocyte(Arif et al., 2017)(Ibrahim et al., 2014). 3 hours after MI and hAFS-EV administration via intra-myocardial injection, PKH67+ EV were traced into the myocardium and gene expression profile analysis revealed a positive trend in the up-regulation of the cardio-active miRNAs miR-210, miR-199a-3p, with more specific enhancement of miR-146a (*$p<0.05$) within the cardiac tissue [Fig.22C].

The hAFS secretome chemokine and cytokine profiling

Following chemokine and cytokine profiling, we found that hAFS secretome contains several trophic factors, such as: growth differentiation factor 15 (GDF-15), MCP-1, OPN, FGF-19; IL-6, IL-8, OPN, macrophage migration inhibitory factor (MIF) and IL-11. Notably, hypoxic preconditioning of hAFS led to a positive trend in the enrichment within their secretome (hypoxic hAFS-CM) of the following soluble factors, when compared to control normoxic hAFS-CM: IL-8, IL-6, OPN. FGF-19, MCP-1 and GDF-15 were enhanced by 2- up to almost 9-fold, while MIF and IL-11, were expressed to a less extent and IL-17a, SFD-1α and PAI-1 similarly, [Fig.23] and [Supplementary Table 2]. Notably, hypoxic hAFS-CM was also supplemented with EMMPRIN and IGFBP-2, which were not detectable in the normoxic counterpart.

Figures

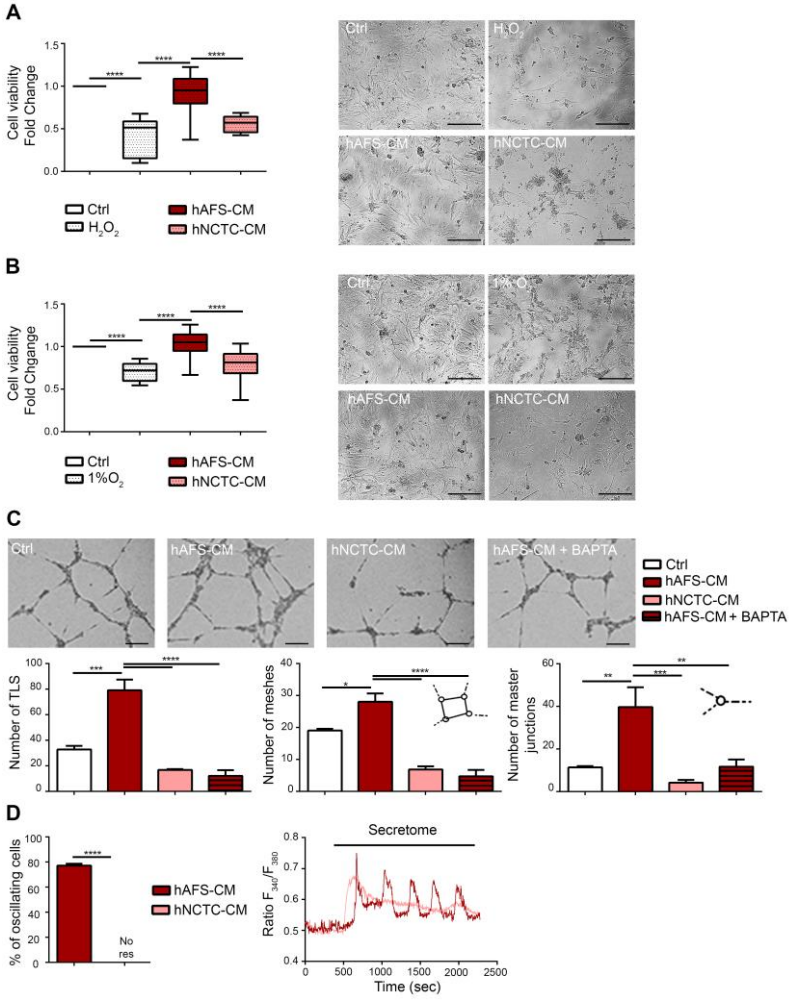

Figure 17. Cardioprotective and angiogenic paracrine effects driven by the hAFS secretome in vitro.

A) mNVCM viability following 150µM H_2O_2 oxidative stress (H_2O_2) with or without pre-incubation with 80µg/ml of hAFS-CM or hNCTC-CM, compared to untreated cells (Ctrl) and evaluated by MTT assay. All values are expressed as mean ± s.e.m of n=3 experiments as fold

change over Ctrl condition (H_2O_2: 0.41±0.07; hAFS-CM: 0.93±0.05; hNCTC-CM: 0.56±0.03; ****p<0.0001). On the right, mNVCM representative pictures: untreated cells (Ctrl), cells exposed to oxidative stress (H_2O_2), cells pre-incubated with hAFS-CM and exposed to oxidative stress (hAFS-CM), and cells pre-incubated with hNCTC-CM and exposed to oxidative stress (hNCTC-CM); scale bar 100µm. **B)** mNVCM viability after exposure to 1%O_2 hypoxic injury, with or without pre-incubation with 80µg/ml of hAFS-CM or hNCTC-CM, compared to untreated cells (Ctrl) and evaluated by MTT assay. All values are expressed as mean ± s.e.m of n=3 experiments as fold change over Ctrl condition (1%O_2: 0.71±0.02; hAFS-CM: 1.04±0.03; hNCTC-CM: 0.78±0.05; ****p<0.0001). On the right, representative pictures of mNVCM: untreated cells (Ctrl), cells exposed to 1%O_2 (1%O_2), cells pre-incubated with hAFS-CM and exposed to 1%O_2 (hAFS-CM) and cells pre-incubated with hNCTC-CM and exposed to 1%O_2 (hNCTC-CM); scale bar 100µm**. C)** Tubulogenesis assay by hECFC with or without (Ctrl) treatment with 80µg/ml of hAFS-CM (hAFS-CM), hNCTC-CM (hNCTC-CM) or hAFS-CM in presence of Ca^{2+} signalling inhibitor BAPTA (hAFS-CM + BAPTA). Digital images of endothelial tubes were obtained by bright-field light microscopy 10 hours after plating cells on Matrigel-coated wells. All values are expressed as mean ± s.e.m of n=3 experiments. From left to right: number of total TLS per picture (Ctrl: 32.67±2.91; hAFS-CM: 79.00±8.41; hNCTC-CM: 16.80±0.58; hAFS-CM+BAPTA: 12.00±4.62; ***p<0.001, p=0.0001, ****p<0.0001); number of meshes per picture (Ctrl: 19.00±0.58; hAFS-CM: 28.00±2.65; hNCTC-CM: 6.80±1.02; hAFS-CM+BAPTA: 4.67±2.03; *p<0.05, (p=0.0185), ****p<0.0001<); number of master junctions per pictures (Ctrl: 11.33±0.67; hAFS-CM: 39.67±9.26; hNCTC-CM: 4.2±1.24; hAFS-CM+BAPTA: 11.67±3.33; **p<0.01, (p=0.0059), ***p<0.001, (p=0.0005), hNCTC-CM versus hAFS-CM; §§p<0.01, (p=0.0064), hAFS-CM + BAPTA versus hAFS-CM). **D)** Percentage of hECFC displaying an oscillatory increase in [Ca^{2+}] in response to different

treatement; all values are expressed as mean ± s.e.m of n=195 cells for hAFS-CM and 102 cells for hNCTC-CM. (hAFS-CM: 77.23±1.48; hNCTC-CM: no response; ****p<0.0001). Right panel: representative tracings of the increase in $[Ca^{2+}]_i$ induced by secretome treatment in hECFC. *Ctrl: control untreated cells; H_2O_2: hydrogen peroxide; hAFS-CM: human Amniotic Fluid Stem Cell-Conditioned Medium; hNCTC-CM: human keratinocyte NCTC cell-Conditioned Medium; hECFC: human Endothelial Colony Forming Cells; TLS: Tube-Like Structure length.*

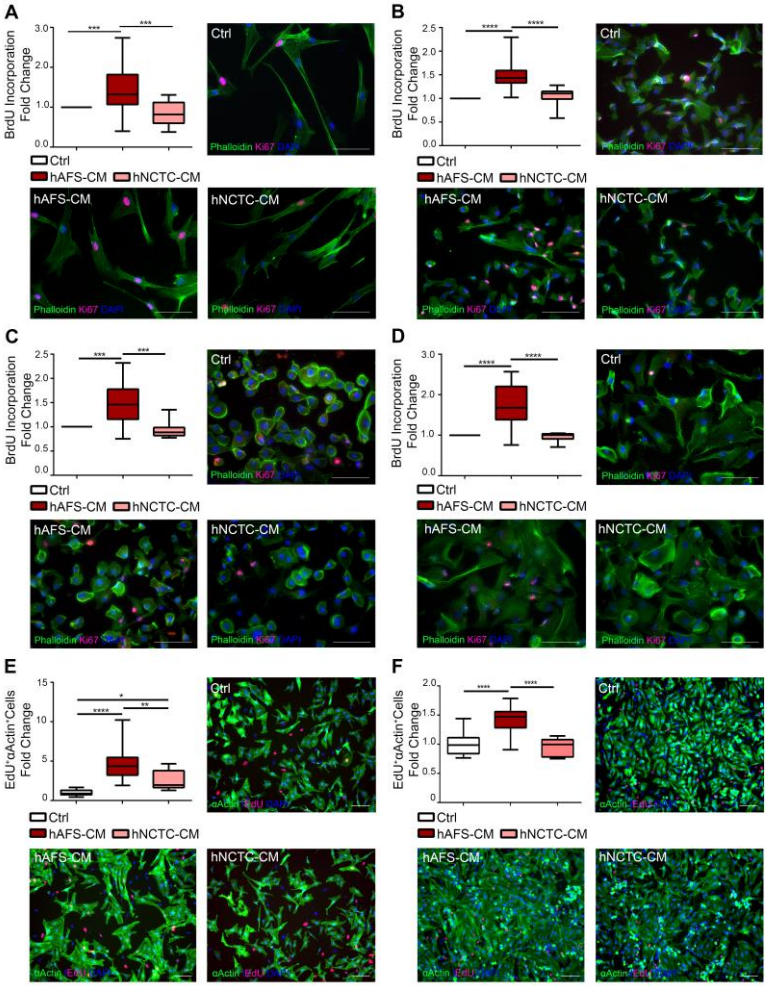

Figure 18. In vitro proliferative paracrine effects on human CPC and rat NVCM by hAFS secretome

A-D) Evaluation of proliferative response from different CPC subpopulations after treatment with 80µg/ml of either hAFS-CM or hNCTC-CM, compared to untreated cells (Ctrl) by BrdU ELISA. All values are expressed as mean ± s.e.m of at least n=3 experiments as fold change over Ctrl condition, with representative pictures of cells in control conditions (Ctrl) or following treatment with either hAFS-CM (hAFS-CM) or hNCTC-CM (hNCTC-CM) stained with KI67 (pink), Phalloidin (Green) and DAPI (Blue); scale bar 200µm in all pictures but for A) which is 100µm. **A)** Adult hCPC (hAFS-CM: 1.47±0.11; hNCTC-CM: 0.86±0.09; ***p<0.001, (p=0.0001 hAFS-CM versus Ctrl; p=0.0002 hNCTC versus hAFS-CM). **B)** fSca1+hCPC (hAFS-CM: 1.47±0.05; hNCTC-CM: 1.05±0.07; **** p<0.0001). **C)** Adult hEPDCc (hAFS-CM: 1.50±0.07; hNCTC-CM: 0,94±0.06. ***p<0.001, p=0.0003, hAFS-CM versus Ctrl and p=0.0002 as versus hNCTC-CM). **D)** Adult hEPDCs (hAFS-CM: 1.70±0.09; hNCTC-CM: 0.96±0.03; ****p<0.0001). **E-F)** Analysis of proliferation of rNVCM exposed to 80µg/ml of either hAFS-CM or hNCTC-CM compared to untreated cells (Ctrl). All values are expressed as mean ± s.e.m of at least n=3 experiments and evaluated as fold change over control condition (Ctrl) of EdU- and α cardiac actin-positive cells with representative pictures of cells in control conditions (Ctrl) or following treatment with either hAFS-CM (hAFS-CM) or hNCTC-CM (hNCTC-CM) stained with EdU (red), cardiac αActin (Green) and DAPI(Blue), scale bar 100µm**. E)** rNVCM isolated from 2-days-old rat hearts, n=3 experiments (Ctrl: 1.00±0.09; hAFS-CM: 4.63±0.34; hNCTC-CM: 2.60±0.43; ****p<0.0001, **p<0.01, p=0.0028, *p<0.05, p=0.0407). **F)** rNVCM isolated from 5-days-old rat hearts, n= 3 experiments (Ctrl: 1.00±0.07; hAFS-CM: 1.43±0.05; hNCTC-CM: 0.96±0.05 ****p<0.0001).

BrDU: 5-Bromo-2'-DeoxyUridine; EdU: 5-Ethynyl-2´-deoxyUridine; αActin: cardiac alpha actin; DAPI: 4',6-DiAmidino-2-PhenylIndole.

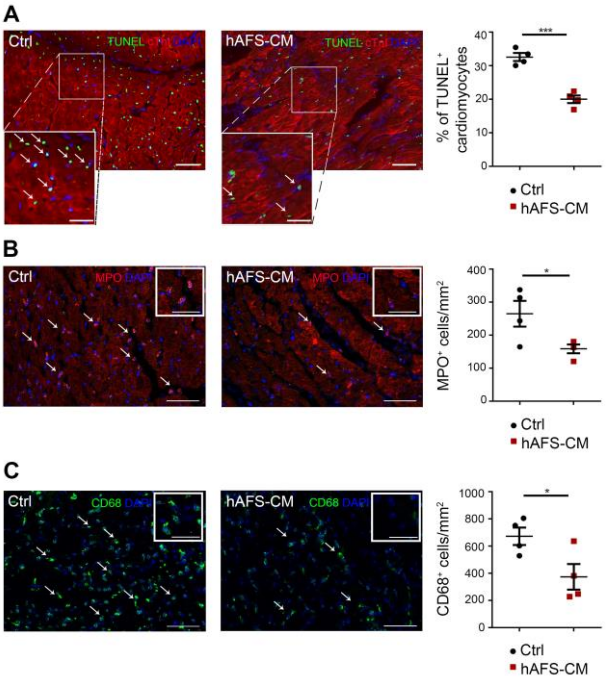

Figure 19. hAFS secretome provides cardioprotection and curbs acute inflammation in the short term after myocardial infarction.

A) Representative images and evaluation of apoptotic cardiomyocytes as detected by TUNEL assay in the myocardial tissue 24h post MI following 100µg hAFS-CM (hAFS-CM) intra-myocardial delivery versus serum-free vehicle-treated animals (Ctrl). All values are expressed as mean ± s.e.m and evaluated as percentage of TUNEL-positive cells over total cells (Ctrl: 32.57±1.20%, n=4; hAFS-CM: 20.01±1.15%, n=4; ***p<0.001, p=0.0003). On the left: representative image of cardiac tissue stained for TUNEL (green, nuclei), cTnT (red) and DAPI (blue). Scale bar: 100µm and 50µm inlet magnification. **B-C)** Assessment of inflammatory cells infiltrating the cardiac tissue at 24h post MI following 100µg hAFS-CM (hAFS-CM) treatment versus serum free vehicle-treated animals (Ctrl). All values are expressed as mean ± s.e.m and evaluated as percentage of MPO-positive neutrophils or CD68-positive

macrophages over total cells. **B)** Infiltrating neutrophils (Ctrl: 264.60±38.89 MPO^+ cells/mm^2, n=4; hAFS-CM: 158.50±13.28 MPO^+ cells/mm^2, n=3; *p<0.05, p=0.0416). On the left: representative image of cardiac tissue 24h post MI stained for MPO (red) and DAPI (blue). **C)** Infiltrating macrophages (Ctrl: 672.60±63.94 $CD68^+$ cells/mm^2, n=4; hAFS-CM 374.00±93.96 $CD68^+$ cells/mm^2, n=4; *p<0.05, p=0.0392). On the left: representative image of myocardium at 24h post MI stained for CD68 (green) and DAPI (blue). Scale bars: 50µm and 25µm inlet magnification. *TUNEL: Terminal deoxynucleotidyl transferase dUTP Nick End Labeling; MPO: MyeloPerOxidase.*

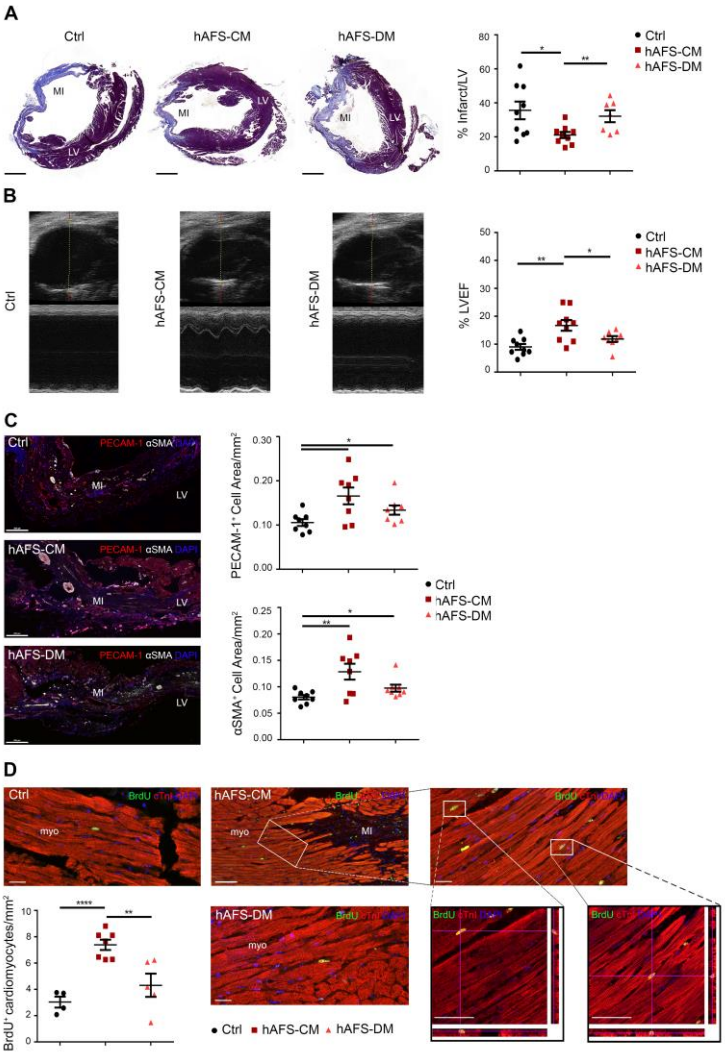

Figure 20. hAFS secretome enhances cardiac repair, rescue cardiac function and support myocardial renewal following myocardial infarction .

A) Analysis of pathological remodelling 28 days post MI following 100µg hAFS-CM (hAFS-CM) or 100µg hAFS-DM (hAFS-DM) intra-myocardial injection compared to serum-free vehicle-treated animals

(Ctrl). Infarct fibrotic scar has been evaluated as percentage of collagen scar area over total left ventricle by Masson's Trichrome staining. All values are expressed as mean ± s.e.m (Ctrl: 35.61±5.17%, n=9; hAFS-CM: 21.13±1.82%, n=9; hAFS-DM: 32.19±3.51%, n=7, *p<0.05, p=0.0178, and **p<0.01, p=0.0098); scale bar 1000 µm. **B)** Evaluation of cardiac function via ultrasounds echocardiography analysis via the measurement of the percentage of left ventricular ejection fraction (%LVEF) in mice at 28 days post MI following 100µg hAFS-CM (hAFS-CM) or 100µg hAFS-DM (hAFS-DM) intra-myocardial injection compared to serum-free vehicle-treated animals (Ctrl). All values are expressed as mean ± s.e.m (Ctrl: 8.97±1.04%, n=9; hAFS-CM 16.69±1.92%, n=9; hAFS-DM 11.82±1.05%, n=9; **p<0.01, p=0.0027, and *p<0.05, p=0.0487). On the left handside: representative image of the heart during ultrasound analysis. **C)** Analysis of local angiogenesis via assessment of PECAM-1 and αSMA-positive cell area and in the infarct border area in mice at 28 days post MI following 100µg hAFS-CM (hAFS-CM) or 100µg hAFS-DM (hAFS-DM) intra-myocardial injection compared to serum-free vehicle-treated animals (Ctrl). All values are expressed as mean ± s.e.m (upper panel, Ctrl: 0.11±0.01 PECAM-1$^+$ cell area/mm^2, n=8; hAFS-CM: 0.17±0.02 PECAM-1$^+$ cell area/mm^2, n=8; hAFS-DM: 0.13±0.01 PECAM-1$^+$ cell area/mm^2, n=7; *p<0.05, p=0.0115 and p=0.0493; lower panel, Ctrl: 0.08±0.004 αSMA$^+$ cell area /mm^2, n=8; hAFS-CM: 0.13±0.02 αSMA$^+$ cell area /mm^2, n=8; hAFS-DM: 0.10±0.01 αSMA$^+$ cell area /mm^2, n=8; **p<0.01, p=0.0081 and *p<0.05, p=0.0466). On the left: representative images of border area cardiac tissue stained for PECAM-1 (red); αSMA (white) and DAPI (blue); scale bar: 50 µm. **D)** Assessment of cardiomyocyte proliferation as detected by BrdU incorporation via co-expression with cTnI at 28 days post MI following 100µg hAFS-CM (hAFS-CM) or 100µg hAFS-DM (hAFS-DM) intra-myocardial injection compared to serum-free vehicle-treated animals (Ctrl). All values are expressed as mean ± s.e.m (Ctrl: 3.03±0.42 BrdU$^+$ cardiomyocytes/mm^2, n=4, hAFS-CM:

7.38±0.39 BrdU^{+} cardiomyocytes/mm^{2}, n=7; hAFS-DM: 4.31±0.88 BrdU^{+} cardiomyocytes/mm^{2}, n=5; ****p<0.0001 and **p<0.01, p=0.0053). Representative images of border area myocardial tissue stained for cTnI (red); BrdU (green) and DAPI (blue). Scale bar: 50µm and 100µm. Inlet magnifications showing confocal microscopy analysis of BrDu+ nuclei. *MI: Myocardial Infarct; LV: Left Ventricle; LVEF: Left Ventricle Ejection Fraction; PECAM-1: Platelet and Endothelial Cell Adhesion Molecule-1; αSMA: alpha Smooth Muscle Actin.*

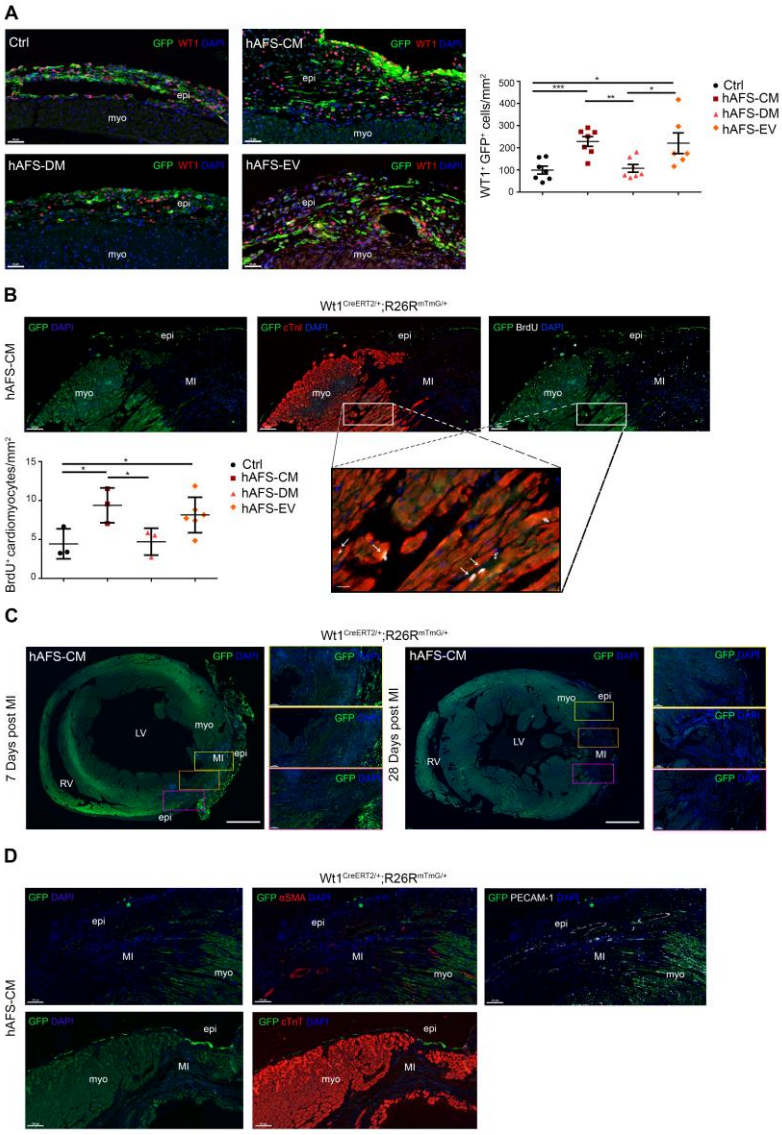

Figure 21. hAFS secretome triggers endogenous regenerative mechanisms from within the heart, including WT1+ EPDC activation.

A) Re-activated WT1+ EPDC traced by GFP genetic labelling in Wt1CreERT2/+;R26RmTmG/+ mice at 7 days post MI following intra

myocardial injection of either 100µg hAFS-CM (hAFS-CM) or hAFS-DM (hAFS-DM) or 4.5 µg hAFS-EV (hAFS-EV) versus serum-free vehicle-treated animals (Ctrl). All values are expressed as mean ± s.e.m (right panel, Ctrl: 98.92±17.80 $WT1^+$ GFP^+ cells/mm^2, n= 7; hAFS-CM: 228.40±22.20 $WT1^+$ GFP^+ cells/mm^2, n= 7; hAFS-DM: 107.20±17.31 $WT1^+$ GFP^+ cells/mm^2, n= 6; hAFS-EV: 220.80±46.64 $WT1^+$ GFP^+ cells/mm^2, n= 5, ***p<0.001, p=0.0007; *p<0.05, p=0.0251 and p=0.0336, and **p<0.01, p=0.001); left panel: representative images of heart tissue 7 days post MI stained for WT1 (red); GFP (green) and DAPI (blue), scale bar: 50µm. **B)** Representative images of hAFS-CM treated-cardiac tissue from $Wt1^{CreERT2/+}R26R^{mTmG/+}$ mice at 7 days post MI showing no expression for GFP (green) in cTnI-(red) and BrDU-positive (white nuclei) cardiomyocytes in the infarct border area, scale bar 100 µm and 50 µm in the inlet magnification. Left panel, evaluation of GFP-negative BrDU-positive resident cardiomyocytes at 7 days post MI following intra-myocardial injection of either 100µg hAFS-CM (hAFS-CM) or hAFS-DM (hAFS-DM) or 4.5µg hAFS-EV (hAFS-EV) versus serum-free vehicle-treated animals (Ctrl). All values are expressed as mean ± s.e.m (Ctrl: 4.44±1.11 $BrdU^+$ cardiomyocytes/mm^2, n= 3; hAFS-CM: 9.39±1.29 $BrdU^+$ cardiomyocytes/mm^2, n= 3; hAFS-DM: 4.72±1.00 $BrdU^+$ cardiomyocytes/mm^2, n= 3; hAFS-EV: 8.15±0.93 $BrdU^+$ cardiomyocytes/mm^2, n= 6; *p<0.05, p=0.0442, p=0.0471 and p=0.0462). **C)** Representative pictures of $Wt1Cre^{ERT2/+}R26R^{mTmG/+}$ mouse heart sections showing $WT1^+$ EPDC reactivation as assessed by GFP staining (green) within 7 days post MI and their decrease at 28 days following injury. $WT1^+$ GFP^+ EPDC remained confined in the epicardial and sub-epicardial area as shown by inlet magnifications of the border and infarct area; scale bar: 1000 µm and 100 µm in inlet magnifications. **D)** Representative images of infarct border area within the hearts of hAFS-CM treated $Wt1^{CreERT2/+}R262^{mTmG/+}$ mice at 28 days post MI showing no co-expression of GFP (green) with either αSMA

(red), PECAM-1 (white) or cTnT (red); scale bar: 100 µm. Green star indicating few WT1⁺ GFP⁺ EPDC in the epicardium. *Epi: Epicardium; Myo: Myocardium; hAFS-EV: human Amniotic Fluid Stem cells-Extracellular Vesicles; MI: Myocardial Infarct.*

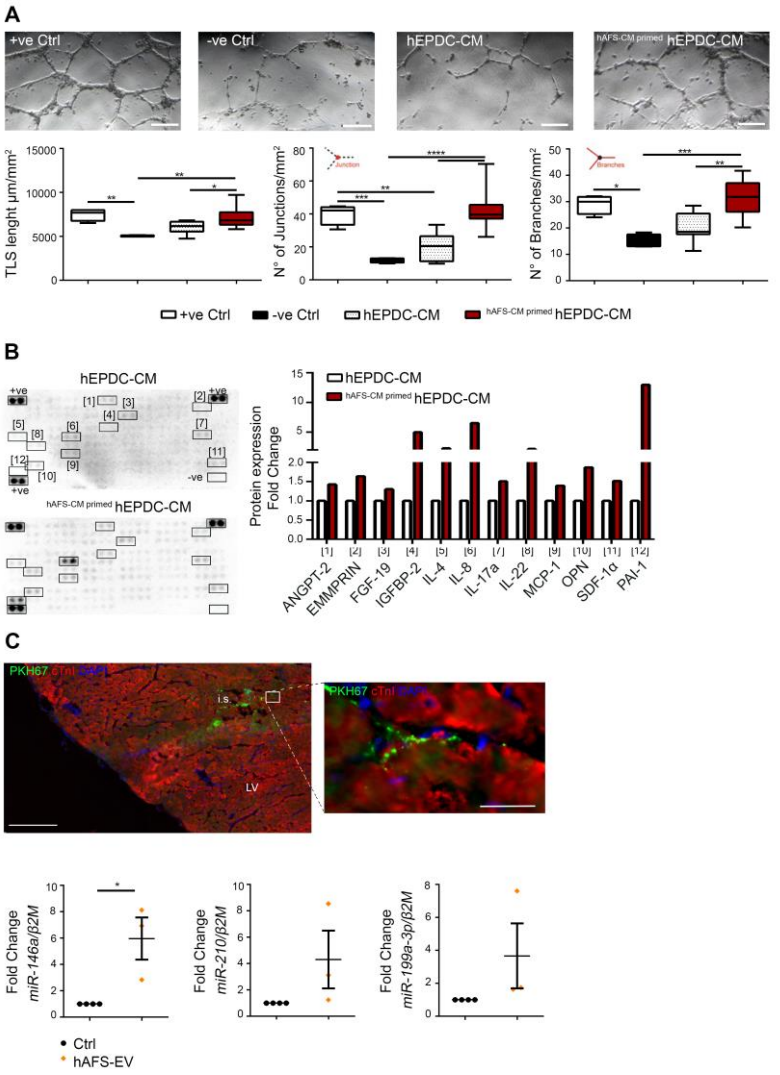

Figure 22. Putative mechanism of action: paracrine cascade and exosomal miRNA horizontal transfer

A) In vitro HUVEC tubologenesis assay following incubation with: human EPDC-conditioned medium (hEPDC-CM) or with hEPDC-CM obtained after priming hEPDC in vitro with hAFS-CM ($^{hAFS\text{-}CM\ primed}$hEPDC-CM), compared to cells grown in EGM-2 endothelial medium as positive control (+ve Ctrl) or to cells grown in 1% FBS hEPDCs medium (-ve Ctrl). Representative digital images of endothelial tube formation were obtained by bright-field light microscopy 18 hours after plating cells in Matrigel, scale bar: 50 μm. Lower panel, evaluation of TLS, junction and branches developed by HUVEC. All values are expressed as mean ± s.e.m (TLS total length, n=4 experiments; +ve Ctrl: 7489±341.4 μm/mm^2, -ve Ctrl: 5044±39.34 μm/mm^2, hEPDC-CM: 6011±266.1 μm/mm^2, $^{hAFS\text{-}CM\ primed}$hEPDC-CM: 7147±282.3 μm/mm^2, *p<0.05, p=0.0436, **p<0.01, p=0.0028 and p=0.0013); number of junctions, n=4 experiments, +ve Ctrl: 39.81±3.14 junctions/mm^2, -ve Ctrl: 11.89±0.70 junctions/mm^2, hEPDC-CM: 19.32±3.26 junctions/mm^2, $^{hAFS\text{-}CM\ primed}$ hEPDC-CM: 41.96±2.72 junctions/mm^2, **p<0.01, p=0.005, ***p<0.001, p=0.0007, ****p<0.0001; number of branches, n=4 experiments, +ve Ctrl: 28.99±1.77 branches/mm^2; -ve Ctrl: 14.99±1.22 branches/mm^2, hEPDC-CM: 20.36±2.16 branches/mm^2; $^{hAFS\text{-}CM\ primed}$ hEPDC-CM: 31.24±1.79 branches/mm^2;; *p<0.05, p=0.0109, **p<0.01, p=0.0022, and **p<0.001, p=0.0002. **B)** Cytokine and chemokine array of unprimed hEPDC-Conditioned Medium (hEPDC-CM), $^{hAFS\text{-}CM\ primed}$ hEPDC-CM assessed by quantification of positive pixels for each selected cytokine. Left panel: representative images of array membranes in which numbers indicate the corresponding chemokine/cytokine as reported in the graph below. Values are expressed as fold change compared to hEPDC-CM and reported in Supplementary Table 1 **C)** Horizontal transfer of hAFS-EV and their exosomal miRNA content into myocardial tissue at 3 hours following intra-myocardial injection and MI, as measured by real time qRT-PCR for human *miR-146a*; *miR-210* and *miR-199a* expression over beta 2

microglobulin as house-keeping reference gene. Values are expressed as fold change mean ± s.e.m of *miR-146a*; *miR-210* and *miR-199a* expression in hAFS-EV injected versus serum free vehicle-treated animals (*miR-146a*, Ctrl: 1; hAFS-EV: 5.97±1.60, *p<0,05, p=0.014 n=3; *miR-210*: Ctrl: 1; hAFS-EV: 4.30±2.19 n=3; *miR-199a*: Ctrl: 1; hAFS-EV: 3.67±1.97 n=3). Upper panel: representative images showing PKH67-positive myocardial tissue following hAFS-EV treatment 3 hours post MI, scale bar: 200 µm and 20µm. *HUVEC: Human Umbilical Vein Endothelial Cells; +ve Ctrl: positive control; +ve: positive reference control; -ve: negative reference control; β2M: beta2 Microglobulin; i.s.: injection site.*

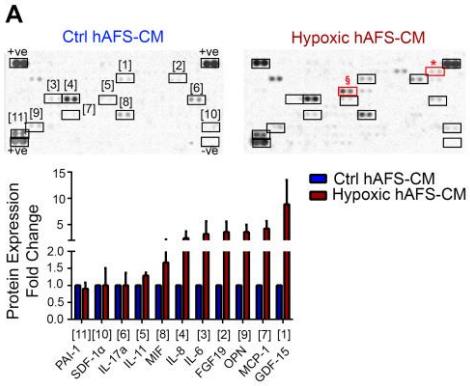

Figure 23. Cytokine and chemokine profiling of the hAFS secretome

A) Cytokine and chemokine array of hypoxic hAFS secretome (Hypoxic hAFS-CM) compared to normoxic control one (Ctrl hAFS-CM) assessed by quantification of positive pixels for each selected cytokine. Upper panel: representative images of array membranes in which numbers indicate the corresponding chemokine/cytokine as reported in the graph below. Red boxes indicated EMMPRIN (*) and IGFBP-2 (§), which are not expressed by Ctrl hAFS-CM. Values are expressed as fold change of Hypoxic hAFS-CM over Ctrl hAFS-CM and reported in

Supplementary Table 2. *+ve: positive reference control; -ve: negative reference control.*

SUPPLEMENTARY MATERIALS

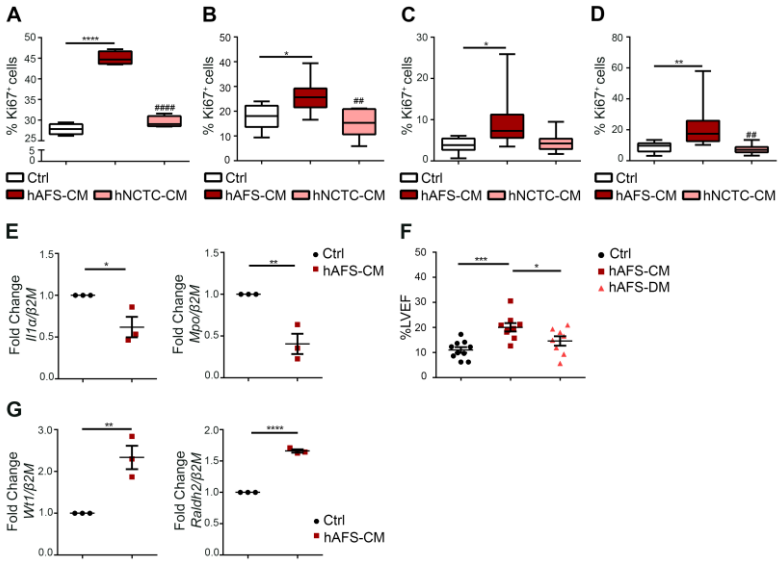

Supplementary Figure 1

A-D) Evaluation of proliferative response from different CPC subpopulations after treatment with 80µg/ml of either hAFS-CM or hNCTC-CM, compared to untreated cells (Ctrl) by Ki67 staining. All values are expressed as mean ± s.e.m of the percentage of Ki67-positive cells, n=3 experiments. **A)** Adult hCPC (Ctrl: 27.82±0.66%; hAFS-CM: 45.01±0.82%; hNCTC-CM: 29.50±0.71%. **** and ####p<0.0001 refers to hAFS-CM versus hNCTC-CM). **B)** fSca1+hCPC (Ctrl: 17.73±2.13%; hAFS-CM: 26.52±1.46%; hNCTC-CM: 15.13±2.44%. *p<0.05 p=0.011; ##p<0.01, p=0.0011, refers to hAFS-CM versus hNCTC-CM). **C)** Adult hEPDCc (Ctrl: 3.87±0.60%; hAFS-CM: 9.57±1.23%; hNCTC-CM: 4.52±0.95%; *p<0.05, p=0.0131). **D)** Adult hEPDCs (Ctrl: 8.83±1.19%; hAFS-CM: 21.17±2.08%; hNCTC-CM: 7.37±1.01%; **p<0.01, p=0.0083; ##p<0.01, p=0.0018, refers to hAFS-CM versus hNCTC-CM). **E)** Real Time qRT-PCR showing significant down-regulation of *Mpo* and *Il1α* expression in the hearts

treated with hAFS-CM at 24h post MI, compared to the serum free vehicle-treated animals (Ctrl). Values are expressed as mean ± s.e.m. fold change of *Mpo* and *Il1α* expression compared to β2M as house keeping reference gene (*Il1α*: n=3, Ctrl:1; hAFS-CM: 0.62±0.12; *p<0.05, p=0.0354; *Mpo*: n=3, Ctrl:1; hAFS-CM: 0.41±0.12; **p<0.01 p=0.0079). **F)** Cardiac function analysis via ultrasounds echocardiography by measurement of left ventricular ejection fraction percentage (%LVEF) in mice at 7 days post MI following either 100µg hAFS-CM (hAFS-CM) or 100µg hAFS-DM (hAFS-DM) intra-myocardial injection compared to serum-free vehicle-treated animals (Ctrl). All values are expressed as mean ± s.e.m (Ctrl: 10.99±1.13%, n=10; hAFS-CM 20.02±1.66%, n=8; hAFS-DM 14.58±1.86%, n=8. ***p<0.001, p=0.0001; *p<0.05, p=0.0446). **G)** Real Time qRT-PCR showing significant up-regulation of *Wt1* and *Raldh2* expression in the heart treated with hAFS-CM 7 days post MI, compared to the serum free vehicle-treated animals (Ctrl). Values are expressed as mean ± s.e.m. fold change of *Wt1* and *Raldh2* expression compared to β2M as house keeping reference gene (*Wt1*: n=3, Ctrl:1; hAFS-CM: 2.33±0.28; **p<0.01, p=0.0089; *Raldh2*: n=3, Ctrl:1; hAFS-CM: 1.66±0.03; ****p<0.0001 n=3). *Il1α: Interleukin-1 alpha; β2M: beta 2 Microglobulin; Mpo: MyeloPerOxidase; Wt1: Wilms' Tumor 1; Raldh2: Retinaldehyde dehydrogenase 2.*

Supplementary Table 1. Cytokine and chemokine profiling of hEPDC secretome primed with either hAFS-CM or hAFS-DM.

	hEPDC-CM	**hAFS-CM primed hEPDC-CM**
ANGPT-2	1	1.42
FGF-19	1	1.30
MCP-1	1	1.39

IL-17	1	1.51
SDF-1α	1	1.52
EMMPRIN	1	1.64
OPN	1	1.87
IL-22	1	2.16
IL-4	1	2.24
IGFBP-2	1	4.96
IL-8	1	6.54
PAI-1	1	12.99

Values are assessed by quantification of positive pixels for each selected cytokine on the array membrane and are expressed as mean of fold change cytokine/chemokine expression over control un-primed hEPDC conditioned medium (hEPDC-CM). ANGPT-2: Angiopoietin-2; EMMPRIN: Extracellular Matrix MetalloPRoteinase Inducer; FGF-19: Fibroblast Growth Factor 19; IGFBP-2: Insulin like Growth Factor Binding Protein-2; IL-4: Interleukin-4; IL-8: Interleukin-8; IL-17a: Interleukin-17a; IL-22: Interleukin-22; MCP-1: Monocyte Chemotactic Protein-1; OPN: Osteopontin; SDF-1α: Stromal cell-Derived Factor 1-alpha; PAI-1: Plasminogen Activator Inhibitor-1.

Supplementary Table 2. Cytokine and chemokine profiling of hAFS secretome obtained following hypoxic preconditioning and compared to normoxic conditions (Ctrl hAFS-CM).

	Ctrl hAFS-CM	**Hypoxic hAFS-CM**
PAI-1	1	0.91±0.18
IL-17a	1	1.00±0.36
SDF-1α	1	1.00±0.50
IL-11	1	1.29±0.1

MIF	1	1.67±0,50
IL-8	1	2.40±1.31
IL-6	1	3.20±2.41
OPN	1	3.55±1.43
FGF-19	1	3.58±1.98
MCP-1	1	4.23±2.51
GDF-15	1	8.87±4.64

Values are assessed by quantification of positive pixels for each selected cytokine on the array membrane and are expressed as mean of fold change cytokine/chemokine expression of hypoxic hAFS secretome (Hypoxic hAFS-CM) over control normoxic hAFS-CM (Ctrl hAFS-CM); FGF-19: Fibroblast Growth Factor 19; GDF-15: Growth/differentiation factor 15; IL-6: Interleukin-6; IL-11: Interleukin-11;IL-17a: Interleukin- 17a; MCP-1: Monocyte Chemotactic Protein-1; MIF: Macrophage migration inhibitory factor; OPN: Osteopontin; SDF-1α: Stromal cell-Derived Factor 1-alpha; PAI-1: Plasminogen Activator Inhibitor-1.

DISCUSSION

These data provide robust evidence, gathered from different *in vitro* and *in vivo* models, suggesting that the hAFS secretome is endowed with appealing paracrine cardio-active potential for future cardiovascular regenerative medicine.

The cardioprotective profile of the whole hAFS secretome obtained following hypoxic preconditioning of the cells, namely the hypoxic hAFS-CM, has here been confirmed also in chemotherapy-induced cardiotoxicity model, as demonstrating to effectively neutralises doxorubicin collateral damage on both CPC and cardiomyocytes by increasing their survival and counteracting premature senescence. Notably, hAFS-CM administration resulted in the prompt activation of several synergic responses in the target cells, such as: the decrease of DNA damage response, the increased expression of the Multidrug Resistance Protein 1 encoded by the Abcb1b gene, so to reduced unspecific drug uptake by cardiac cells and a more articulated anti-apoptotic paracrine feedback, mainly based on direct activation of a signaling cascade, starting with the the PI3K/Akt-dependent pathway, via the induction of NF-KB resulting in the trascription of its target genes, the pro-survival cytokines Il6 and Cxcl1, playing a picvotal role. Indeed, IL-6 is released by stressed cardiomyocytes and promotes cardiac cell survival in an autocrine/paracrine fashion (Craig et al., 2000). It acts through several intracellular mediators, including PI3K/Akt (Fahmi et al., 2013)(Smart et al., 2006) which raises the possibility of a feed-forward signalling loop, whereby PI3K/Akt promote the transcription of Il6 and IL-6 activates PI3K/Akt . Furthermore, CXCL1, the murine homologue of IL-8, is an established angiogeneic factor (Lee et al., 1995)(Belo et al., 2005) and has been reported to exert anti-inflammatory and pro-survival effects in a mouse model of autoimmune myocarditis. As doxorubicin-induced left ventricular

dysfunction and heart failure are relatively common and by themselves have clinical burden, cause hospitalization, and carry a risk of mortality (Molinaro et al., 2015)(Lipshultz et al., 2013), our results holds high translational value and great promise for future therapeutic strategies. Indeed, the experiments presented here integrate earlier findings on the cardioprotective potential of hAFS in a acute model of rat ischemia/reperfusion injury (Bollini et al., 2011) and confirm that, in general, the hAFS secretome is a valuable source of pro-survival factors for future cardiac paracrine therapy, extending their application for the prevention not only of ischemic cardiomyopathy but to drug-derived cardiac disease as well. Nevertheless, some limitations of this part of the project must be acknowledged. First, sustained incubation of cardiomyocytes and CPC with the hAFS-CM in the long term has not been investigated. Second, *in vivo* studies on cardiac-specific delivery of the hAFS-CM treatment to antagonize doxorubicin cardiotoxicity are needed in order to evaluate the effects of the hAFS-CM on cardiomyocytes and CPCs while they are in their own microenvironment, which comprises other cell types possibly influenced by the hAFS-CM. This is a critical aspect to address so to exploit the hAFS secretome as a future implementation strategy for cancer therapies by maintaining their specific antitumor effects while counteracting doxorubicin side effects on the cardiac tissue.

EV play critical roles in paracrine inter-cellular crosstalks, as reported by several studies. Here I have showed for the first time strong evidence that hAFS dynamically secrete EV as fundamental mediators of distinct proliferative, anti-apoptotic, immunomodulatory, pro-angiogenic and anti-inflammatory effects. Uptake analysis confirmed the role of hAFS-EV as biological mediators of cell communication via rapid incorporation by the target cells within few hours. More specifically, these results demonstrate that short hypoxic preconditioning of hAFS can be exploited as working strategy to improve the hAFS-EV yield while strengthening their paracrine

potential. Moreover, hAFS-EV and in particular the hypoxic hAFS-EV, possibly mediate significant regenerative effects on responding cells by targeting their post-transcriptional regulation and translational apparatus both by horizontal reprogramming via direct miRNA transfer and by transporting proteins involved in translational elongation, RNA metabolism and gene expression processes. These results have provided new interesting insights on the specific modulatory role of hAFS-EV from within the whole secretome produced by these promising fetal progenitor cells. Notably, hAFS-EV showed specific enrichment of the miR-210 and miR-199a-3p pair, previously reported to be crucial for mediating cardioprotection (Barile et al., 2014), sustaining angiogenesis (Zeng et al., 2014)(Alaiti et al., 2012) and triggering cardiomyocyte proliferation (Eulalio et al., 2012a)(Bodempudi et al., 2014). Therefore, they may represent an appealing tool to be exploited for enhancing cardiac repair and activating cardiac regeneration, following myocardial ischemia.

In light of these evidences, I focused the last part of my PhD project on unveiling the specific role of the whole hAFS secretome (hAFS-CM) over hAFS-EV to unlock true cardiac endogenous regeneration in a preclinical mouse model of myocardial infarct, mainly by evaluating its influence on several mechanisms: enhancement of cardiac repair; re-activation of quiescent WT1+ epicardial progenitor cells and restoration of resident surviving cardiomyocytes.
So far, the results obtained confirmed that not only the whole secretome (hAFS-CM) confirmed its remarkable cardioprotective potential *in vitro*, on cardiomyocytes challenged by hypoxic and oxidative stress, but it also showed to significantly enhance the proliferation of different CPC. Remarkably, a single topical administration of hAFS secretome within the myocardium soon after MI, showed to exert significant beneficial effects on cardiac function, while mediating myocardial protection from apoptosis, increasing

angiogenesis and sustaining cardiomyocyte proliferation up to 4 weeks later. Epicardial WT1+ progenitors, previously shown to significantly contribute to cardiac repair and regeneration either by paracrine modulation of the surrounding microenvironment (Zhou and Pu, 2012) or by direct de novo contribution to cardiovascular lineages, including functionally mature cardiomyocytes (Smart et al., 2011), were significantly stimulated by the hAFS secretome, by increasing their activation and proliferation. Since progenitor cells represents a limited reservoir residing in the cardiac tissue that following suitable paracrine stimulation can actively trigger cardiac regeneration, these results are highly valuable. So far, I've also noticed that administration of the whole secretome, namely hAFS-CM has been more effective than its counterpart depleted of extracellular vesicles (hAFS-DM) in increasing both activation of resident epicardial progenitor cells and general cardiac function. Furthermore hAFS-EV were also tested in the myocardial preclinical model showing an important role in increasing activation of epicardial progenitor cells and proliferation of resident cardiomyocyte.

In this scenario, a significant aspect to take into account is represented by the administration regime of this hAFS secretome paracrine therapy. While the delivery route adopted here represents the more relevant for the clinical scenario (i.e. a single administration within the myocardial tissue via a guided catheter at the time of myocardial infarct would be feasible as the patient undergoes primary percutaneous coronary intervention to open the occluded coronary vessel in the hospital), there is general consensus that stem cell paracrine effect is usually a prompt and short-term response. Hence, to sustain beneficial effects for longer and/or to induce a more articulated and time-consuming response such as the functional differentiation of re-activated epicardial CPC, further evaluation is needed to determine whether either higher-dose or more frequent systemic administration of hAFS-secretome can boost their paracrine potential even more and maintain it over time.

CONCLUSIONS

In conclusion, the results obtained from my PhD project so far substantiate the concept of a stem cell based paracrine approach via the cell-free delivery of bioactive factors to prevent cardiac disease for different pathological scenarios: from chemoterapy induced cardiotoxicity to ischemic injury, such as myocardial infarction.

In addition, they may lay the ground for future research work, using the hAFS secretome as an easily obtainable and appealing source of paracrine cardioactive molecules that can become an advanced medicinal product for new cardiac regeneration strategies, without some of the ethical and technical issues associated with embryonic and adult stem cell use. Indeed, in the quest to find the most suitable stem cell source for future paracrine therapy, important limitations with ES and iPS or bone marrow MSC should not be overlooked: ES are not free of ethical issues, and culture of iPS is technically challenging and quite time-consuming. These drawbacks are not encountered with adult bone marrow MSC, which, however, are obtained by invasive sampling with low yield and present limited self-renewal potential.

By contrast, there is no ethical concern related to hAFS, as they are obtained from the amniotic fluid that is anyway collected by amniocentesis for prenatal screening or at term during scheduled caesarean delivery procedure.

Notably Being hAFS immature foetal cells and developmentally very “young”, they are likely to possess a more powerful paracrine potential than adult stem cells. This is significantly relevant when approaching a challenging field such as cardiac regeneration, which may be achieved by restoring quiescent or defective mechanisms from within the injured adult heart (namely CPC reactivation, cardiomyocyte proliferation and cardiac repair) only by very strong, focused and effective stimulation.

Last, but not least, hAFS, withstand cryopreservation for a long time while maintaining a stable karyotype, which makes their banking and

scale up expansion very feasible, thus representing an ideal paracrine source to be exploited.

REFERENCES

Alaiti, M. A., Ishikawa, M., Masuda, H., Simon, D. I., Jain, M. K., Asahara, T., et al. (2012). Up-regulation of miR-210 by vascular endothelial growth factor in ex vivo expanded CD34+ cells enhances cell-mediated angiogenesis. *J. Cell. Mol. Med.* 16, 2413–21. doi:10.1111/j.1582-4934.2012.01557.x.

Altieri, P., Barisione, C., Lazzarini, E., Garuti, A., Bezante, G. P., Canepa, M., et al. (2016). Testosterone Antagonizes Doxorubicin-Induced Senescence of Cardiomyocytes. *J Am Hear. Assoc* 5. doi:10.1161/JAHA.115.002383.

Arif, M., Pandey, R., Alam, P., Jiang, S., Sadayappan, S., Paul, A., et al. (2017). MicroRNA-210-mediated proliferation, survival, and angiogenesis promote cardiac repair post myocardial infarction in rodents. *J. Mol. Med. (Berl).* 95, 1369–1385. doi:10.1007/s00109-017-1591-8.

Arslan, F., Lai, R. C., Smeets, M. B., Akeroyd, L., Choo, A., Aguor, E. N. E., et al. (2013). Mesenchymal stem cell-derived exosomes increase ATP levels, decrease oxidative stress and activate PI3K/Akt pathway to enhance myocardial viability and prevent adverse remodeling after myocardial ischemia/reperfusion injury. *Stem Cell Res.* 10, 301–312. doi:10.1016/j.scr.2013.01.002.

Bachmaier, K., Toya, S., and Malik, A. B. (2014). Therapeutic administration of the chemokine CXCL1/KC abrogates autoimmune inflammatory heart disease. *PLoS One* 9, e89647. doi:10.1371/journal.pone.0089647.

Balbi, C., Piccoli, M., Barile, L., Papait, A., Armirotti, A., Principi, E., et al. (2017). First Characterization of Human Amniotic Fluid Stem Cell Extracellular Vesicles as a Powerful Paracrine Tool Endowed with Regenerative Potential. *Stem Cells Transl. Med.* 6, 1340–1355. doi:10.1002/sctm.16-0297.

Balmer, G. M., Bollini, S., Dubé, K. N., Martinez-Barbera, J. P., Williams, O., and Riley, P. R. (2014). Dynamic haematopoietic cell contribution to the developing and adult epicardium. *Nat. Commun.* 5, 4054. doi:10.1038/ncomms5054.

Barile, L., Lionetti, V., Cervio, E., Matteucci, M., Gherghiceanu, M., Popescu, L. M., et al. (2014). Extracellular vesicles from human cardiac progenitor cells inhibit cardiomyocyte apoptosis and

improve cardiac function after myocardial infarction. *Cardiovasc. Res.* 103, 530–41. doi:10.1093/cvr/cvu167.

Bekeredjian-Ding, I., Foermer, S., Kirschning, C. J., Parcina, M., and Heeg, K. (2012). Poke weed mitogen requires Toll-like receptor ligands for proliferative activity in human and murine B lymphocytes. *PLoS One* 7, e29806. doi:10.1371/journal.pone.0029806.

Belo, A. V, Leles, F., Barcelos, L. S., Ferreira, M. A. N. D., Bakhle, Y. S., Teixeira, M. M., et al. (2005). Murine chemokine CXCL2/KC is a surrogate marker for angiogenic activity in the inflammatory granulation tissue. *Microcirculation* 12, 597–606. doi:10.1080/10739680500253535.

Bergmann, O., Bhardwaj, R. D., Bernard, S., Zdunek, S., Barnabé-Heider, F., Walsh, S., et al. (2009). Evidence for cardiomyocyte renewal in humans. *Science* 324, 98–102. doi:10.1126/science.1164680.

Bian, S., Zhang, L., Duan, L., Wang, X., Ying, M., and Yu, H. Extracellular vesicles derived from human bone marrow mesenchymal stem cells promote angiogenesis in a rat myocardial infarction model. doi:10.1007/s00109-013-1110-5.

Bobis-Wozowicz, S., Kmiotek, K., Sekula, M., Kedracka-Krok, S., Kamycka, E., Adamiak, M., et al. (2015). Human Induced Pluripotent Stem Cell-Derived Microvesicles Transmit RNAs and Proteins to Recipient Mature Heart Cells Modulating Cell Fate and Behavior. *Stem Cells* 33, 2748–61. doi:10.1002/stem.2078.

Bodempudi, V., Hergert, P., Smith, K., Xia, H., Herrera, J., Peterson, M., et al. (2014). miR-210 promotes IPF fibroblast proliferation in response to hypoxia. *Am. J. Physiol. Lung Cell. Mol. Physiol.* 307, L283-94. doi:10.1152/ajplung.00069.2014.

Bollini, S., Cheung, K. K., Riegler, J., Dong, X., Smart, N., Ghionzoli, M., et al. (2011). Amniotic Fluid Stem Cells Are Cardioprotective Following Acute Myocardial Infarction. *Stem Cells Dev.* 20, 1985–1994. doi:10.1089/scd.2010.0424.

Bollini, S., Gentili, C., Tasso, R., and Cancedda, R. (2013). The Regenerative Role of the Fetal and Adult Stem Cell Secretome. *J. Clin. Med.* 2, 302–327. doi:10.3390/jcm2040302.

Bottai, D., Cigognini, D., Nicora, E., Moro, M., Grimoldi, M. G., Adami, R., et al. (2012). Third trimester amniotic fluid cells with the

capacity to develop neural phenotypes and with heterogeneity among sub-populations. *Restor. Neurol. Neurosci.* 30, 55–68. doi:10.3233/RNN-2011-0620.

Bruno, S., Grange, C., Collino, F., Deregibus, M. C., Cantaluppi, V., Biancone, L., et al. (2012). Microvesicles derived from mesenchymal stem cells enhance survival in a lethal model of acute kidney injury. *PLoS One* 7, e33115. doi:10.1371/journal.pone.0033115.

Cahill, T. J., Choudhury, R. P., and Riley, P. R. (2017). Heart regeneration and repair after myocardial infarction: translational opportunities for novel therapeutics. *Nat. Rev. Drug Discov.* 16, 699–717. doi:10.1038/nrd.2017.106.

Caradec, J., Kharmate, G., Hosseini-Beheshti, E., Adomat, H., Gleave, M., and Guns, E. (2014). Reproducibility and efficiency of serum-derived exosome extraction methods. *Clin. Biochem.* 47, 1286–92. doi:10.1016/j.clinbiochem.2014.06.011.

Chen, E. Y., Tan, C. M., Kou, Y., Duan, Q., Wang, Z., Meirelles, G. V, et al. (2013). Enrichr: interactive and collaborative HTML5 gene list enrichment analysis tool. *BMC Bioinformatics* 14, 128. doi:10.1186/1471-2105-14-128.

Chiavegato, A., Bollini, S., Pozzobon, M., Callegari, A., Gasparotto, L., Taiani, J., et al. (2007). Human amniotic fluid-derived stem cells are rejected after transplantation in the myocardium of normal, ischemic, immuno-suppressed or immuno-deficient rat. *J. Mol. Cell. Cardiol.* 42, 746–59. doi:10.1016/j.yjmcc.2006.12.008.

Connolly, K. D., Guschina, I. A., Yeung, V., Clayton, A., Draman, M. S., Von Ruhland, C., et al. (2015). Characterisation of adipocyte-derived extracellular vesicles released pre- and post-adipogenesis. *J. Extracell. vesicles* 4, 29159. doi:10.3402/jev.v4.29159.

Craig, R., Larkin, A., Mingo, A. M., Thuerauf, D. J., Andrews, C., McDonough, P. M., et al. (2000). p38 MAPK and NF-kappa B collaborate to induce interleukin-6 gene expression and release. Evidence for a cytoprotective autocrine signaling pathway in a cardiac myocyte model system. *J. Biol. Chem.* 275, 23814–24. doi:10.1074/jbc.M909695199.

De Angelis, A., Piegari, E., Cappetta, D., Marino, L., Filippelli, A.,

Berrino, L., et al. (2010). Anthracycline cardiomyopathy is mediated by depletion of the cardiac stem cell pool and is rescued by restoration of progenitor cell function. *Circulation* 121, 276–92. doi:10.1161/CIRCULATIONAHA.109.895771.

De Coppi, P., Bartsch, G., Siddiqui, M. M., Xu, T., Santos, C. C., Perin, L., et al. (2007). Isolation of amniotic stem cell lines with potential for therapy. *Nat. Biotechnol.* 25, 100–106. doi:10.1038/nbt1274.

de Masson, A., Le Buanec, H., and Bouaziz, J.-D. (2014). Purification and immunophenotypic characterization of human B cells with regulatory functions. *Methods Mol. Biol.* 1190, 45–52. doi:10.1007/978-1-4939-1161-5_4.

Deyhle, M. R., Gier, A. M., Evans, K. C., Eggett, D. L., Nelson, W. B., Parcell, A. C., et al. (2016). Skeletal Muscle Inflammation Following Repeated Bouts of Lengthening Contractions in Humans. *Front. Physiol.* 6. doi:10.3389/fphys.2015.00424.

Dragoni, S., Laforenza, U., Bonetti, E., Lodola, F., Bottino, C., Berra-Romani, R., et al. (2011). Vascular Endothelial Growth Factor Stimulates Endothelial Colony Forming Cells Proliferation and Tubulogenesis by Inducing Oscillations in Intracellular Ca2+ Concentration. *Stem Cells* 29, 1898–1907. doi:10.1002/stem.734.

Dragoni, S., Reforgiato, M., Zuccolo, E., Poletto, V., Lodola, F., Ruffinatti, F. A., et al. (2015). Dysregulation of VEGF-induced proangiogenic Ca2+ oscillations in primary myelofibrosis-derived endothelial colony-forming cells. *Exp. Hematol.* 43, 1019–1030.e3. doi:10.1016/j.exphem.2015.09.002.

El-Awady, R. A., Semreen, M. H., Saber-Ayad, M. M., Cyprian, F., Menon, V., and Al-Tel, T. H. (2015). Modulation of DNA damage response and induction of apoptosis mediates synergism between doxorubicin and a new imidazopyridine derivative in breast and lung cancer cells. *DNA Repair* 37, 1–11. doi:10.1016/j.dnarep.2015.10.004.

Eulalio, A., Mano, M., Dal Ferro, M., Zentilin, L., Sinagra, G., Zacchigna, S., et al. (2012a). Functional screening identifies miRNAs inducing cardiac regeneration. *Nature* 492, 376–81. doi:10.1038/nature11739.

Eulalio, A., Mano, M., Ferro, M. D., Zentilin, L., Sinagra, G.,

Zacchigna, S., et al. (2012b). Functional screening identifies miRNAs inducing cardiac regeneration. *Nature* 492, 376–381. doi:10.1038/nature11739.

Fabbi, P., Spallarossa, P., Garibaldi, S., Barisione, C., Mura, M., Altieri, P., et al. (2015). Doxorubicin impairs the insulin-like growth factor-1 system and causes insulin-like growth factor-1 resistance in cardiomyocytes. *PLoS One* 10, e0124643. doi:10.1371/journal.pone.0124643.

Fahmi, A., Smart, N., Punn, A., Jabr, R., Marber, M., and Heads, R. (2013). p42/p44-MAPK and PI3K are sufficient for IL-6 family cytokines/gp130 to signal to hypertrophy and survival in cardiomyocytes in the absence of JAK/STAT activation. *Cell. Signal.* 25, 898–909. doi:10.1016/j.cellsig.2012.12.008.

Fish, J. E., Santoro, M. M., Morton, S. U., Yu, S., Yeh, R.-F., Wythe, J. D., et al. (2008). miR-126 regulates angiogenic signaling and vascular integrity. *Dev. Cell* 15, 272–84. doi:10.1016/j.devcel.2008.07.008.

Gambini, E., Pompilio, G., Biondi, A., Alamanni, F., Capogrossi, M. C., Agrifoglio, M., et al. (2011). C-kit+ cardiac progenitors exhibit mesenchymal markers and preferential cardiovascular commitment. *Cardiovasc Res* 89, 362–373. doi:10.1093/cvr/cvq292.

Gnecchi, M., Zhang, Z., Ni, A., and Dzau, V. J. (2008). Paracrine mechanisms in adult stem cell signaling and therapy. *Circ. Res.* 103, 1204–19. doi:10.1161/CIRCRESAHA.108.176826.

Grisendi, G., Finetti, E., Manganaro, D., Cordova, N., Montagnani, G., Spano, C., et al. (2015). Detection of microparticles from human red blood cells by multiparametric flow cytometry. *Blood Transfus.* 13, 274–80. doi:10.2450/2014.0136-14.

Hanley, F. L., Heinemann, M. K., Jonas, R. A., Mayer, J. E., Cook, N. R., Wessel, D. L., et al. (1993). Repair of truncus arteriosus in the neonate. *J. Thorac. Cardiovasc. Surg.* 105, 1047–56. Available at: http://www.ncbi.nlm.nih.gov/pubmed/8501932 [Accessed December 7, 2016].

Heredia, J. E., Mukundan, L., Chen, F. M., Mueller, A. A., Deo, R. C., Locksley, R. M., et al. (2013). Type 2 innate signals stimulate fibro/adipogenic progenitors to facilitate muscle regeneration. *Cell* 153, 376–88. doi:10.1016/j.cell.2013.02.053.

Huang, C., Zhang, X., Ramil, J. M., Rikka, S., Kim, L., Lee, Y., et al. (2010). Juvenile exposure to anthracyclines impairs cardiac progenitor cell function and vascularization resulting in greater susceptibility to stress-induced myocardial injury in adult mice. *Circulation* 121, 675–83. doi:10.1161/CIRCULATIONAHA.109.902221.

Ibrahim, A. G.-E. E., Cheng, K., and Marbán, E. (2014). Exosomes as critical agents of cardiac regeneration triggered by cell therapy. *Stem cell reports* 2, 606–19. doi:10.1016/j.stemcr.2014.04.006.

Irizarry, R. A., Hobbs, B., Collin, F., Beazer-Barclay, Y. D., Antonellis, K. J., Scherf, U., et al. (2003). Exploration, normalization, and summaries of high density oligonucleotide array probe level data. *Biostatistics* 4, 249–264. doi:10.1093/biostatistics/4.2.249.

Itahana, K., Itahana, Y., and Dimri, G. P. (2013). Colorimetric detection of senescence-associated beta galactosidase. *Methods Mol Biol* 965, 143–156. doi:10.1007/978-1-62703-239-1_8.

Judge, T. A., Wu, Z., Zheng, X. G., Sharpe, A. H., Sayegh, M. H., and Turka, L. A. (1999). The role of CD80, CD86, and CTLA4 in alloimmune responses and the induction of long-term allograft survival. *J. Immunol.* 162, 1947–51.

Keerthikumar, S., Chisanga, D., Ariyaratne, D., Saffar, H. Al, Anand, S., Zhao, K., et al. (2015). ExoCarta: A Web-Based Compendium of Exosomal Cargo. *J. Mol. Biol.* doi:10.1016/j.jmb.2015.09.019.

Kordelas, L., Rebmann, V., Ludwig, A.-K., Radtke, S., Ruesing, J., Doeppner, T. R., et al. (2014). MSC-derived exosomes: a novel tool to treat therapy-refractory graft-versus-host disease. *Leukemia* 28, 970–3. doi:10.1038/leu.2014.41.

Krishnamurthy, K., Vedam, K., Kanagasabai, R., Druhan, L. J., and Ilangovan, G. (2012). Heat shock factor-1 knockout induces multidrug resistance gene, MDR1b, and enhances P-glycoprotein (ABCB1)-based drug extrusion in the heart. *Proc Natl Acad Sci U S A* 109, 9023–9028. doi:10.1073/pnas.1200731109.

Laflamme, M. A., and Murry, C. E. (2011). Heart regeneration. *Nature* 473, 326–35. doi:10.1038/nature10147.

Lai, R. C., Arslan, F., Lee, M. M., Sze, N. S. K., Choo, A., Chen, T. S.,

et al. (2010). Exosome secreted by MSC reduces myocardial ischemia/reperfusion injury. *Stem Cell Res.* 4, 214–222. doi:10.1016/j.scr.2009.12.003.

Lazzarini, E., Balbi, C., Altieri, P., Pfeffer, U., Gambini, E., Canepa, M., et al. (2016). The human amniotic fluid stem cell secretome effectively counteracts doxorubicin-induced cardiotoxicity. *Sci. Rep.* 6, 29994. doi:10.1038/srep29994.

Lee, J., Cacalano, G., Camerato, T., Toy, K., Moore, M. W., and Wood, W. I. (1995). Chemokine binding and activities mediated by the mouse IL-8 receptor. *J. Immunol.* 155, 2158–64. Available at: http://www.ncbi.nlm.nih.gov/pubmed/7636264 [Accessed September 27, 2017].

Levy, D., Kenchaiah, S., Larson, M. G., Benjamin, E. J., Kupka, M. J., Ho, K. K. L., et al. (2002). Long-term trends in the incidence of and survival with heart failure. *N. Engl. J. Med.* 347, 1397–402. doi:10.1056/NEJMoa020265.

Lipshultz, S. E., Cochran, T. R., Franco, V. I., and Miller, T. L. (2013). Treatment-related cardiotoxicity in survivors of childhood cancer. *Nat. Rev. Clin. Oncol.* 10, 697–710. doi:10.1038/nrclinonc.2013.195.

Lodola, F., Laforenza, U., Cattaneo, F., Ruffinatti, F. A., Poletto, V., Massa, M., et al. (2017). VEGF-induced intracellular Ca2+ oscillations are down-regulated and do not stimulate angiogenesis in breast cancer-derived endothelial colony forming cells. *Oncotarget* 8, 95223–95246. doi:10.18632/oncotarget.20255.

López, Y., Lutjemeier, B., Seshareddy, K., Trevino, E. M., Hageman, K. S., Musch, T. I., et al. (2013). Wharton's jelly or bone marrow mesenchymal stromal cells improve cardiac function following myocardial infarction for more than 32 weeks in a rat model: a preliminary report. *Curr. Stem Cell Res. Ther.* 8, 46–59. doi:CSCRT-EPUB-20121224-7 [pii].

Lötvall, J., Hill, A. F., Hochberg, F., Buzás, E. I., Di Vizio, D., Gardiner, C., et al. (2014). Minimal experimental requirements for definition of extracellular vesicles and their functions: a position statement from the International Society for Extracellular Vesicles. *J. Extracell. vesicles* 3, 26913. doi:http://dx.doi.org/10.3402/jev.v3.26913.

Mareschi, K., Castiglia, S., Sanavio, F., Rustichelli, D., Muraro, M., Defedele, D., et al. (2016). Immunoregulatory effects on T lymphocytes by human mesenchymal stromal cells isolated from bone marrow, amniotic fluid, and placenta. *Exp. Hematol.* 44, 138–150.e1. doi:10.1016/j.exphem.2015.10.009.

Massa, M., Rosti, V., Ramajoli, I., Campanelli, R., Pecci, A., Viarengo, G., et al. (2005). Circulating CD34 $^{+}$, CD133 $^{+}$, and Vascular Endothelial Growth Factor Receptor 2–Positive Endothelial Progenitor Cells in Myelofibrosis With Myeloid Metaplasia. *J. Clin. Oncol.* 23, 5688–5695. doi:10.1200/JCO.2005.09.021.

Messina, E., Angelis, L. De, Frati, G., Morrone, S., Chimenti, S., Fiordaliso, F., et al. (2004). Isolation and Expansion of Adult Cardiac Stem Cells From Human and Murine Heart. *Circ. Res.* 95, 911–921. doi:10.1161/01.RES.0000147315.71699.51.

Mirabella, T., Cilli, M., Carlone, S., Cancedda, R., and Gentili, C. (2011). Amniotic liquid derived stem cells as reservoir of secreted angiogenic factors capable of stimulating neo-arteriogenesis in an ischemic model. *Biomaterials* 32, 3689–3699. doi:10.1016/j.biomaterials.2011.01.071.

Mirabella, T., Hartinger, J., Lorandi, C., Gentili, C., van Griensven, M., and Cancedda, R. (2012). Proangiogenic Soluble Factors from Amniotic Fluid Stem Cells Mediate the Recruitment of Endothelial Progenitors in a Model of Ischemic Fasciocutaneous Flap. *Stem Cells Dev.* 21, 2179–2188. doi:10.1089/scd.2011.0639.

Mirebella, T., Poggi, A., Scaranari, M., Mogni, M., Lituania, M., Baldo, C., et al. (2011). Recruitment of host's progenitor cells to sites of human amniotic fluid stem cells implantation. *Biomaterials* 32, 4218–4227. doi:10.1016/j.biomaterials.2010.12.028.

Mirotsou, M., Jayawardena, T. M., Schmeckpeper, J., Gnecchi, M., and Dzau, V. J. (2011). Paracrine mechanisms of stem cell reparative and regenerative actions in the heart. *J Mol Cell Cardiol* 50, 280–289. doi:10.1016/j.yjmcc.2010.08.005.

Moccia, F., and Poletto, V. (2015). May the remodeling of the Ca2+ toolkit in endothelial progenitor cells derived from cancer patients suggest alternative targets for anti-angiogenic treatment? *Biochim. Biophys. Acta - Mol. Cell Res.* 1853, 1958–1973. doi:10.1016/j.bbamcr.2014.10.024.

Moccia, F., Tanzi, F., and Munaron, L. (2014). Endothelial remodelling and intracellular calcium machinery. *Curr. Mol. Med.* 14, 457–80. Available at: http://www.ncbi.nlm.nih.gov/pubmed/24236452 [Accessed December 14, 2017].

Moerkamp, A. T., Lodder, K., van Herwaarden, T., Dronkers, E., Dingenouts, C. K. E., Tengström, F. C., et al. (2016). Human fetal and adult epicardial-derived cells: a novel model to study their activation. *Stem Cell Res. Ther.* 7, 174. doi:10.1186/s13287-016-0434-9.

Molinaro, M., Ameri, P., Marone, G., Petretta, M., Abete, P., Di Lisa, F., et al. (2015). Recent Advances on Pathophysiology, Diagnostic and Therapeutic Insights in Cardiac Dysfunction Induced by Antineoplastic Drugs. *Biomed Res. Int.* 2015, 1–14. doi:10.1155/2015/138148.

Mozaffarian, D., Benjamin, E. J., Go, A. S., Arnett, D. K., Blaha, M. J., Cushman, M., et al. (2015). Heart Disease and Stroke Statistics—2015 Update. *Circulation* 131, e29–e322. doi:10.1161/CIR.0000000000000152.

Nichols, M., Townsend, N., Scarborough, P., and Rayner, M. Cardiovascular disease in Europe 2014: epidemiological update. doi:10.1093/eurheartj/ehu299.

Octavia, Y., Tocchetti, C. G., Gabrielson, K. L., Janssens, S., Crijns, H. J., and Moens, A. L. (2012). Doxorubicin-induced cardiomyopathy: From molecular mechanisms to therapeutic strategies. *J. Mol. Cell. Cardiol.* 52, 1213–1225. doi:10.1016/j.yjmcc.2012.03.006.

Perkins, D. N., Pappin, D. J., Creasy, D. M., and Cottrell, J. S. (1999). Probability-based protein identification by searching sequence databases using mass spectrometry data. *Electrophoresis* 20, 3551–67. doi:10.1002/(SICI)1522-2683(19991201)20:18<3551::AID-ELPS3551>3.0.CO;2-2.

Piccoli, M., Franzin, C., Bertin, E., Urbani, L., Blaauw, B., Repele, A., et al. (2012). Amniotic fluid stem cells restore the muscle cell niche in a HSA-Cre, SmnF7/F7 mouse model. *Stem Cells* 30, 1675–1684. doi:10.1002/stem.1134.

Piegari, E., De Angelis, A., Cappetta, D., Russo, R., Esposito, G., Costantino, S., et al. (2013). Doxorubicin induces senescence and impairs function of human cardiac progenitor cells. *Basic*

Res Cardiol 108, 334. doi:10.1007/s00395-013-0334-4.
Poloni, A., Rosini, V., Mondini, E., Maurizi, G., Mancini, S., Discepoli, G., et al. (2008). Characterization and expansion of mesenchymal progenitor cells from first-trimester chorionic villi of human placenta. *Cytotherapy* 10, 690–697. doi:10.1080/14653240802419310.
Pozzobon, M., Piccoli, M., Schiavo, A. A., Atala, A., and De Coppi, P. Isolation of c-Kit+ Human Amniotic Fluid Stem Cells from Second Trimester. *Kursad Turksen Methods Mol. Biol.* 1035. doi:10.1007/978-1-62703-508-8_16.
Pozzobon, M., Piccoli, M., Schiavo, A. A., Atala, A., and De Coppi, P. (2013). Isolation of c-Kit+ human amniotic fluid stem cells from second trimester. *Methods Mol Biol* 1035, 191–198. doi:10.1007/978-1-62703-508-8_16.
Radisic, M., Euloth, M., Yang, L., Langer, R., Freed, L. E., and Vunjak-Novakovic, G. (2003). High-density seeding of myocyte cells for cardiac tissue engineering. *Biotechnol Bioeng* 82, 403–414. doi:10.1002/bit.10594.
Rani, S., Ryan, A. E., Griffin, M. D., and Ritter, T. (2015). Mesenchymal Stem Cell-derived Extracellular Vesicles: Toward Cell-free Therapeutic Applications. *Mol. Ther.* 23, 812–23. doi:10.1038/mt.2015.44.
Rauniyar, N., Gao, B., McClatchy, D. B., and Yates, J. R. (2013). Comparison of protein expression ratios observed by sixplex and duplex TMT labeling method. *J. Proteome Res.* 12, 1031–9. doi:10.1021/pr3008896.
Schiavo, A. A., Franzin, C., Albiero, M., Piccoli, M., Spiro, G., Bertin, E., et al. (2015). Endothelial properties of third-trimester amniotic fluid stem cells cultured in hypoxia. *Stem Cell Res Ther* 6, 209. doi:10.1186/s13287-015-0204-0.
Senyo, S. E., Steinhauser, M. L., Pizzimenti, C. L., Yang, V. K., Cai, L., Wang, M., et al. (2013). Mammalian heart renewal by pre-existing cardiomyocytes. *Nature* 493, 433–6. doi:10.1038/nature11682.
Shamim, E. A., Rider, L. G., and Miller, F. W. (2000). Update on the genetics of the idiopathic inflammatory myopathies. *Curr. Opin. Rheumatol.* 12, 482–91.
Smart, N., Bollini, S., Dubé, K. N., Vieira, J. M., Zhou, B., Davidson,

S., et al. (2011). De novo cardiomyocytes from within the activated adult heart after injury. *Nature* 474, 640–4. doi:10.1038/nature10188.

Smart, N., Mojet, M. H., Latchman, D. S., Marber, M. S., Duchen, M. R., and Heads, R. J. (2006). IL-6 induces PI 3-kinase and nitric oxide-dependent protection and preserves mitochondrial function in cardiomyocytes. *Cardiovasc. Res.* 69, 164–77. doi:10.1016/j.cardiores.2005.08.017.

Smart, N., Risebro, C. A., Melville, A. A. D., Moses, K., Schwartz, R. J., Chien, K. R., et al. (2007). Thymosin beta4 induces adult epicardial progenitor mobilization and neovascularization. *Nature* 445, 177–82. doi:10.1038/nature05383.

Tan, C. Y., Lai, R. C., Wong, W., Dan, Y. Y., Lim, S.-K., and Ho, H. K. (2014). Mesenchymal stem cell-derived exosomes promote hepatic regeneration in drug-induced liver injury models. *Stem Cell Res. Ther.* 5, 76. doi:10.1186/scrt465.

Tao, H., Han, Z., Han, Z. C., and Li, Z. (2016). Proangiogenic Features of Mesenchymal Stem Cells and Their Therapeutic Applications. *Stem Cells Int.* 2016, 1314709. doi:10.1155/2016/1314709.

Tasev, D., Konijnenberg, L. S. F., Amado-Azevedo, J., van Wijhe, M. H., Koolwijk, P., and van Hinsbergh, V. W. M. (2016). CD34 expression modulates tube-forming capacity and barrier properties of peripheral blood-derived endothelial colony-forming cells (ECFCs). *Angiogenesis* 19, 325–338. doi:10.1007/s10456-016-9506-9.

Tersteeg, C., Roest, M., Mak-Nienhuis, E. M., Ligtenberg, E., Hoefer, I. E., de Groot, P. G., et al. (2012). A fibronectin-fibrinogen-tropoelastin coating reduces smooth muscle cell growth but improves endothelial cell function. *J. Cell. Mol. Med.* 16, 2117–26. doi:10.1111/j.1582-4934.2011.01519.x.

Tetta, C., Ghigo, E., Silengo, L., Deregibus, M. C., and Camussi, G. (2013). Extracellular vesicles as an emerging mechanism of cell-to-cell communication. *Endocrine* 44, 11–19. doi:10.1007/s12020-012-9839-0.

Tidball, J. G., and Villalta, S. A. (2010). Regulatory interactions between muscle and the immune system during muscle regeneration. *AJP Regul. Integr. Comp. Physiol.* 298, R1173–

R1187. doi:10.1152/ajpregu.00735.2009.
Van Den Borne, S. W. M., Van De Schans, V. A. M., Strzelecka, A. E., Vervoort-Peters, H. T. M., Lijnen, P. M., Cleutjens, J. P. M., et al. (2009). Mouse strain determines the outcome of wound healing after myocardial infarction. *Cardiovasc. Res.* 84, 273–282. doi:10.1093/cvr/cvp207.
van Vliet, P., Roccio, M., Smits, A. M., van Oorschot, A. A. M., Metz, C. H. G., van Veen, T. A. B., et al. (2008). Progenitor cells isolated from the human heart: a potential cell source for regenerative therapy. *Neth. Heart J.* 16, 163–9. doi:10.1007/BF03086138.
Won Kim, H., Haider, H. K., Jiang, S., and Ashraf, M. (2009). Ischemic Preconditioning Augments Survival of Stem Cells via miR-210 Expression by Targeting Caspase-8-associated Protein 2. *J. Biol. Chem.* 284, 33161–33168. doi:10.1074/jbc.M109.020925.
Xin, H., Li, Y., Buller, B., Katakowski, M., Zhang, Y., Wang, X., et al. (2012). Exosome-mediated transfer of miR-133b from multipotent mesenchymal stromal cells to neural cells contributes to neurite outgrowth. *Stem Cells* 30, 1556–64. doi:10.1002/stem.1129.
Xu, W., Qian, H., Zhang, B., Wang, M., Gong, , aihua, Zhang, X., et al. HucMSC-exosome Mediated -Wnt4 Signaling is Required for Cutaneous Wound Healing. doi:10.1002/stem.1771.
Zani, A., Cananzi, M., Fascetti-Leon, F., Lauriti, G., Smith, V. V, Bollini, S., et al. (2014). Amniotic fluid stem cells improve survival and enhance repair of damaged intestine in necrotising enterocolitis via a COX-2 dependent mechanism. *Gut* 63, 300–9. doi:10.1136/gutjnl-2012-303735.
Zeng, L., He, X., Wang, Y., Tang, Y., Zheng, C., Cai, H., et al. (2014). MicroRNA-210 overexpression induces angiogenesis and neurogenesis in the normal adult mouse brain. *Gene Ther.* 21, 37–43. doi:10.1038/gt.2013.55.
Zhang, Z., Sun, H., Dai, H., Walsh, R., Imakura, M., Schelter, J., et al. (2009). MicroRNA miR-210 modulates cellular response to hypoxia through the MYC antagonist MNT. *Cell Cycle* 8, 2756–2768. doi:10.4161/cc.8.17.9387.
Zhou, B., Honor, L. B., Ma, Q., Oh, J.-H., Lin, R.-Z., Melero-Martin, J. M., et al. (2012). Thymosin beta 4 treatment after myocardial

infarction does not reprogram epicardial cells into cardiomyocytes. *J. Mol. Cell. Cardiol.* 52, 43–7. doi:10.1016/j.yjmcc.2011.08.020.

Zhou, B., Ma, Q., Rajagopal, S., Wu, S. M., Domian, I., Rivera-Feliciano, J., et al. (2008). Epicardial progenitors contribute to the cardiomyocyte lineage in the developing heart. *Nature* 454, 109–13. doi:10.1038/nature07060.

Zhou, B., and Pu, W. T. (2012). Epicardial epithelial to mesenchymal transition in injured heart. *J. Cell. Mol. Med.* 15, 2781–2783. doi:10.1111/j.1582-4934.2011.01450.x.Epicardial.

LIST OF PUBLICATIONS AND OTHER ACTIVITIES

Publications in International Peer-Reviewed Journals:

1. Bollini S, Silini AR, Banerjee A, Wolbank S, **Balbi C**, Parolini O. *Cardiac Restoration Stemming from the Placenta Tree: Insights from Fetal and Perinatal Cell Biology*. **Frontiers in Physiology**. Accepted

2. **Balbi C,** Bollini S. *Fetal and Perinatal Stem Cells in Cardiac Regeneration: Moving Forward to the Paracrine Era.* **Placenta** 2017 Apr. 12 doi: 10.1016/j.placenta.2017.04.008 I.F 2.759

3. **Balbi C,** Piccoli M, Barile L, Papait A, Armirotti A, Principi E, Reverberi D, Pascucci L, Becherini P, Varesio L, Mogni M, Coviello D, Bandiera T, Pozzobon M, Cancedda R, Bollini S. *First Characterization of Human Amniotic Fluid Stem Cell Extracellular Vesicles as a Powerful Paracrine Tool Endowed with Regenerative Potential.* **Stem Cells Translational Medicine.** 2017 Mar 8. doi: 10.1002/sctm.16-0297. I.F. 4

4. Lo Sicco C, Reverberi D, **Balbi C**, Ulivi V, Principi E, Pascucci L, Becherini P, Bosco MC, Varesio L, Franzin C, Pozzobon M, Cancedda R, Tasso R. *Mesenchymal Stem Cell-Derived Extracellular Vesicles as Mediators of Anti-Inflammatory Effects: Endorsement of Macrophage Polarization.* **Stem Cells Translational Medicine.** 2017 Mar;6(3):1018-1028. doi: 10.1002/sctm.16-0363. I.F. 4

5. Lazzarini E*., **Balbi C.***, Altieri P., Pfeffer U., Gambini E., Canepa M., Varesio L., Bosco MC., Coviello D., Pompilio G., Brunelli C., Cancedda R., Ameri P., Bollini S. *The human amniotic fluid stem cell secretome effectively counteracts doxorubicin-induced*

cardiotoxicity. **First Joint Authorship.* **Scientific Reports.** 2016 Jul 21;6:29994. doi:10.1038/srep29994. I.F. 4.259

Presentations at National and International Meetings:

- SIRC XXI CONGRESSO NAZIONALE 2017 16 18 November with the following **oral presentation**

"The human Amniotic Stem Cell Secretome as a new paracrine tool to unlock endogenous cardiac regeneration"

- TERMIS-EU 2017 26-30 June with the following poster presentation

"First characterization of human amniotic fluid stem cell extracellular vesicles as a powerful paracrine tool endowed with regenerative potential"

"The human Amniotic Stem Cell Secretome as a new paracrine tool to unlock endogenous cardiac regeneration"

- SCR Italy 2017 Chieti 25-27 May with the following poster and **oral presentation**, respectively

"The human Amniotic Stem Cell Secretome as a new paracrine tool to unlock endogenous cardiac regeneration"

"First characterization of human amniotic fluid stem cell extracellular vesicles as a powerful paracrine tool endowed with regenerative potential"

- PhD Students Meeting: Life Sciences for a Better Future 2017 11-13 May with the following **oral presentation**

"First characterization of human amniotic fluid stem cell extracellular vesicles as a powerful paracrine tool endowed with regenerative potential"

- FCVB 2016 Florence 21-23 June with the following poster presentations

"The Regenerative Potential of the Amniotic Fluid Stem Cell Microvescicles"

"The human Amniotic Stem Cell Secretome as a new paracrine tool to unlock endogenous cardiac regeneration"

- LSCM 2016 Lugano 20-21 June with the following poster presentation

"The Regenerative Potential of the Amniotic Fluid Stem Cell Microvescicles"

- SIRC Forum 2016 Genoa 18 June with the selected following **oral presentation**

"The human Amniotic Stem Cell Secretome as a new paracrine tool to unlock endogenous cardiac regeneration"

- AICC 2016 Rome 9-10 June with the following poster presentation

"The Regenerative Potential of the Amniotic Fluid Stem Cell Microvescicles"

- ISEV 2016 Rotterdam 4-7 May with the following poster presentation

"The Regenerative Potential of the Amniotic Fluid Stem Cell Microvescicles"

- GISM 2015 Brescia 8-9 October with the following poster presentation

"Human Amniotic Fluid Stem Cells provide Cardioprotection by paracrine effect in a Doxorubicin-induced Cardiotoxicity model"

"The Regenerative Potential of the Amniotic Fluid Stem Cell Microvescicles"

Awards:

- Award "Giovane Ricercatore 2017" Best Oral Presentation – SIRC XXI Congresso Nazionale 2017, Imola 16-18 Nov 2017

- Young Investigator Award for Best Poster Presentation – GISM (*Gruppo Italiano cellule Staminali Mesenchimali*, Italian Mesenchymal Stem Cell Group) Annual Meeting 2015, Brescia, 8-9 October 2015
- Paolo Bianco Award for Best Oral Presentation – SCR Italy (*Stem Cell Research Italy*) Annual meeting 2017, Chieti 25-27 May 2017

Workshop Training:

- BD Multicolor Training - Milano (Italy) 28 Jan 2016 (open access)
- EMBL course: Extracellular Vesicles: from Biology to Biomedical Applications – Heidelberg 19-24 Sep 2016 (selected as 1 of 20 in a total of 100 applicants):

Responsabilities:

- Review Editor for the Editorial Board of Stem Cell Research, a specialty of Frontiers in Bioengineering and Biotechnology, Cell and Developmental Biology, Genetics and Oncology.
- University of Genova teaching tutor of Faculty of Medicine - 2016/2017

Other Training Activities:

- From 09.11.15 to 22.11.15

Visiting PhD Student at SIRM – Swiss Institute of Regenerative Medicine – Laboratory of Molecular and Cellular Cardiology, CardioCentro Ticino Foundation-CCT, Lugano, Swiss, under the supervision of Dr.Lucio Barile to acquire specific know.how on the

isolation of human cardiac progenitor cells from cardiac biospy as clinical waste material.

- From 09.07.2017 – 31.12.2018

Visiting PhD Student at LUMC – Leiden University Medical Center – Department of Molecular Cell Biology – Leiden, The Netherlands under the supervision of Prof.Marie-Josè Goumans and Dr. Anke Smits.

ACKNOWLEDGEMENTS

Nonostante tutto, questo è forse il capitolo più difficile della mia tesi.
Ringrazio la Professoressa Bollini che in un mondo di porte chiuse mi ha tenuto una porta aperta, dandomi la possibilità di svolgere il mio dottorato nel migliore dei modi possibili; ringrazio anche Sveva che ha contribuito a tenere la porta aperta ma soprattutto ad alleggerire questi tre anni, tra chiacchiere, gatti e cibo, tanto cibo.
Ringrazio il Professor Quarto direttore della nostra scuola di Dottorato.
I would also like to thank Prof.Marie-Josè Goumans for hosting me in her lab and Dr.Anke Smits for supervising me during my period at Leiden University Medical Center: thank you so much!!! It was a pleasure for me to be there.
I would like to thank Kirsten who having surgery on so many mice all around the clock with also the most annoying mice line in the history and Tessa who was always so kind and helped me with the experiments. Also thank to all the STAR group it was a very nice experience.
Grazie anche a tutto il laboratorio di Medicina Rigenerativa, devo dire che probabilmente senza di voi più della metà dei bei ricordi non esisterebbero.
Sprono che anche non volendo è, a tutti gli effetti, la motivatrice del gruppo; si sa che se anche lei è in crisi vuol dire che siamo veramente nello sterco (da notare l'educazione del termine che ho usato). Claudia con la quale ho sfogato i miei momenti di down sapendo di trovare sempre una comprensione, thank you Cansu, because you are wonderfully crazy and with your craziness you brought a necessary breath of joy in that lab.
Poi ci sono le altre gioie del lab: Alessandro, Van, Racalina, Simonetta, Alessio e Martolina. Siete fantastici, con voi fare un discorso serio è impossibile ed è il motivo per cui vi adoro tutti…ovviamente Martolina un po' di più di tutti, ma lo sapete quindi nessun rancore :)

Grazie ai “Malatestiani” sempre pronti ad aiutare trovando, a volte, soluzioni spesso troppo complicate per il genere umano.
Grazie ad Ambra, sei super in gamba, non smetterò mai di dirtelo, buona fortuna per tutto e ad Elisa, sono stata fortunata a poter condividere gioie e dolori (freddo e caldo) di quella stanza con te.
Poi ci sono tutti quelli passati dal lab, ma non passati dall’esser per me persone speciali come Barbara (mamma mia come manca la tua risata) e gli “Amici del Gusto” una fortuna che auguro a tutti quella di trovare una seconda famiglia come loro: Raffy le tue battute mancano sempre (lo so sono bugiarda) e Dani tu dovresti fare un video con le tue imitazioni, così quando un è un po’ giù se le guarda e si risolleva la giornata! Lucia, l’unica saggia del gruppo che ci ha visto lungo ed è andata a fare un lavoro vero da subito :) e Fede, con il quale ho condiviso 2 anni di follia in quel lab, è stato bello ri-averti lì per un po’. Chri e Mary, bhè lo sapete amici, quando volete andare da qualche parte e mangiare e bere bene, noi ci siamo sempre :).
Poi i ringraziamenti passano alla mia famiglia, mio Padre che credo non abbia mai capito il perché io abbia fatto la scelta di fare questo lavoro, ma nonostante ciò mi ha sempre sostenuto nel farlo e i miei Zii sempre piacevolmente molto orgogliosi di me. E poi ovviamente, anche se non c’è più un grazie va sempre e andrà per sempre a mia madre, ho iniziato questo dottorato esattamente quando tu te ne sei andata questo ha reso questi tre anni i più difficili della mia vita, ti amo come ti ho sempre amato e come tu sai.
Infine, come dicono i migliori speaker: LAST BUT NOT LEAST grazie a Edoardo. Sei stato la mia fortuna, niente di tutto ciò sarebbe stato possibile senza te accanto, sei il mio miglior amico, colui che più mi fa ridere al mondo e con cui le giornate volano e sono indimenticabili allo stesso tempo. Grazie di questi anni insieme, e grazie per quelli che verranno, ti amo.
Ah, e ovviamente, tante tante ma tante grazie a **ME**.